
Article:
Aad, G. orcid.org/0000-0002-6665-4934, Aakvaag, E. orcid.org/0000-0001-7616-1554, Abbott, B. orcid.org/0000-0002-5888-2734 et al. (2915 more authors) (2024) Fiducial and differential cross-section measurements of electroweak Wy j j production in pp collisions at √s = 13 TeV with the ATLAS detector. The European Physical Journal C, 84. 1064. ISSN 1434-6044

https://doi.org/10.1140/epjc/s10052-024-13311-6

Eur. Phys. J. C (2024) 84:1064
https://doi.org/10.1140/epjc/s10052-024-13311-6

THE EUROPEAN PHYSICAL JOURNAL C

Regular Article - Experimental Physics

Fiducial and differential cross-section measurements of electroweak $W\gamma jj$ production in pp collisions at $\sqrt{s} = 13$ TeV with the ATLAS detector

ATLAS Collaboration[⋆]

CERN, 1211 Geneva 23, Switzerland

Received: 6 March 2024 / Accepted: 28 August 2024

Abstract The observation of the electroweak production of a W boson and a photon in association with two jets, using pp collision data at the Large Hadron Collider at a centre of mass energy of $\sqrt{s} = 13$ TeV, is reported. The data were recorded by the ATLAS experiment from 2015 to 2018 and correspond to an integrated luminosity of 140 fb^{-1}. This process is sensitive to the quartic gauge boson couplings via the vector boson scattering mechanism and provides a stringent test of the electroweak sector of the Standard Model. Events are selected if they contain one electron or muon, missing transverse momentum, at least one photon, and two jets. Multivariate techniques are used to distinguish the electroweak $W\gamma jj$ process from irreducible background processes. The observed significance of the electroweak $W\gamma jj$ process is well above six standard deviations, compared to an expected significance of 6.3 standard deviations. Fiducial and differential cross sections are measured in a fiducial phase space close to the detector acceptance, which are in reasonable agreement with leading order Standard Model predictions from MadGraph5+Pythia8 and Sherpa. The results are used to constrain new physics effects in the context of an effective field theory.

Contents

1 Introduction

The scattering of two vector bosons, e.g. $WZ \to W\gamma$, is sensitive to both the triple and quartic electroweak-boson self-interactions [1,2]. In proton–proton (pp) collisions, the $W\gamma jj$ final state can be produced via many different mechanisms, as shown in Fig. 1. Electroweak (EW) $W\gamma jj$ production concerns exclusively electroweak interactions of order α_{EW}^4 at tree level [3], where α_{EW} is the electroweak coupling constant. Although the contributions of interest are vector boson scattering (VBS) interactions involving quartic gauge couplings (QGCs), these cannot be distinguished from other electroweak contributions in a gauge-invariant manner. Thus, the signal process studied in this paper is the combination of all processes of order α_{EW}^4 shown in Fig. 1a–c. The dominant background for EW $W\gamma jj$ production concerns processes of order $\alpha_{\mathrm{S}}^2\alpha_{\mathrm{EW}}^2$ at tree level in Fig. 1d, where α_{S} is the strong coupling constant and the jets are produced via strong interaction vertices; these processes are collectively referred to as strong $W\gamma jj$ production in this paper. Triboson diagrams, such as the one shown in Fig. 1b, do contribute to EW $W\gamma jj$ production. However, due to their distinct topology they require separate signal selection and background estimation methods and are thus generally the subject of separate studies.

The large cross-section of EW $W\gamma jj$ production predicted by the SM allows differential cross-sections to be measured with higher precision than other VBS processes. The differ-

⋆ e-mail: atlas.publications@cern.ch

Published online: 15 October 2024

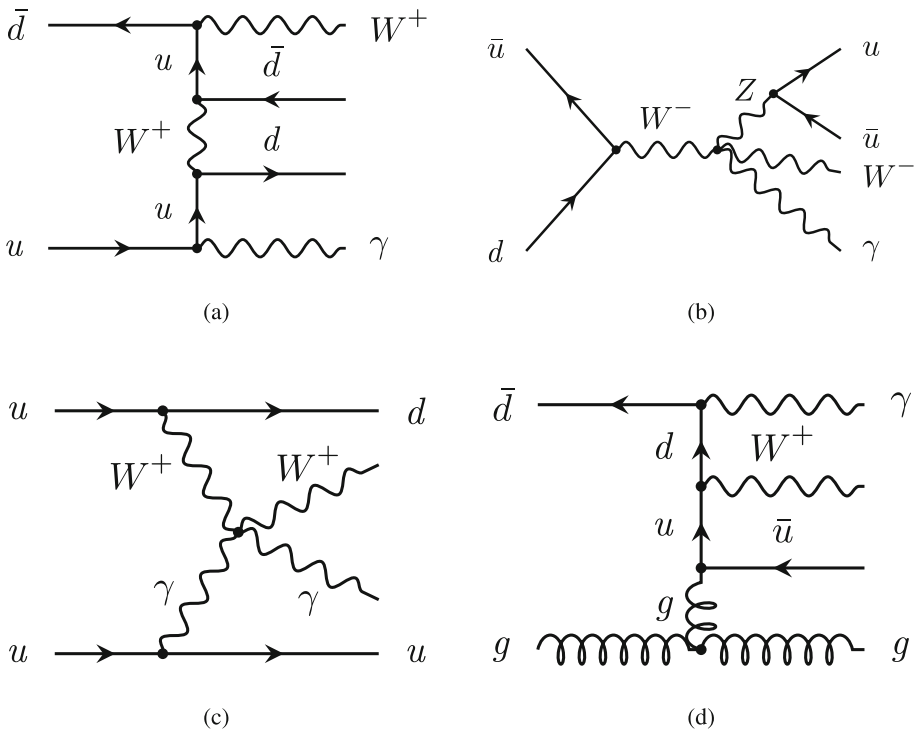

Fig. 1 Representative Feynman diagrams for the $W\gamma jj$ final state: **a** EW $W\gamma jj$ production involving no gauge boson self-interactions, **b** Bremsstrahlung EW $W\gamma jj$ non-VBS production involving quartic gauge boson interactions, **c** $W\gamma$ VBS involving quartic gauge boson interactions, and **d** Strong $W\gamma jj$ production

ential measurements further enhance our sensitivity to potential anomalous quartic couplings of $WW\gamma\gamma$ and $WW\gamma Z$. In addition to the VBS topology characterised by the two energetic jets in the forward and backward region, the leptonic decay channel of the EW $W\gamma jj$ production has a clean signature in the detector with exactly one charged lepton, missing transverse momentum, and at least one photon. This paper reports fiducial and differential cross-section measurements in the EW $W\gamma jj$ final state using 140 fb^{-1} of data recorded between 2015 and 2018 with the ATLAS detector.

The CMS Collaboration reported the observation of the EW $W\gamma jj$ process [4] and measured EW $W\gamma jj$ differential cross-sections [5]. This analysis exploits two innovations compared to the CMS publication. First, multivariate techniques involving a neural network are used to isolate the EW $W\gamma jj$ signal from the strong $W\gamma jj$ background in a VBS-enhanced phase space; the resulting observed yield is corrected for detector effects and a fiducial cross-section is reported in a fiducial phase space at particle level as close as possible to the reconstruction level. Secondly, observables sensitive to the charge conjugation (C) and parity (P) structure of $WW\gamma\gamma$ and $WW\gamma Z$ couplings are measured. These measurements can be used to explore new sources of CP violation (CPV) in the gauge-boson sector that may partly explain the predominance of matter over anti-matter in the universe. The differential cross-sections for EW $W\gamma jj$ production are measured as functions of two types of observables: *VBS observables* and *charge conjugation and parity observables*.

- The VBS observables are those that are used to characterise specifically the VBS nature of events; they are additionally sensitive to anomalous QGCs (aQGCs) via dimension-8 operators of an effective field theory (EFT), which can be parameterised in the Éboli basis [2]. These observables include the invariant mass of the dijet system, m_{jj}, the transverse momentum of the two jets, p_{T}^{jj}, the lepton transverse momentum, p_{T}^{l}, and the invariant mass of the lepton and the photon, $m_{l\gamma}$.
- The charge conjugation and parity observables probe the CP structure of $WW\gamma\gamma$ and $WW\gamma Z$ couplings. Two observables are studied: the signed azimuthal angle difference between the two jets, $\Delta\phi_{jj} = \phi_f^j - \phi_b^j$, where the two highest transverse-momentum jets are ordered by rapidity y such that $y_f^j > y_b^j$, and the signed azimuthal angle difference between the lepton and the photon, $\Delta\phi_{l\gamma} = \phi_f - \phi_b$, where the lepton and the photon are ordered such that $y_f > y_b$. Measurements of $\Delta\phi_{jj}$ have previously been proposed to constrain the CP-odd component involving Higgs boson couplings in Vector Boson Fusion (VBF) processes [6] and the $t\bar{t}H$ process [7].

The paper is organised as follows. Section 2 briefly describes the ATLAS detector. Section 3 documents the simulated signal and background samples used in this analysis. The object reconstruction and event selection is presented in Sect. 4. The background estimate is detailed in Sect. 5. The methodologies used for the fiducial and differential cross-section measurements are discussed in Sect. 6. Corrections for detector effects are described in Sect. 7, followed by a

description of the systematic uncertainties in Sect. 8. The fiducial and differential EW $W\gamma jj$ cross-sections are presented in Sect. 9. Section 10 presents constraints on the Wilson coefficients of dimension-8 EFT.

2 ATLAS detector

The ATLAS detector [8] at the LHC covers nearly the entire solid angle around the collision point.[1] It consists of an inner tracking detector surrounded by a thin superconducting solenoid, electromagnetic and hadronic calorimeters, and a muon spectrometer incorporating three large superconducting air-core toroidal magnets.

The inner-detector system (ID) is immersed in a 2T axial magnetic field and provides charged-particle tracking in the range $|\eta| < 2.5$. The high-granularity silicon pixel detector covers the vertex region and typically provides four measurements per track, the first hit generally being in the insertable B-layer (IBL) installed before Run 2 [9,10]. It is followed by the SemiConductor Tracker (SCT), which usually provides eight measurements per track. These silicon detectors are complemented by the transition radiation tracker (TRT), which enables radially extended track reconstruction up to $|\eta| = 2.0$. The TRT also provides electron identification information based on the fraction of hits (typically 30 in total) above a higher energy-deposit threshold corresponding to transition radiation.

The calorimeter system covers the pseudorapidity range $|\eta| < 4.9$. Within the region $|\eta| < 3.2$, electromagnetic calorimetry is provided by barrel and endcap high-granularity lead/liquid-argon (LAr) calorimeters, with an additional thin LAr presampler covering $|\eta| < 1.8$ to correct for energy loss in material upstream of the calorimeters. Hadronic calorimetry is provided by the steel/scintillator-tile calorimeter, segmented into three barrel structures within $|\eta| < 1.7$, and two copper/LAr hadronic endcap calorimeters. The solid angle coverage is completed with forward copper/LAr and tungsten/LAr calorimeter modules optimised for electromagnetic and hadronic energy measurements respectively.

The muon spectrometer (MS) comprises separate trigger and high-precision tracking chambers measuring the deflection of muons in a magnetic field generated by the superconducting air-core toroidal magnets. The field integral of the toroids ranges between 2.0 and 6.0T m across most of the detector. Three layers of precision chambers, each consisting of layers of monitored drift tubes, cover the region $|\eta| < 2.7$, complemented by cathode-strip chambers in the forward region, where the background is highest. The muon trigger system covers the range $|\eta| < 2.4$ with resistive-plate chambers in the barrel, and thin-gap chambers in the endcap regions.

The luminosity is measured mainly by the LUCID–2 [11] detector that records Cherenkov light produced in the quartz windows of photomultipliers located close to the beampipe.

Events are selected by the first-level trigger system implemented in custom hardware, followed by selections made by algorithms implemented in software in the high-level trigger [12]. The first-level trigger accepts events from the 40MHz bunch crossings at a rate below 100kHz, which the high-level trigger further reduces in order to record complete events to disk at about 1kHz.

A software suite [13] is used in data simulation, in the reconstruction and analysis of real and simulated data, in detector operations, and in the trigger and data acquisition systems of the experiment.

3 Monte Carlo event simulation

Monte Carlo (MC) event generators are used in the analysis to simulate signal and background events produced in pp collisions. These simulated samples are used to design and optimise the analysis, evaluate systematic uncertainties, and characterise the effects of detector inefficiency and resolution.

Electroweak $W\gamma jj$ production is simulated with the Sherpa 2.2.12 [14] generator. Matrix elements at leading order (LO) in QCD with up to one additional emission are matched to a parton shower based on Catani–Seymour dipole factorisation [15,16] using the MEPS@LO prescription [17–20]. Samples are simulated using the NNPDF3.0nnlo parton distribution function (PDF) set [21], along with the dedicated set of tuned parton-shower parameters developed by the Sherpa authors. An alternative EW $W\gamma jj$ signal sample is produced using MadGraph5_aMC@NLO [22] at LO accuracy with the default dynamical scale choice and the NNPDF3.1lo PDF set. Pythia 8.240 with the dipole recoil option turned on is used to add parton showering, hadronisation, and underlying-event activity. The A14 [23] set of tuned parton-shower parameters is used for Pythia 8.240, and EvtGen [24] is used for the properties of bottom and charmed hadron decays. This alternative EW $W\gamma jj$ sample is used to evaluate a systematic uncertainty of the signal production due to the choice of event generator.

[1] ATLAS uses a right-handed coordinate system with its origin at the nominal interaction point (IP) in the centre of the detector and the z-axis along the beam pipe. The x-axis points from the IP to the centre of the LHC ring, and the y-axis points upwards. Polar coordinates (r, ϕ) are used in the transverse plane, ϕ being the azimuthal angle around the z-axis. The pseudorapidity is defined in terms of the polar angle θ as $\eta = -\ln\tan(\theta/2)$ and is equal to the rapidity $y = \frac{1}{2}\ln\left(\frac{E+p_z c}{E-p_z c}\right)$ in the relativistic limit. Angular distance is measured in units of $\Delta R \equiv \sqrt{(\Delta y)^2 + (\Delta\phi)^2}$.

The dominant background process, strong $W\gamma jj$, is simulated using SHERPA 2.2.11 [14]. Matrix elements at next-to leading order (NLO) QCD accuracy for up to one additional parton and LO accuracy for up to three additional parton emissions are matched and merged with the SHERPA parton shower based on Catani–Seymour dipole factorisation [15,16] using the MEPS@NLO prescription [17–20]. This sample uses NNPDF3.0NNLO for the matrix element calculation with default parameters for parton showering, hadronisation, and underlying-event activity. An alternative strong $W\gamma jj$ sample is produced using MADGRAPH5_AMC@NLO at NLO accuracy for events with up to three partons in the final state with the NNPDF3.0NLO PDF set and is interfaced with PYTHIA 8.240 with A14 parameters to provide parton showering, hadronisation, and underlying-event activity. This alternative strong $W\gamma jj$ sample is used to evaluate a systematic uncertainty of the strong $W\gamma jj$ background estimate due to the choice of event generator.

Prompt background events are those that contain at least one prompt photon, exactly one prompt charged lepton, and two jets. SHERPA 2.2.12, with the same settings as EW and strong $W\gamma jj$, is also used to simulate EW and strong $Z\gamma jj$ production. The remaining prompt backgrounds can arise from $tW\gamma$, $tq\gamma$, and $t\bar{t}\gamma$ processes, which are simulated using MADGRAPH5_AMC@NLO[22] with NNPDF2.3NLO for $tW\gamma$ and $t\bar{t}\gamma$ at LO, and $tq\gamma$ at NLO. To provide parton showering, hadronisation, and underlying-event activity these samples are interfaced PYTHIA 8.235, PYTHIA 8.212, and PYTHIA 8.240, respectively, with A14 parameters.

Contributions from background events arising from jets misidentified as leptons or photons, non-prompt leptons or photons from decays of hadrons, electrons reconstructed as photons, and photons arising from a separate pp interaction ("pile-up photons") are estimated by using the data-driven methods that are outlined in Sect. 5. The term *fake leptons* is used to collectively refer to either non-prompt leptons or hadronic jets misreconstructed as leptons. MC simulated samples including W+jets, Z+jets, tW, $t\bar{t}$, diboson, and multijet events are used in the validation of data-driven methods and the evaluation of systematic uncertainties of the background estimations. In particular, simulated W+jets and Z+jets events, which are used in the validation of the non-prompt photon estimate, are produced at NLO accuracy using SHERPA 2.2.11 with NNPDF3.0NNLO and default parameter tunes for parton showering, hadronisation, and underlying-event activity. Background events from electrons misreconstructed as photons can arise from tW, $t\bar{t}$, and Z+jets processes. The tW and $t\bar{t}$ processes are simulated using POWHEG at NLO accuracy with NNPDF3.0NNLO and PYTHIA 8.230 with A14 parameters to provide parton showering, hadronisation, and underlying-event activity. Diboson and multijet events are used in the data-driven estimate of fake leptons. The diboson sample is simulated with SHERPA 2.2.2 at NLO with NNPDF3.0NLO and default parameter tunes for parton showering, hadronisation, and underlying-event activity. The multijet sample is simulated using PYTHIA 8.235 at LO accuracy with NNPDF2.3LO and A14 tunes for parton showering.

All simulated signal and background events are processed through the full ATLAS detector simulation using GEANT4 [25] and then reconstructed using the same algorithms as the recorded data events. Differences between reconstructed leptons, photons, jets and missing transverse momentum in simulations and data are corrected using event-by-event scale factors with p_{T} and η dependence. The effect of multiple interactions in the same and neighbouring bunch crossings (pile-up) is modelled by overlaying the simulated hard-scattering event with inelastic pp events simulated with PYTHIA 8.186 [26] using the NNPDF2.3LO set of PDFs [27] and the A3 set of tuned parton-shower parameters [28].

4 Object reconstruction and event selection

This analysis is performed using pp collision data collected between 2015 and 2018 at a centre-of-mass energy of $\sqrt{s} = 13$ TeV, corresponding to an integrated luminosity of 140 fb^{-1} [29].

Events are required to satisfy the unprescaled single-lepton triggers that have transverse momentum thresholds of 20–26 GeV, depending on the charged lepton flavour and data-taking periods [30,31]; this is complemented by triggers with higher p_{T} thresholds and no isolation requirements to increase the overall trigger efficiency. Events are also required to satisfy detector and data quality requirements during stable beam conditions [32]. Candidate pp interaction vertices are reconstructed using charged-particle tracks; each candidate vertex must have at least two tracks with $p_{\mathrm{T}} > 500$ MeV [33]. The vertex with the highest scalar sum of track p_{T}^2 is selected as the primary vertex. Events must contain at least one electron or muon, missing transverse momentum, at least one photon, and at least two jets.

Muons are reconstructed by matching tracks in the MS to a corresponding track in the ID. Each muon must satisfy the *tight* identification criteria and *tight* isolation working point [34]. Muons are constrained to originate from the primary vertex by requiring $|d_0/\sigma_{d_0}| < 3$ and $|z_0 \sin\theta| < 0.5$ mm, where d_0 is the distance of closest approach to the primary vertex in the transverse plane, with an uncertainty σ_{d_0}, and z_0 is the longitudinal difference between the point at which d_0 is defined and the primary vertex. Selected muons are required to have $p_{\mathrm{T}} > 30$ GeV and $|\eta| < 2.5$.

Electrons are reconstructed from clusters of energy deposits in the ECAL and matched to a track reconstructed in the ID. Each electron must satisfy the *tight* identification and *tight* isolation working points [35]. Electrons are required to have $p_{\mathrm{T}} > 30$ GeV and $|\eta| < 2.47$, excluding the calorime-

ter transition region $1.37 < |\eta| < 1.52$, $|d_0/\sigma_{d_0}| < 5$ and $|z_0 \sin\theta| < 0.5$ mm.

Photons are also reconstructed from clusters of energy deposits in the ECAL. Both converted and unconverted photons are used in the analysis. Converted photons are defined as photon clusters that are matched to one or two ID tracks consistent with a conversion vertex, while unconverted photons are defined as photon clusters that are matched to neither an ID electron track nor a conversion vertex. Each photon is required to satisfy *tight* identification and *tight* isolation working points [35]. Photons passing a *loose* identification requirement are retained in the analysis to define control regions for the data-driven background estimation method used to determine the background from jets misidentified as photons, which is described in Sect. 5. The *tight* isolation requirement is defined as $E_{\mathrm{T}}^{\mathrm{cone40}} < 0.022 \times p_{\mathrm{T}} + 2.45$ GeV, where $E_{\mathrm{T}}^{\mathrm{cone40}}$ is computed as the sum of transverse energies of positive-energy topological clusters in the calorimeter within a distance of $\Delta R = 0.4$ around the photon candidate [35]. Photons are required to have $p_{\mathrm{T}} > 22$ GeV and $|\eta| < 2.37$, excluding the calorimeter transition region $1.37 < |\eta| < 1.52$.

Jets are reconstructed using a particle-flow method [36] that combines charged-particle tracks in the ID with topo-clusters formed from energy deposits in the calorimeters. The anti-k_t algorithm [37] with radius parameter $R = 0.4$ is used to define the jet. Each jet is required to have $p_{\mathrm{T}} > 25$ GeV and $|\eta| < 4.4$. Jets with $p_{\mathrm{T}} < 60$ GeV and $|\eta| < 2.4$ are required to originate from the primary vertex by using the *tight* working point of the jet vertex tagger (JVT) [38]. Jets that originate from noise bursts in the calorimeters are removed [39]. Events must have at least two jets with $p_{\mathrm{T}} > 50$ GeV. Jets with $|\eta| < 2.5$ that contain b-hadrons are identified by a multivariate algorithm (DL1r) [40] with 85% tagging efficiency working point. Events identified as containing a b-jet by the DL1r algorithm are excluded to suppress backgrounds from processes involving top quarks.

The magnitude of the missing transverse momentum, $E_{\mathrm{T}}^{\mathrm{miss}}$, and its direction are calculated from the negative vector sum of a track-based soft term and all reconstructed electrons, muons, photons, and jets [41]. The soft term is calculated from tracks from the primary vertex that are not matched to any hard physics objects. Events are required to satisfy $E_{\mathrm{T}}^{\mathrm{miss}} > 30$ GeV.

To resolve ambiguities in the object reconstruction, an overlap removal procedure is applied. Jet candidates are removed if $\Delta R(j, l) < 0.2$ ($l = e, \mu$). Then, leptons are removed if $\Delta R(l, j) < 0.4$, and photons are removed if $\Delta R(\gamma, l) < 0.4$ or $\Delta R(\gamma, j) < 0.4$. Finally, electron candidates are removed if shared ID tracks exist between a muon and an electron.

Events are required to satisfy $m_{\mathrm{T}}^{W} > 30$ GeV, where $m_{\mathrm{T}}^{W} = \sqrt{2 p_{\mathrm{T}}^{l} E_{\mathrm{T}}^{\mathrm{miss}} (1 - \cos\Delta\phi)}$ and $\Delta\phi$ is the azimuthal angle difference between the lepton and missing transverse momentum in the transverse plane, relative to the beam axis. In addition, to reject events that have topologies consistent with leptonic Z decays in which one charged lepton is reconstructed as a photon, the invariant mass of the lepton and the photon must satisfy $|m_{l\gamma} - m_Z| > 10$ GeV. To further remove events containing two prompt charged leptons consistent with a Z boson or two W bosons, events are rejected if a second lepton satisfying the following requirements is present: $p_{\mathrm{T}} > 7$ GeV, the lepton-specific pseudorapidity requirements, both track impact parameter requirements, and *loose* identification [34,35]. Finally, the two leading jets must have a rapidity difference $|\Delta y_{jj}| > 2$ and invariant mass $m_{jj} > 500$ GeV, which ensures a topology consistent with EW $W\gamma jj$ production.

The preceding selection criteria comprise the baseline selection. Baseline selected events are further divided into different signal and control regions, which differ depending on the purpose. The selection for the fiducial cross-section measurement of EW $W\gamma jj$ production divides the baseline region into a signal region, $\mathrm{SR}^{\mathrm{fid}}$, and a control region, $\mathrm{CR}^{\mathrm{fid}}$, by counting jets in the rapidity interval between the two leading jets, $N_{\mathrm{jets}}^{\mathrm{gap}}$. In EW $W\gamma jj$ events, the two leading jets are produced via an electroweak interaction and there is thus little hadronic activity between them; hence each event in $\mathrm{SR}^{\mathrm{fid}}$ is required to satisfy $N_{\mathrm{jets}}^{\mathrm{gap}} = 0$, and $\mathrm{CR}^{\mathrm{fid}}$ is defined by $N_{\mathrm{jets}}^{\mathrm{gap}} > 0$.

For the differential cross-section measurement, it is additionally required that events have $m_{jj} > 1$ TeV to enhance the EW $W\gamma jj$ signal purity; these events are then divided into three control regions ($\mathrm{CR_A}$, $\mathrm{CR_B}$, and $\mathrm{CR_C}$) and one signal region (SR). The centrality of the lepton-photon system relative to the VBS tagged jets, j_1 and j_2, is defined as $\xi_{l\gamma} = |(y_{l\gamma} - (y_{j_1} + y_{j_2})/2)/(y_{j_1} - y_{j_2})|$ and is used to form three control regions ($\mathrm{CR_A}$, $\mathrm{CR_B}$, and $\mathrm{CR_C}$) and one signal region (SR), where $y_{l\gamma}$ is the rapidity of the lepton-photon system. In EW $W\gamma jj$ events, the W boson and photon are generally produced centrally, between the two leading jets, and thus these events have low $\xi_{l\gamma}$. The variables $\xi_{l\gamma}$ and $N_{\mathrm{jets}}^{\mathrm{gap}}$ are chosen to define the four regions because they are uncorrelated. The SR is defined by requiring that there must be little hadronic activity in the region between the two leading jets and that the reconstructed $l\gamma$ system is produced centrally ($N_{\mathrm{jets}}^{\mathrm{gap}} = 0$, $\xi_{l\gamma} < 0.35$). The remaining three regions are control regions with small EW $W\gamma jj$ contribution, and are used to constrain the dominant background from strong $W\gamma jj$ production: $\mathrm{CR_A}$ ($N_{\mathrm{jets}}^{\mathrm{gap}} > 0$, $\xi_{l\gamma} < 0.35$), $\mathrm{CR_B}$ ($N_{\mathrm{jets}}^{\mathrm{gap}} > 0$, $0.35 < \xi_{l\gamma} < 1$), and $\mathrm{CR_C}$ ($N_{\mathrm{jets}}^{\mathrm{gap}} = 0$, $0.35 < \xi_{l\gamma} < 1$).

Table 1 Summary table for signal and control regions for the fiducial and differential cross-section measurements

Fiducial cross-section	SR^{fid} $N_{\text{jets}}^{\text{gap}} = 0$		CR^{fid} $N_{\text{jets}}^{\text{gap}} > 0$	
Differential cross-section	SR	CR_A	CR_B	CR_C
$m_{jj} > 1$ TeV	$N_{\text{jets}}^{\text{gap}} = 0$	$N_{\text{jets}}^{\text{gap}} > 0$	$N_{\text{jets}}^{\text{gap}} > 0$	$N_{\text{jets}}^{\text{gap}} = 0$
	$\xi_{l\gamma} < 0.35$	$\xi_{l\gamma} < 0.35$	$0.35 < \xi_{l\gamma} < 1$	$0.35 < \xi_{l\gamma} < 1$

Table 2 Expected number of events in the signal and control regions used for the fiducial cross-section measurement and observation of EW $W\gamma jj$ production. Statistical and systematic uncertainties estimated in Sect. 8 are included for each component. The number of observed events in each region are included for comparison. The "non-prompt" background category includes non-prompt photons and fake leptons

	SR^{fid} $\left(N_{\text{jets}}^{\text{gap}} = 0\right)$	CR^{fid} $\left(N_{\text{jets}}^{\text{gap}} > 0\right)$
EW $W\gamma jj$	520 ± 141	120 ± 49
Strong $W\gamma jj$	1550 ± 830	1970 ± 950
Non-prompt	692 ± 57	698 ± 58
Top quark processes	109 ± 18	183 ± 37
EW + strong $Z\gamma jj$	128 ± 34	163 ± 77
Total	3000 ± 830	3140 ± 960
Data	3341	3143

The signal and control region selection requirements for both the fiducial and differential cross-section measurements are summarised in Table 1.

Table 2 shows the number of signal and background events in SR^{fid} and CR^{fid}, after computing the data-driven backgrounds, as described in Sect. 5. The strong $W\gamma jj$ process accounts for 63% of the event yield in CR^{fid} and 52% in the SR^{fid}. The remaining prompt backgrounds, including top quark processes and EW and strong $Z\gamma jj$ processes, contribute 11% in CR^{fid} and 8% in SR^{fid}, while the non-prompt background fraction is 22% in CR^{fid} and 23% in SR^{fid}.

5 Background estimation

The main source of background arises from strong $W\gamma jj$ production. This background is estimated by using MC simulation and constrained using data in the control regions defined in Table 1; a detailed description of this procedure is provided in Sect. 6. Additional prompt backgrounds arise from $Z\gamma jj$ production and the production of one or more top quarks in association with photons. These prompt backgrounds are estimated by using MC simulations described in Sect. 3.

The largest non-prompt background arises primarily from W+jet production, where a jet is misidentified as a photon. This non-prompt photon background is estimated by using a data-driven template fit to the p_{T}-corrected photon isolation energy ($E_{\text{T}}^{\text{iso},\gamma} = E_{\text{T}}^{\text{cone40}} - 0.022 \times p_{\text{T}}$) distributions of prompt and non-prompt photons. The prompt photon template is determined from prompt photons in $W\gamma jj$ MC simulation. A control region enriched with non-prompt photons is defined by requiring photons to satisfy the *loose* identification criteria but fail to satisfy the selection criteria for at least one of four variables in the *tight* identification that define the photon shower shape. This selection is referred to as *LoosePrime4* [35]. The shape of the non-prompt photon template is extracted by parameterising the $E_{\text{T}}^{\text{iso},\gamma}$ distribution in this control region. Contributions from processes with prompt photons in the non-prompt photon control region are minimal but are accounted for with a systematic uncertainty of the background estimate. The fractions of prompt and non-prompt photons are extracted for each bin of each distribution using an unbinned, maximum-likelihood fit of the prompt and non-prompt templates to data. The extracted yields are verified using an "ABCD sideband method" [42] with the two dimensional plane defined by photon identification and isolation requirements. The dominant uncertainty in the non-prompt photon background is due to the choice of photon identification criteria used to define the non-prompt template regions. This non-prompt photon definition is varied by requiring photons to fail to satisfy at least one of two, three, or five shower shape selection variables used to define the tight identification [35], and the systematic uncertainty due to this identification choice varies from 4% to 16%. Other sources of systematic uncertainty arise from statistical uncertainties of the samples in the template and fit regions; prompt photon leakage into the non-prompt template regions, estimated from signal MC simulation; and the effect of photon isolation energy modelling uncertainties on the prompt photon templates.

A "fake factor" method is used to estimate the background from fake leptons: charged leptons arising from misreconstructed jets or in-flight decays of hadrons. The method defines *tight* leptons as those satisfying all selection criteria described in Sect. 4 and *non-tight* leptons as those failing to satisfy either the *tight* identification or *tight* isolation criteria. *Non-tight* leptons must still satisfy *loose* identification in addition to the identification and isolation requirements associated with the single lepton triggers. The fake factor is defined as the ratio of events with one *tight* lepton to those events with one *non-tight* lepton. It is calculated differentially in lepton p_{T} and η in a non-prompt control region

defined by exactly one lepton and at least one jet. Contributions from processes with prompt leptons are subtracted from the data prior to calculating the fake factor. The non-prompt lepton background is then determined in each bin of each measured distribution by applying the fake factor to prompt, background-subtracted data events that satisfy all the selection criteria except the *tight* lepton criteria. Sources of uncertainty arise from data and MC sample size in the control regions, relative fractions between heavy flavour decays and photon conversions, control region definitions for fake factor calculation, theoretical uncertainties of the prompt background, and the binning in p_{T}^{l} and η.

An electron can be misreconstructed as a converted photon ($e \to \gamma$) if the track reconstruction algorithm either fails to associate a B-layer hit to the track or associates a spurious conversion track to the electron. This background arises predominantly from Z+jets and $t\bar{t}$ processes, and the fake rate is determined using data by selecting candidate ee and $e\gamma$ events in a range of ± 20 GeV around the Z boson mass. The object selections for the electron and photon candidates satisfies the same criteria specified in Sect. 4. Compared with the analysis region selections described in Sect. 4, events must satisfy the following criteria: $E_{\mathrm{T}}^{\mathrm{miss}} < 20$ GeV, $m_{\mathrm{T}}^{W} < 20$ GeV, and there are no jet requirements. The ee and $e\gamma$ event yields are obtained by fitting a double-sided Crystal Ball function [43] to m_{ee} or $m_{e\gamma}$ to model the Z boson decay along with an exponential function to account for backgrounds. The ratio of $N_{e\gamma}/N_{ee}$ is parameterised as functions of electron p_{T} and η and applied to data events with $eejj$ and $e\mu jj$ final states, where one electron replaces the photon in the event selection, to estimate the $e \to \gamma$ background in electron and muon channels, respectively. Sources of systematic uncertainties for the $e \to \gamma$ fake rate arise from variations in the invariant mass fit range, varying the binning in p_{T} and η, and replacing the exponential background parameterisation with a fourth-order Bernstein polynomial [44].

No explicit requirement is imposed on the longitudinal position of the photon relative to the primary vertex, Δz_{γ}, as it is not well-measured for unconverted photons. As a result, a combinatorial background arises whereby a photon originating from one pp interaction is selected alongside a Wjj event from another pp interaction from the same bunch crossing. This pile-up photon background is estimated by using a data-driven method [45] that exploits the difference in Δz_{γ} between hard scatter and pile-up photons. Because the pile-up photon fraction, f_{PU}, is independent of the photon conversion status, events are selected if they contain a converted photon with two tracks and a conversion vertex with radius < 125 mm such that the conversion occurs within the pixel detector, allowing for an accurate measurement of Δz_{γ}. The sidebands of the Δz_{γ} distribution in background-subtracted data and $W\gamma jj$ simulation are used to estimate the fraction of events in each analysis region that have photons originating from a pile-up interaction. A control region dominated by pile-up photon background is defined by $|\Delta z_{\gamma}| > 50$ mm. Due to the limited number of events in this data control region, the statistical precision of f_{PU} is almost 90% while the systematic uncertainty is negligible compared with the statistical uncertainty. The pile-up background contains a component where a pile-up jet can be misidentified as a photon. The fraction of prompt photons is estimated by using inclusive prompt photon events obtained from data recorded using single photon triggers, and f_{PU} is then multiplied by this fraction. The estimated f_{PU} is $(1.7 \pm 1.6)\%$ in $\mathrm{SR}^{\mathrm{fid}}$ and $(0.45 \pm 0.39)\%$ in $\mathrm{CR}^{\mathrm{fid}}$; it is neglected for the differential cross-section measurement due to the limited number of events in the control region of pile-up photons arising from the additional requirement of $m_{jj} > 1$ TeV. The procedure to extract the EW $W\gamma jj$ fiducial cross-section is repeated without the pile-up photon background, and the uncertainty on the fiducial cross-section is unchanged.

6 Signal extraction

6.1 Signal extraction for observation

A neural network (NN) is used to classify signal and background processes. The NN is trained on the EW $W\gamma jj$ process as the signal model and the sum of strong $W\gamma jj$, $Z\gamma jj$, and top quark processes as the background model, which are weighted according to their cross-sections. All events used in the training satisfy the signal region $\mathrm{SR}^{\mathrm{fid}}$ selection described in Sect. 4. Two NN classifiers are created after training on two statistically independent but otherwise identical samples. A binary cross-entropy loss function is used during the training and the loss for each event is weighted by its weight. The NN consists of a batch normalisation layer followed by three densely connected hidden layers of 512 nodes each. Each hidden node uses a LeakyRelu activation function [46]. The last hidden layer is densely connected with the output layer that uses a sigmoid activation function. The model is trained with the Adam learning rate optimiser [47] with an initial learning rate of 3×10^{-5}. The NN is trained to discriminate signal from background using 13 kinematic observables. These 13 observables, ranked according to importance, consist of the lepton-photon centrality, $\xi_{l\gamma}$; pseudorapidity difference between the two jets, $\Delta\eta_{jj}$; angular distance between the lepton-photon system and the dijet system, $\Delta R(l\gamma, jj)$; p_{T}^{γ}; p_{T}^{l}; photon centrality, ξ_{γ}; angular distance between leading jet and photon, $\Delta R(j_{\mathrm{lead}}, \gamma)$; angular distance between lepton and photon, $\Delta R(l, \gamma)$; transverse momentum of the lepton-photon system, $p_{\mathrm{T}}^{l\gamma}$; azimuthal angle difference between the lepton-photon and the dijet system, $\Delta\phi(l\gamma, jj)$; m_{T}^{W}; leading jet

transverse momentum, $p_{\mathrm{T}}^{j_{\mathrm{lead}}}$; and $\eta_{j_{\mathrm{lead}}}$. The optimal hyperparameters are determined using a grid search by repeating the training with different combinations of the number of hidden layers, number of nodes, and learning rate; the model architecture with the lowest loss on test data is chosen. The NN trained on one statistically independent sample is applied to the other for evaluation. No significant differences between the two NNs are found, and thus the average value of the two NN output scores is used for data and data-driven background events.

A profile likelihood fit to the NN score in the $\mathrm{SR}^{\mathrm{fid}}$ and $\mathrm{CR}^{\mathrm{fid}}$ region is performed simultaneously to maximise the likelihood for observing n^{data} events given the number of predicted events. The expected number of events depends on two floating normalisation factors: μ_{strong} for strong $W\gamma jj$ and μ_{EW} as the EW $W\gamma jj$ signal strength. The likelihood function $\mathcal{L}$ can be written in a simplified form as the product of Poisson distributions multiplied by the product of Gaussian constraints,

$$\mathcal{L} = \prod_r \prod_i P(n_{r,i}^{\mathrm{data}} | \mu_{\mathrm{EW}} S_{r,i}(\boldsymbol{\theta}) + B_{r,i}(\mu_{\mathrm{strong}}, \boldsymbol{\theta})) \times \prod_j G(\theta_j), \quad (1)$$

where r is either $\mathrm{SR}^{\mathrm{fid}}$ or $\mathrm{CR}^{\mathrm{fid}}$, i represents the bin number of the NN score in region r, $\boldsymbol{\theta}$ refers to nuisance parameters constrained by the Gaussian term $G(\theta_j)$ for each systematic uncertainty source j, $S_{r,i}(\boldsymbol{\theta})$ is the number of predicted events from EW $W\gamma jj$ simulation, and $B_{r,i}(\boldsymbol{\theta})$ is the number of background events.

The shape of the NN score for EW $W\gamma jj$ and strong $W\gamma jj$ is taken from the corresponding MC while the normalisation for each process is floated, namely, μ_{EW} and μ_{strong}, respectively. The other backgrounds are allowed to vary within their respective uncertainties. The EW $W\gamma jj$ measurement depends on a set of nuisance parameters that represent the impact of uncertainties on the fit; these uncertainties are discussed in Sect. 8. The observed significance is evaluated by performing a background-only simultaneous fit to data in $\mathrm{SR}^{\mathrm{fid}}$ and $\mathrm{CR}^{\mathrm{fid}}$ to estimate the probability of rejecting the background-only hypothesis. The signal region was blinded when analysis decisions and optimisations were made to avoid biasing the measurement.

Figure 2 shows the top three ranked observables of the NN in the signal region with the values of nuisance parameters and normalisation factors obtained from the fit of the NN score distributions to templates in different variables results and Fig. 3 shows the output NN score in $\mathrm{SR}^{\mathrm{fid}}$ and $\mathrm{CR}^{\mathrm{fid}}$ after performing the profile likelihood fit in the corresponding observables. Good agreement with the observed data is seen in both the regions except for the slight shape difference in $\xi_{l\gamma}$ between MC and data. Instead of injecting the nuisance parameter from the fit to the NN score, the maximum-likelihood fit was performed to $\xi_{l\gamma}$ directly to obtain the nuisance parameters, resulting in excellent agreement between MC and data after the fit. Therefore the maximum-likelihood fit has sufficient flexibility to give reliable results despite mismodelling between MC and data before the fit.

6.2 Signal extraction for the differential cross-section measurement

The EW $W\gamma jj$ event yields are also extracted differentially as functions of m_{jj}, p_T^{jj}, $\Delta\phi_{jj}$, p_{T}^{l}, $m_{l\gamma}$, and $\Delta\phi_{l\gamma}$ using the methodology documented in Ref. [48]. This method exploits signal and control regions in a binned log-likelihood fit [49,50], which are used to constrain both the shape and normalisation of the strong $W\gamma jj$ background. The data are split into four regions (SR, $\mathrm{CR_A}$, $\mathrm{CR_B}$, and $\mathrm{CR_C}$) by imposing the selection criteria for $\xi_{l\gamma}$ and $N_{\mathrm{jets}}^{\mathrm{gap}}$ defined in Table 1 in Sect. 4. The variables $\xi_{l\gamma}$ and $N_{\mathrm{jets}}^{\mathrm{gap}}$ are uncorrelated, and are thus chosen to define these four regions. The EW $W\gamma jj$ event is produced centrally and has little hadronic activity in between the forward and backward jets, hence each event in the SR is required to satisfy $N_{\mathrm{jets}}^{\mathrm{gap}} = 0$ and $\xi_{l\gamma} < 0.35$. The control regions are deficient in EW $W\gamma jj$, and are defined by inverting the requirement on either $\xi_{l\gamma}$ or $N_{\mathrm{jets}}^{\mathrm{gap}}$.

The binned log likelihood is defined as:

$$\ln \mathcal{L} = -\sum_{r,i} \nu_{ri}^{s} + \sum_{r,i} N_{ri}^{\mathrm{data}} \ln \nu_{ri}^{s},$$

where r corresponds to one of the four regions SR, $\mathrm{CR_A}$, $\mathrm{CR_B}$, and $\mathrm{CR_C}$, i corresponds to the bin of the kinematic observable, N_{ri}^{data} corresponds to the data yield in bin i of region r, and ν_{ri}^{s} corresponds to the prediction that relies on the s sources of experimental systematic uncertainty.

The fitted number of events in region r and bin i is expressed as

$$\nu_{ri} = \mu_{\mathrm{EW},i}\, \nu_{ri}^{\mathrm{EW,MC}} + \nu_{ri}^{\mathrm{strong}} + \nu_{ri}^{\mathrm{other,bkg}}, \quad (2)$$

where $\mu_{\mathrm{EW},i}$ is the signal strength of EW $W\gamma jj$ in bin i, and $\nu_{ri}^{\mathrm{EW,MC}}$ and $\nu_{ri}^{\mathrm{other,bkg}}$ correspond to the EW $W\gamma jj$ prediction and contributions from reducible background processes, respectively. The strong $W\gamma jj$ prediction is constrained using the signal-suppressed control regions based on the following four relations:

$$\begin{aligned} \nu_{\mathrm{CR_A},i}^{\mathrm{strong}} &= b_{\mathrm{L},i}\, \nu_{\mathrm{CR_A},i}^{\mathrm{strong,MC}}, & \nu_{\mathrm{CR_B},i}^{\mathrm{strong}} &= b_{\mathrm{H},i}\, \nu_{\mathrm{CR_B},i}^{\mathrm{strong,MC}}, \\ \nu_{\mathrm{SR},i}^{\mathrm{strong}} &= b_{\mathrm{L},i}\, c\, \nu_{\mathrm{SR},i}^{\mathrm{strong,MC}}, \text{ and } & \nu_{\mathrm{CR_C},i}^{\mathrm{strong}} &= b_{\mathrm{H},i}\, c\, \nu_{\mathrm{CR_C},i}^{\mathrm{strong,MC}}. \end{aligned} \quad (3)$$

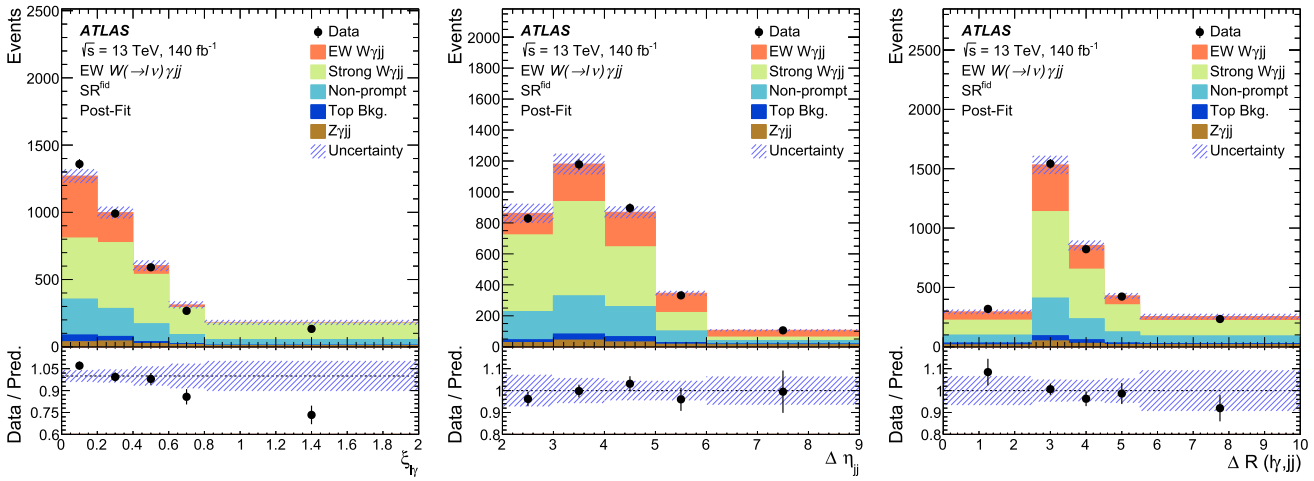

(a) (b) (c)

Fig. 2 Distributions of the predicted and observed yields for the three highest ranked variables in the NN after performing the profile likelihood fit, as functions of **a** $\xi_{l\gamma}$, **b** $\Delta\eta_{jj}$, and **c** $\Delta R(l\gamma, jj)$. The observed data is represented by solid circles and the associated vertical error bar represents the statistical uncertainty of the data. The predicted yields comprise simulated EW $W\gamma jj$ signal, backgrounds from non-prompt photons and leptons that are estimated by using data-driven methods, and backgrounds that are estimated with simulation. The hashed band represents the quadrature sum of the statistical and systematic uncertainties

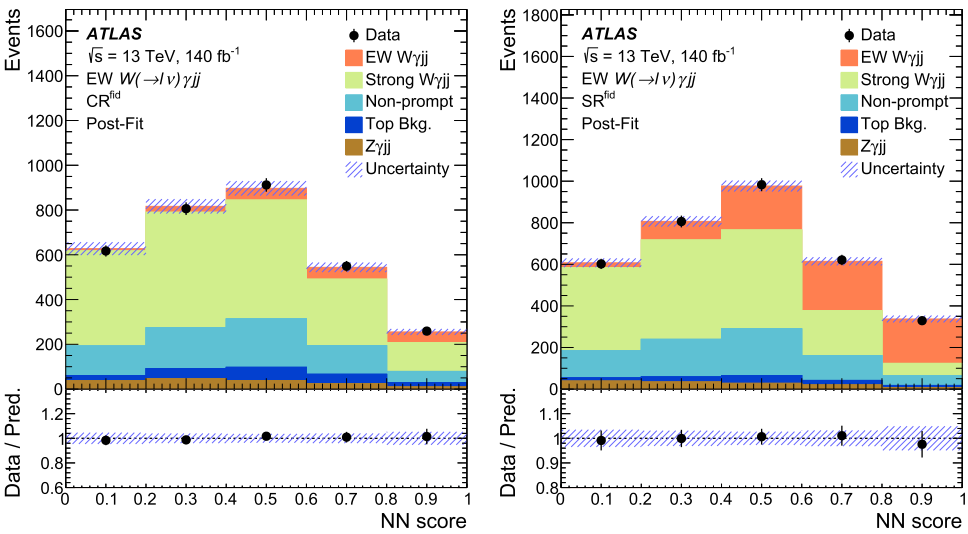

(a) (b)

Fig. 3 Distribution of the predicted and observed yields as a function of the NN score in the CR^{fid} (**a**) and SR^{fid} (**b**) regions after performing the profile likelihood fit. Data is represented by solid circles, and the associated vertical error bar represents the statistical uncertainty on the data. The predicted yields comprise simulated EW $W\gamma jj$ signal, backgrounds from non-prompt photons and leptons that are estimated by using data-driven methods, and backgrounds that are estimated with simulation. The hashed band represents the quadrature sum of the statistical and systematic uncertainties

The parameters $b_{\mathrm{L},i}$ and $b_{\mathrm{H},i}$ are sets of bin-dependent free parameters that correspond to the $\xi_{l\gamma} < 0.35$ and $\xi_{l\gamma} > 0.35$ regions, respectively. The low-$\xi_{l\gamma}$ parameter, $b_{\mathrm{L},i}$, is primarily constrained by $\mathrm{CR_A}$, while $b_{\mathrm{H},i}$ is primarily constrained by $\mathrm{CR_B}$. These two sets of parameters introduce additional degrees of freedom to the predicted strong $W\gamma jj$ event yield to allow the fitted number of strong $W\gamma jj$ events to be more consistent with the observed data. A floating parameter c is used to provide a residual correction that can account for any mismodelling across $N_{\mathrm{jets}}^{\mathrm{gap}}$. This configuration is less prone to fit instabilities coming from the limited number of observed events than is the two-parameter linear fit of Ref. [48].

For each bin i, the binned maximum-likelihood fit consists of the following free parameters: the signal strength $\mu_{\mathrm{EW},i}$, the free parameter c, and the $b_{\mathrm{L},i}$ and $b_{\mathrm{H},i}$ corrections to the strong $W\gamma jj$ process. This constitutes an overall number of $3 \times N_{\mathrm{bins}} + 1$ parameters that are constrained by the $4 \times N_{\mathrm{bins}}$ measurements in data, where N_{bins} corresponds to the number of bins in the measurement of the differential observable.

The alternative predictions for EW $W\gamma jj$ and strong $W\gamma jj$ introduced in Sect. 3 are used to assess the systematic uncertainties discussed in Sect. 8. The statistical uncertainty arising from the limited size of the data and simulated MC samples is evaluated using the bootstrap method [51],

each with 10 000 toy experiments. The signal extraction is repeated for each toy experiment, where the event yields in each bin of the signal and control regions are sampled according to a Poisson distribution. The mean and RMS of the extracted event yields among these toy experiments are used to define the extracted EW $W\gamma jj$ yield and associated statistical uncertainty. Each source of systematic uncertainty is varied and applied to the templates coherently in each region and propagated through the fit. The theory uncertainties due to QCD scales, PDFs, and α_S are evaluated following the procedures discussed in Sect. 8.

Figure 4 shows the pre- and post-fit agreement between data and predicted yields as functions of m_{jj} in SR, $\mathrm{CR_A}$, $\mathrm{CR_B}$, and $\mathrm{CR_C}$. The floating parameter c ranges from 1.06 to 1.22 depending on the observable while the overall scaling factor for strong $W\gamma jj$ ($b_{\mathrm{L},i}\, c$) ranges between 1.07 and 1.39. Good post-fit agreement between the predicted yields and data is observed in all four regions. The pre-fit systematic uncertainties presented on the figures are estimated as documented in Sect. 8. The three control regions allow for a constraint of the systematic uncertainties, in particular the strong $W\gamma jj$ modelling uncertainties.

The differential EW $W\gamma jj$ signal extraction method is validated with two procedures. In the first cross-check, a different choice of control regions for the strong $W\gamma jj$ process is assigned in Eq. (3), where $b_{\mathrm{L},i}$ and $b_{\mathrm{H},i}$ instead link the strong background yields at same $N_{\mathrm{jets}}^{\mathrm{gap}}$ values, and are thus constrained at high $\xi_{l\gamma}$, and the free parameter c provides residual corrections considering the mismodelling across $\xi_{l\gamma}$. In the second method, the data-driven corrections to the strong $W\gamma jj$ contributions are derived only in either $\mathrm{CR_A}$ or $\mathrm{CR_C}$. The extracted EW $W\gamma jj$ event yields obtained using each of these two methods are consistent with the nominal results.

7 Correction for detector effects

The fiducial and differential cross-sections at particle level are obtained by correcting the reconstruction-level EW $W\gamma jj$ event yield for the detector effects of inefficiency and resolution.

The particle-level regions are defined using all final-state stable particles with a mean lifetime of $c\tau > 10$ mm. To reduce model-dependence associated with extrapolations across phase space, the particle-level selection is defined to mimic the detector-level event selection described in Sect. 4. Particle-level dressed leptons are formed by combining the four momenta of each prompt electron or muon with the prompt photons that lie within $\Delta R = 0.1$ of the prompt lepton excluding electrons or muons from tau decays. Events must contain exactly one dressed lepton with $p_{\mathrm{T}} > 30$ GeV. Leptons are required to fall within the same detector acceptance as the reconstruction level, with muons satisfying $|\eta| < 2.5$ and electrons satisfying $|\eta| < 2.47$ excluding the region $1.37 < |\eta| < 1.52$. Events must contain at least one prompt photon with $p_{\mathrm{T}} > 22$ GeV and $|\eta| < 2.37$, excluding the region $1.37 < |\eta| < 1.52$. At particle level, the photon isolation energy, $E_{\mathrm{T}}^{\mathrm{iso}}$ is defined as the sum of the transverse energy of stable particles within a cone of $\Delta R = 0.4$ around the prompt photon, excluding the photon itself and neutrinos. To minimise the model dependence, SHERPA EW $W\gamma jj$ simulation is used to determine a particle-level photon isolation requirement that best mimics the detector-level behaviour; particle-level photons must satisfy $E_{\mathrm{T}}^{\mathrm{iso}} < 0.2E_{\mathrm{T}}^{\gamma}$. Jets are reconstructed with the anti-k_t algorithm using all final-state particles as input except the dressed lepton and prompt neutrinos. Events are required to contain zero jets that fall within $\Delta R = 0.4$ around a b-hadron, and must contain at least two jets with $p_{\mathrm{T}} > 50$ GeV and $|\eta| < 4.4$. The particle-level missing transverse momentum, defined as the vector sum of the transverse momenta of all non-interacting, final-state stable particles, must satisfy $E_{\mathrm{T}}^{\mathrm{miss}} > 30$ GeV. These leptons, jets, and photons are then selected in a VBS topology by using the same requirements as the reconstruction-level selection, which are listed in Table 3. The particle-level phase space definition is slightly different for the fiducial and differential cross-section measurements to ensure the definitions are as close as possible to the signal extraction method at reconstruction level.

The integrated fiducial cross-section, $\sigma_{\mathrm{EW}\ W\gamma jj}^{\mathrm{fid}}$, is defined as:

$$\sigma_{\mathrm{EW}\ W\gamma jj}^{\mathrm{fid}} = \frac{N_{\mathrm{EW}\ W\gamma jj}}{L \cdot C_{\mathrm{EW}\ W\gamma jj}}, \tag{4}$$

where $N_{\mathrm{EW}\ W\gamma jj}$ is the number of extracted EW $W\gamma jj$ events after performing the fit described in Sect. 6.1, L is the integrated luminosity, and $C_{\mathrm{EW}\ W\gamma jj}$ is the correction factor estimated by using the EW $W\gamma jj$ MC. The statistical uncertainty due to the limited size of data and simulation samples are propagated through Eq. (4), along with each source of systematic uncertainty affecting $N_{\mathrm{EW}\ W\gamma jj}$ and $C_{\mathrm{EW}\ W\gamma jj}$, which are treated as fully correlated.

For the differential cross-section measurement each distribution is unfolded using an iterative Bayesian method with two iterations [52,53]. The binnings of the observables are optimised to ensure the relative statistical precision of the extracted EW $W\gamma jj$ event yield is similar across bins using an Asimov dataset [54] formed by the $W\gamma$ and non-$W\gamma$ simulation samples. The binning for each observable is optimised using the EW $W\gamma jj$ and strong $W\gamma jj$ simulation samples, such that a similar statistical precision is obtained for each bin of the extracted yield. An additional requirement that the bin width is not smaller than twice the resolution of the observable is enforced. The number of iterations are determined by minimising the quadrature sum of the bias and the statistical uncertainty due to unfolding, where the bias is estimated by

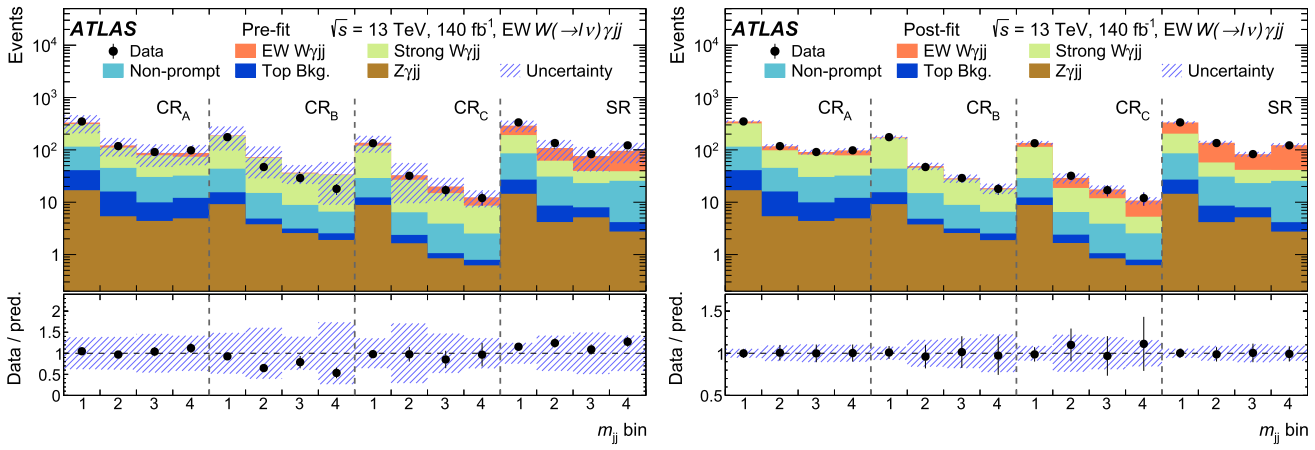

Fig. 4 Distribution of the observed and predicted yields as a function of m_{jj} in the SR, CR_A, CR_B, and CR_C regions, both **a** pre-fit and **b** post-fit. Data is represented by solid circles, and the associated vertical error bar represents the statistical uncertainty of the data. The predicted yields comprise simulated EW $W\gamma jj$ signal, backgrounds from non-prompt photons and leptons that are estimated by using data-driven methods, and backgrounds that are estimated with simulation. The hashed band represents the quadrature sum of the statistical and systematic uncertainties, which are constrained in the fit. The bin edges are (1, 1.4, 1.7, 2,1, 5.3) TeV

Table 3 Particle-level definition for the fiducial and differential EW $W\gamma jj$ measurement

Object	Selection requirements
Dressed muons	$p_{\mathrm{T}} > 30$ GeV and $\lvert\eta\rvert < 2.5$
Dressed electrons	$p_{\mathrm{T}} > 30$ GeV and $\lvert\eta\rvert < 2.47$ (excluding $1.37 < \lvert\eta\rvert < 1.52$)
Isolated photons	$E_{\mathrm{T}}^{\gamma} > 22$ GeV and $\lvert\eta\rvert < 2.37$ (excluding $1.37 < \lvert\eta\rvert < 1.52$) and $E_{\mathrm{T}}^{\mathrm{iso}} < 0.2E_{\mathrm{T}}^{\gamma}$
Jets	At least two jets with $p_{\mathrm{T}} > 50$ GeV and $\lvert y\rvert < 4.4$, $b-$jet veto
Missing transverse momentum	$E_{\mathrm{T}}^{\mathrm{miss}} > 30$ GeV and $m_{\mathrm{T}}^{W} > 30$ GeV
VBS topology	$N_{\ell} = 1$, $N_{\gamma} \geq 1$, $\lvert m_{\ell\gamma} - m_Z\rvert > 10$ GeV
	$\Delta R_{\mathrm{min}}(\ell, j) > 0.4$, $\Delta R_{\mathrm{min}}(\gamma, j) > 0.4$, $\Delta R_{\mathrm{min}}(\ell, \gamma) > 0.4$
	$\Delta R_{\mathrm{min}}(j_1, j_2) > 0.4$, $\Delta\phi_{\mathrm{min}}(E_{\mathrm{T}}^{\mathrm{miss}}, j) > 0.4$
	$N_{\mathrm{jets}} \geq 2$, $p_{\mathrm{T}}^{j1}, p_{\mathrm{T}}^{j2} > 50$ GeV
	$m_{jj} > 500$ GeV, $\lvert\Delta y_{jj}\rvert > 2$
Fiducial measurement	VBS topology
Differential measurement	VBS topology $\oplus$ ($m_{jj} > 1000$ GeV, $N_{\mathrm{jets}}^{\mathrm{gap}} = 0$, and $\xi_{W\gamma} < 0.35$)

comparing the unfolded distribution after a certain number of iterations to the true distribution in the EW $W\gamma jj$ simulation. The value and statistical uncertainty on the fiducial EW $W\gamma jj$ cross-section are derived from the mean and root mean square (RMS) of the 10 000 toy experiments described in Sect. 6.2, propagated through the unfolding. These modified distributions and response matrices are then used to repeat the unfolding procedure for each toy experiment. The statistical uncertainty in each bin corresponds to the standard deviation of the unfolded results from the ensemble of 10 000 toy experiments. Systematic uncertainties that affect both the signal extraction and the unfolding are treated as correlated and propagated through the unfolding to the final results.

8 Systematic uncertainties

Experimental sources of systematic uncertainty arise from the reconstruction and energy calibration of objects including charged leptons, photons, jets, heavy-flavour tagging of jets, and missing transverse momentum. These uncertainties affect both the normalisation and shape of the simulated background processes, the shape of the simulated EW $W\gamma jj$ process in the signal extraction, and the normalisation and shape of simulations used to unfold the inclusive and differential cross-sections of the EW $W\gamma jj$ process.

The lepton trigger efficiencies and lepton and photon reconstruction, identification, and isolation efficiencies in simulations are corrected using scale factors derived from

data, as described in Sect. 4. Systematic uncertainties due to this procedure are evaluated by varying the scale factors based on their associated uncertainties [34,35]. Uncertainties arising from differences between simulation and data in the reconstructed lepton (photon) momentum are evaluated by scaling and smearing the lepton (photon) transverse momentum.

Jets are calibrated using a combination of MC-based and data-driven corrections [55]. Uncertainties in the measurements due to uncertainties in the jet energy scale and resolution corrections are evaluated by scaling and smearing the jet four-momentum in the simulation by the uncertainties associated with each of these corrections. Uncertainties arising from the imperfect modelling of the JVT in the simulation are estimated by varying the JVT requirement. Furthermore, uncertainties arising from differences between simulation and data in b-jet tagging efficiencies are estimated by varying the associated scale factors [40].

Uncertainties from the $E_{\mathrm{T}}^{\mathrm{miss}}$ measurement are estimated by propagating the uncertainties in the transverse momenta of hard physics objects and by applying uncertainties associated with momentum scale and resolution to the track-based term [41].

Additional sources of experimental uncertainty arise due to the modelling of pile-up and the luminosity determination. The uncertainty in the combined 2015–2018 integrated luminosity is 0.83% [29], obtained using the LUCID-2 detector [11] for the primary luminosity measurements, complemented by measurements using the inner detector and calorimeters.

For the EW $W\gamma jj$ fiducial cross-section measurement, each source of experimental systematic uncertainty is introduced as a nuisance parameter using a Gaussian constraint in the likelihood, as described in Sect. 6.1. For the differential signal extraction, 10 000 pseudo-experiments are constructed for simulated MC samples, where each pseudo-experiment samples each simulated MC event with a unit-mean Poisson distribution. For data, in each experiment the number of data events in each bin is determined by sampling a Poisson distribution of mean equal to the nominal bin content. When evaluating the statistical significance of the systematic uncertainties, the distribution of Poisson fluctuations is the same in the nominal as that in the systematic variations. The EW $W\gamma jj$ yield is extracted for each pseudo-experiment, and the effect of the systematic uncertainty on the yield is calculated as the mean of the distribution of differences between the varied and nominal for each pseudo-experiment. The statistical significance of each experimental systematic uncertainty is evaluated by computing the RMS of the distribution of differences between the varied and nominal pseudo-experiments. A smoothing procedure is applied to reduce bin-to-bin statistical fluctuations such that the difference between uncertainties with or without smoothing is statistically insignificant. All experimental systematic uncertainties are treated as correlated among processes and regions. For both the inclusive and differential cross-sections, the dominant experimental systematic uncertainties arise from the calibration of jets and modelling of pile-up conditions, resulting in approximately 4% uncertainty in the inclusive cross-section and 5–9% uncertainty in the differential measurements.

Theoretical uncertainties are accounted for from all simulated signal and background processes that affect the EW $W\gamma jj$ signal extraction. Each source of theoretical uncertainty is estimated by repeating the signal extraction and unfolding procedure with an uncertainty variation applied and propagating this through the unfolded measurements. Theoretical uncertainties arise due to higher-order QCD corrections, the PDFs used in the simulations, the accuracy of the strong coupling constant α_{S}, and the choice of event generators. The effects of higher-order QCD corrections are estimated by varying each of the renormalisation (μ_R) and factorisation (μ_F) scales by a factor of two with $0.5 \leq \mu_F/\mu_R \leq 2.0$. Uncertainties due to the PDFs are evaluated by varying each Hessian eigenvector of the nominal NNPDF3.0NNLO set and comparing results obtained from nominal PDFs to alternative PDFs such as NNPDF3.1NNLO [56], CT18NNLO [57], MSHT2020NNLO [58], and PDF4LHC15NNLO [59]. If the difference between the nominal PDF and alternative PDF is not covered by the quadrature sum of the eigenvector changes in NNPDF3.0NNLO, an additional uncertainty is assigned. The uncertainty due to α_{S} is evaluated with the nominal PDF by varying the nominal $\alpha_{\mathrm{S}} = 0.118$ by ± 0.001. For the EW $W\gamma jj$ signal extraction, the systematic uncertainty arising from the choice of event generator for the strong $W\gamma jj$ and EW $W\gamma jj$ processes is estimated using the symmetrised envelope formed by the difference between the extracted event yield between the nominal generator, SHERPA, and the alternative generator, MADGRAPH5+PYTHIA8. For the differential cross-section measurement, the choice of event generator is extracted using the same method as with the experimental systematic uncertainties.

Treatment of the theory uncertainties is briefly discussed here. For the fiducial cross-section measurement, the QCD scale uncertainties are treated as uncorrelated between signal and control regions, because it is a conservative approach in this case as the QCD scales are varied separately instead of simultaneously in these two regions. The PDF and α_{S} uncertainties are treated as correlated between regions but kept uncorrelated between different processes. Unlike the decorrelation of theory uncertainties across regions for the fiducial cross-section measurement of EW $W\gamma jj$, this treatment of theory uncertainties is not necessary for the differential cross-section measurement for two reasons: first, the differential cross-section is measured in each bin of the observable using the fit described above, hence the theory uncertainties are

Table 4 Impact of uncertainties on the measured fiducial cross-section. Squared values of impacts are obtained by fixing a set of nuisance parameters of the uncertainty sources corresponding to the category to the best-fit values, then calculating the difference between the squares of the resulting uncertainty from the total uncertainty of the nominal fit

Uncertainty source	Fractional uncertainty (%)
MC statistics	11
Jets	8
Lepton, photon, pile-up	8
EW $W\gamma jj$ modelling	7
Data statistics	6
Strong $W\gamma jj$ modelling	6
Non-prompt background	2
Luminosity	2
Other background modelling	2
$E_{\mathrm{T}}^{\mathrm{miss}}$	1

decorrelated between bins of observables; and second, correlations of QCD scale variations across $N_{\mathrm{jets}}^{\mathrm{gap}}$ are taken into account by the floating parameter c in Eq. (3) in Sect. 6.2 such that only the uncertainties in c are required.

Systematic uncertainties related to the unfolding procedure in the differential cross-section measurements are evaluated as follows. First, the EW $W\gamma jj$ process simulated with the alternative generator, MadGraph, is used to extract the EW $W\gamma jj$ signal and unfold the data. The difference from the nominal result is applied as a systematic uncertainty on the unfolded EW $W\gamma jj$ distributions. Second, 10 000 truth toy experiments are generated for the particle-level distribution according to a Gaussian distribution with mean equal to the value of the corresponding bin and RMS equal to the statistical uncertainty of the bin. The nominal response matrix is then applied to the particle-level distribution from each toy experiment to create a reconstruction-level pseudo-dataset, which is then unfolded with the nominal response matrix to produce an unfolded pseudo-dataset. The difference in the observable distribution between the truth toy experiment and the unfolded pseudo-dataset constitutes a systematic uncertainty on the unfolded result.

Table 4 shows the impact of the statistical and systematic uncertainties on the fiducial and differential cross-section measurement. The precision of the fiducial cross-section is limited by the statistical precision of the sample followed by the modelling uncertainties, and the largest experimental uncertainties arise from uncertainties in the jet energy scale and jet energy resolution of reconstructed jets. Figure 5 shows the fractional systematic uncertainties as functions of m_{jj} and p_{T}^{l}. The uncertainties in the differential measurement are mostly dominated by the systematic variations arising from strong $W\gamma jj$ and EW $W\gamma jj$ modelling and the impact of the jet energy scale and resolution uncertainties, for distributions including jets.

9 Results

9.1 Observation and fiducial cross-section for EW $W\gamma jj$ process

The measured signal strength, μ_{EW}, is 1.5 ± 0.5. This includes a significant modelling uncertainty on the prediction of the fiducial cross-section due to the difference in cross-section prediction between Sherpa and MadGraph5+Pythia8, which can be seen in Fig. 6. The observed significance is determined using a likelihood ratio test, and is calculated to be above six standard deviations, compared with an expected significance of 6.3σ. The significance is obtained using the central value of the Sherpa prediction for the SM EW $W\gamma jj$ signal. The large normalisation uncertainty on the predicted cross-section does not impact the calculation of the signal significance.

The measured EW $W\gamma jj$ fiducial cross-section in the phase space defined in Sect. 7 is determined to be $\sigma_{\mathrm{EW}} = 13.2 \pm 2.5$ fb. The difference in fractional uncertainty between μ_{EW} and σ_{EW} is due to a large normalisation component of the signal modelling uncertainty from the choice of event generator. These predictions from Sherpa and MadGraph5+Pythia8 are compared with the measured fiducial cross-section in Fig. 6. The MadGraph5+Pythia8 prediction is in agreement with the data within uncertainties while Sherpa underestimates the data within two standard deviations. The theoretical uncertainties in the predicted cross-sections include systematic uncertainties from the QCD scales, PDFs, and α_S variations. The difference between the predicted cross-section between MadGraph5+Pythia8 and Sherpa arises due to the third parton included in the matrix element of Sherpa [60].

9.2 Differential cross-section for EW $W\gamma jj$ process

Figure 7 shows the differential cross-sections for EW $W\gamma jj$ production as functions of m_{jj}, p_{T}^{jj}, $\Delta\phi_{jj}$, p_{T}^{l}, $m_{l\gamma}$, and $\Delta\phi_{l\gamma}$. The predictions from both MadGraph5+Pythia8 and Sherpa are in agreement with the data within uncertainties.

The presence of anomalous quartic gauge coupling can modify the distributions of these observables at the tails of m_{jj}, p_{T}^{jj}, p_{T}^{l} or $m_{l\gamma}$. This is investigated further in Sect. 10. Enhancement of CP violation of Higgs and gauge boson couplings in the diboson sector may distort the shape of $\Delta\phi_{jj}$ and $\Delta\phi_{l\gamma}$, thus the measurements of these two observables can be used to constrain the presence of CP-odd contributions to the EW $W\gamma jj$ process.

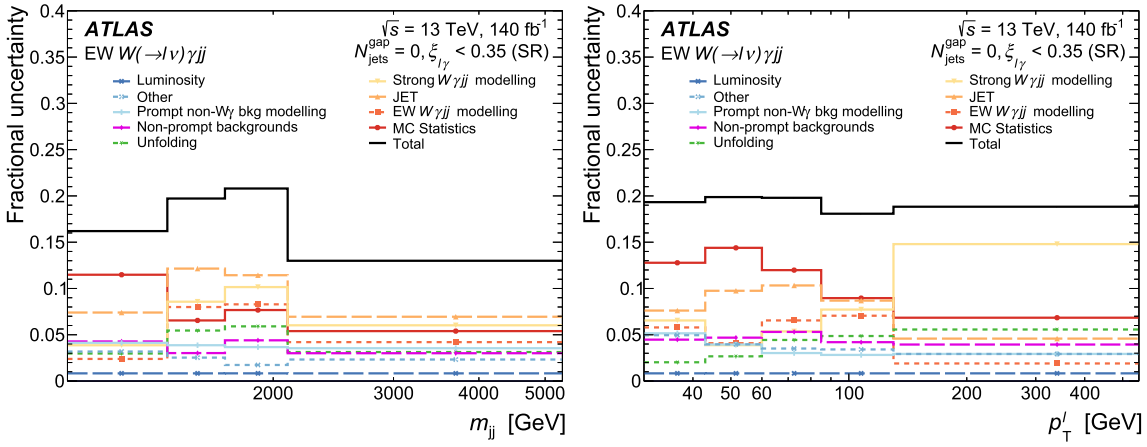

Fig. 5 Fractional uncertainty in the EW $W\gamma jj$ measurement as functions of m_{jj} and p_{T}^{l}. Uncertainties are grouped in categories that are added in quadrature to give total uncertainties. Systematic uncertainties due to reconstruction of leptons, photons, pile-up, and heavy-flavour jets are grouped in the category "Other"

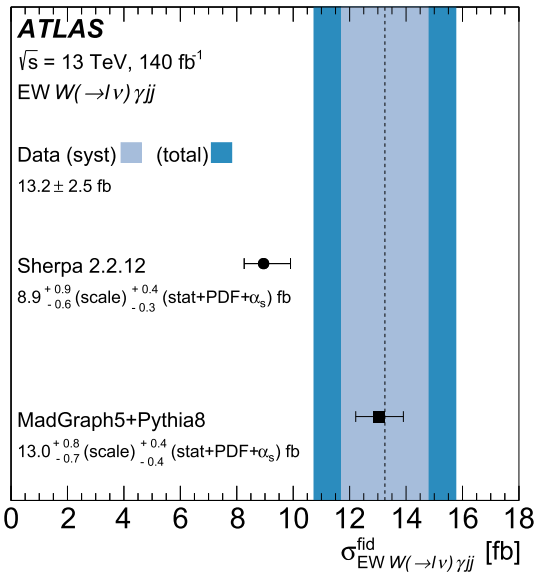

Fig. 6 The measured EW $W\gamma jj$ fiducial cross-section compared with the predictions of SHERPA and MADGRAPH5+PYTHIA8. The central value of the measured fiducial cross-section is represented by a dashed vertical line. The light shaded band represents the total uncertainty on the measured fiducial cross-section, while the darker shaded band represents the systematic uncertainty. Each MC prediction is represented with a solid circle, and the associated horizontal error bars correspond to the quadrature sum of statistical uncertainties and theoretical uncertainties. The impacts of various sources of systematic and theoretical modelling uncertainties in the fiducial cross-section are shown in Table 4

10 EFT interpretation

The differential cross-section measurements presented in Sect. 9 are used to constrain dimension-8 (D-8) operators [2]. These operators are implemented in the Éboli model including twenty independent, charge-conjugation and parity conserving D-8 operators that can change the QGCs. The measured distributions for the six observables are sensitive to sixteen D-8 operators and the most stringent limits from interpretations of these distributions are reported.

The effective Lagrangian, $\mathcal{L}_{\mathrm{eff}}$, including aQGCs represented by the higher dimension operators and the corresponding Wilson coefficients, is given by:

$$\mathcal{L}_{\mathrm{eff}} = \mathcal{L}_{\mathrm{SM}} + \sum_{j} \frac{f_j^{(8)}}{\Lambda^4} O_j^{(8)}, \tag{5}$$

where $\mathcal{L}_{\mathrm{SM}}$ is the SM Lagrangian, $O_i^{(8)}$ correspond to D-8 operators with dimensionless couplings $f_j^{(8)}$ (Wilson coefficients), and Λ is the energy scale of new physics. The D-8 operators are the lowest-order operators that can change QGCs without affecting the triple gauge couplings.[2] It is assumed that the D-6 operators do not affect the EW $W\gamma jj$ or strong $W\gamma jj$ processes. These D-8 operators can be classified into two groups: mixed-scalar operators ($O_{M0,1,2,3,4,5,7}$), consisting of two covariant derivatives of the Higgs field and two field strength tensors, and tensor-type operators, consisting of four field strength tensors ($O_{T0,1,2,3,4,5,6,7}$).

Theoretical predictions for the EW $W\gamma jj$ process are constructed based on the effective Lagrangian in Eq. (5). The amplitude for the EW $W\gamma jj$ process, $\mathcal{M}$, consists of the SM contribution, $\mathcal{M}_{\mathrm{SM}}$, and the pure D-8 part including the aQGCs, $\mathcal{M}_{\mathrm{D-8}}$.

[2] Triple gauge couplings are represented by dimension-6 operators that affect both strong and EW production of VBS processes. These are strongly constrained by vector boson fusion processes.

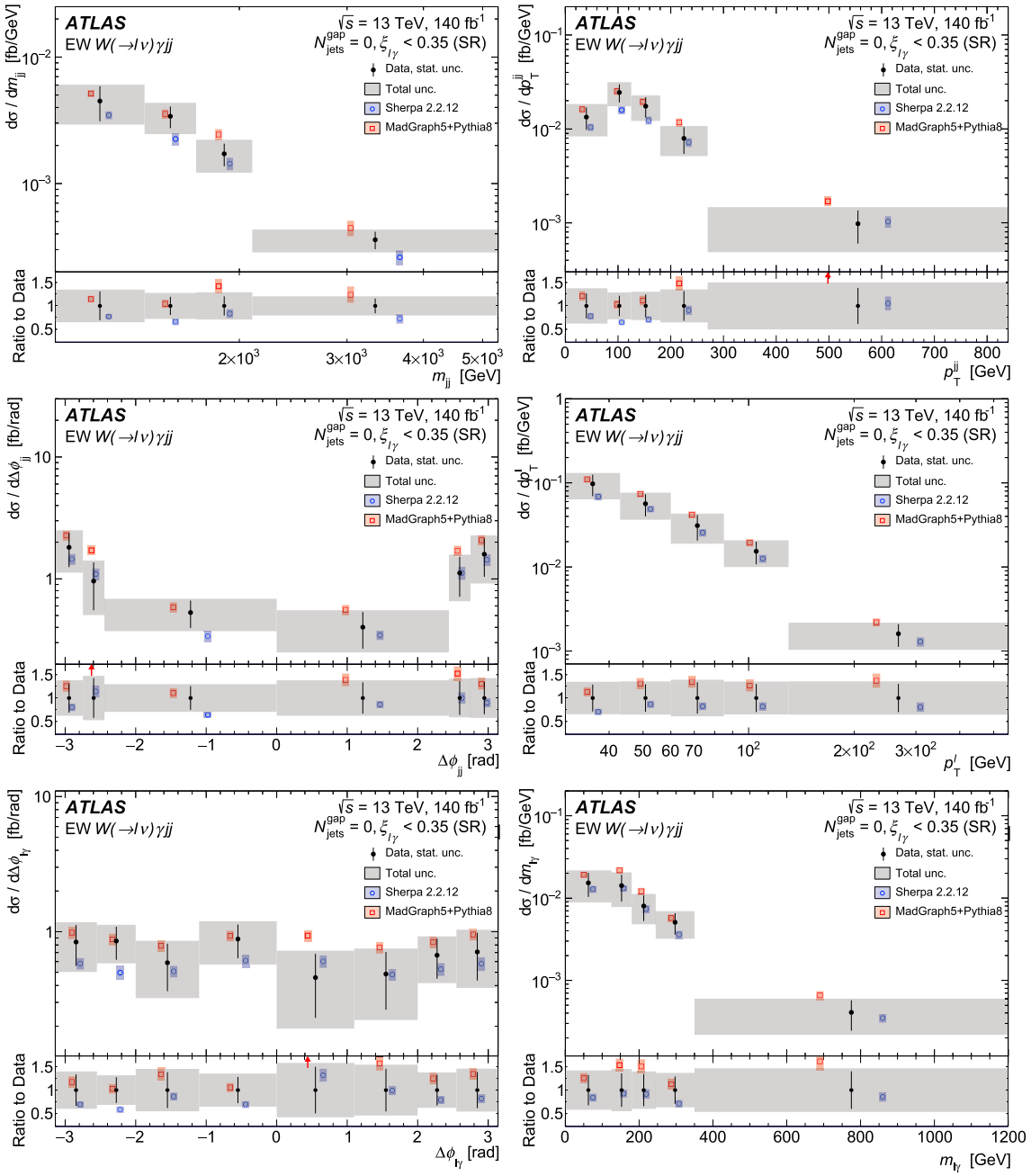

Fig. 7 EW $W\gamma jj$ measured differential cross-section (solid circles) as functions of m_{jj}, p_{T}^{jj}, $\Delta\phi_{jj}$, p_{T}^{l}, $m_{l\gamma}$ and $\Delta\phi_{l\gamma}$ in comparison to SHERPA (open circles) and MADGRAPH5+PYTHIA8 (open squares) predictions. The vertical error bars on the predictions are determined by varying QCD scales, PDFs, α_S (for SHERPA), and MC statistical uncertainties. The vertical (shaded) error bars on the data correspond to the data statistical (total) uncertainties

The differential cross-section can be decomposed into the following three terms:

$$|\mathcal{M}|^2 = |\mathcal{M}_{\mathrm{SM}}|^2 + 2Re(\mathcal{M}^*_{\mathrm{SM}}\mathcal{M}_{\mathrm{D-8}}) + |\mathcal{M}_{\mathrm{D-8}}|^2, \quad (6)$$

where the pure SM term is $|\mathcal{M}_{\mathrm{SM}}|^2$, $|\mathcal{M}_{\mathrm{D-8}}|^2$ is the pure D-8 term that scales quadratically with $f_j^{(8)}$, and the interference term between the SM and D-8 amplitudes is $2Re(\mathcal{M}^*_{\mathrm{SM}}\mathcal{M}_{\mathrm{D-8}})$, which scales linearly with $f_j^{(8)}$. It was

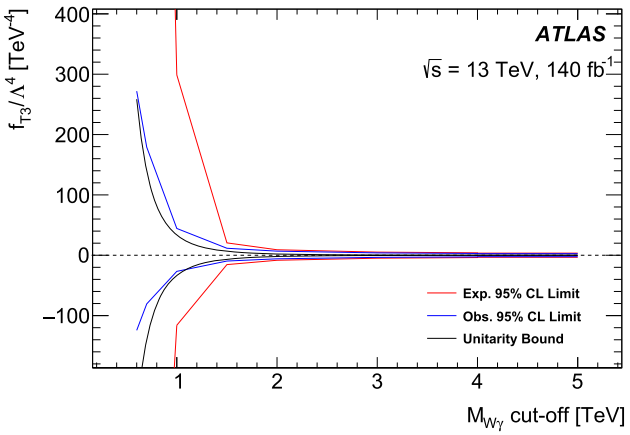

Fig. 8 Expected and observed 95% CL limits of the tensor-type operator coupling f_{T3} from the fit to p_T^{jj} at different values of $m_{W\gamma}$. Bounds from partial wave unitarity constraints are also shown

found that the pure D-8 term affects the differential cross-section measurements significantly more than the interference term. The pure SM part in Eq. (6) is taken to be the LO prediction from MadGraph5+Pythia8, described in Sect. 3. The D-8 and interference terms are generated at LO using MadGraph5+Pythia8, with the same PDF and parameter tunes for modelling as the SM term. QCD scale uncertainties for the EFT contributions are taken directly from the corresponding uncertainty estimate in the SM EW $W\gamma jj$ process using MadGraph5+Pythia8.

Limits on the D-8 operator coefficients are determined using test statistics based on the profile likelihood ratio. The profile likelihood ratio is constructed in terms of the measured cross-section as functions of each of the six observables and the corresponding theoretical prediction parameterised in terms of Wilson coefficients. The profile-likelihood test statistics, which are assumed to follow a χ^2 distribution with one degree of freedom according to Wilks' theorem [61], allows the 95% confidence level (CL) bounds on Wilson coefficients. The expected 95% coverage is further validated using 1000 pseudo experiments.

The most stringent expected limit on each coefficient is obtained from either the p_T^{jj} or p_{T}^{l} distribution. Observed and expected limits on the Wilson coefficients at 95% CL are presented in Tables 5 and 6 with or without unitarity preservation by introducing the clipping technique described in Ref. [62]. The observed limits are tighter than the expected limits because MadGraph5+Pythia8 overshoots the differential measurement shown in Fig. 7.

The limits on the D-8 Wilson coefficients using the clipping technique are estimated as functions of a cut-off scale, and for values of $M_{W\gamma}$ greater than the cut-off scale the anomalous interaction contribution is set to zero. Figure 8 shows a scan of the cut-off scale for the $T3$ operator when fitting the p_T^{jj} distribution. p_T^{jj} is found to be the most sensitive observable to the tensor-type operators while p_{T}^{l} is found to be the most sensitive observable to the mixed scalar operators. The constraints on the f_{T3} and f_{T4} operators represent the first such limits at the LHC.

11 Conclusion

An observation of the electroweak production of $W\gamma jj$ and measurements of its fiducial and differential cross-section are reported, using pp collision data collected with the ATLAS detector at a centre-of-mass energy of $\sqrt{s} = 13$ TeV that correspond to an integrated luminosity of 140 fb^{-1}. This process provides a unique probe of the quartic gauge coupling via the vector boson scattering production mechanism, and measurements of EW $W\gamma jj$ production are therefore sensitive to the $WW\gamma Z$ and $WW\gamma\gamma$ quartic gauge boson couplings.

Advanced machine learning techniques are used to establish the observation of the EW $W\gamma jj$ process with a significance of well above six standard deviations. The measured fiducial cross-section for the EW $W\gamma jj$ process is determined to be 13.2 ± 2.5 fb, consistent with LO predictions from MadGraph5+Pythia8, whereas Sherpa underestimates the measured cross-section. Differential cross-sections are measured as functions of six kinematic observables in a stricter fiducial phase space. These observables are either sensitive to the quartic gauge couplings or the CP violation structure of $WW\gamma Z$ and $WW\gamma\gamma$ couplings. The data are corrected for detector effects of inefficiency and resolution using an iterative Bayesian unfolding method and are compared with theoretical predictions from MadGraph5+Pythia8 and Sherpa 2.2.12. These unfolded distributions are described by LO predictions within uncertainties, in which MadGraph5+Pythia8 tends to overshoot the measurement at high m_{jj} and p_{T}^{jj} while Sherpa 2.2.12 shows reasonable agreement but tends to underestimate the data across the six observables. The shape of these distributions are described reasonably well by both predictions. These differential measurements are used to search for anomalous quartic boson interactions using dimension-8 operators in the context of an effective field theory. The transverse momentum of the dijet system is found to be the most sensitive observable to the tensor-type operators while the charged lepton transverse momentum is found to be the most sensitive observable to the mixed scalar operators. The first LHC constraints on f_{T3} and f_{T4} are presented.

Table 5 Expected and observed limits on dimension-8 operators modifying the $WW\gamma\gamma$ coupling when fitting either the p_{T}^{jj} or p_{T}^{l} distribution

Coefficients (TeV^{-4})	Observable	Expected (TeV^{-4})	Observed (TeV^{-4})
f_{T0}/Λ^4	p_{T}^{jj}	$[-2.4, 2.4]$	$[-1.8, 1.8]$
f_{T1}/Λ^4	p_{T}^{jj}	$[-1.5, 1.6]$	$[-1.1, 1.2]$
f_{T2}/Λ^4	p_{T}^{jj}	$[-4.4, 4.7]$	$[-3.1, 3.5]$
f_{T3}/Λ^4	p_{T}^{jj}	$[-3.3, 3.5]$	$[-2.4, 2.6]$
f_{T4}/Λ^4	p_{T}^{jj}	$[-3.0, 3.0]$	$[-2.2, 2.2]$
f_{T5}/Λ^4	p_{T}^{jj}	$[-1.7, 1.7]$	$[-1.2, 1.3]$
f_{T6}/Λ^4	p_{T}^{jj}	$[-1.5, 1.5]$	$[-1.0, 1.1]$
f_{T7}/Λ^4	p_{T}^{jj}	$[-3.8, 3.9]$	$[-2.7, 2.8]$
f_{M0}/Λ^4	p_{T}^{l}	$[-28, 28]$	$[-24, 24]$
f_{M1}/Λ^4	p_{T}^{l}	$[-43, 44]$	$[-37, 38]$
f_{M2}/Λ^4	p_{T}^{l}	$[-10, 10]$	$[-8.6, 8.5]$
f_{M3}/Λ^4	p_{T}^{l}	$[-16, 16]$	$[-13, 14]$
f_{M4}/Λ^4	p_{T}^{l}	$[-18, 18]$	$[-15, 15]$
f_{M5}/Λ^4	p_{T}^{l}	$[-17, 14]$	$[-14, 12]$
f_{M7}/Λ^4	p_{T}^{l}	$[-78, 77]$	$[-66, 65]$

Table 6 Expected and observed 95% CL limits for specified $M_{W\gamma}$ cut-off values, where the expected limit for some operators intersects with the unitarity bounds derived from partial wave unitarity constraints. Entries with an $M_{W\gamma}$ cut-off scale of "–" indicate that the contribution from the operators do not cross the unitarity bound over the range of the clipping scan. The fit to either the p_{T}^{jj} or p_{T}^{l} distribution is used to extract the limits

Coefficients (TeV^{-4})	Observable	$M_{W\gamma}$ cut-off (TeV)	Expected (TeV^{-4})	Observed (TeV^{-4})
f_{T0}/Λ^4	p_{T}^{jj}	–	[−2.4,2.4]	[−1.7,1.8]
f_{T1}/Λ^4	p_{T}^{jj}	–	[−1.5,1.6]	[−1.1,1.2]
f_{T2}/Λ^4	p_{T}^{jj}	–	[−4.4,4.7]	[−3.1,3.5]
f_{T3}/Λ^4	p_{T}^{jj}	–	[−3.3,3.5]	[−2.4,2.6]
f_{T4}/Λ^4	p_{T}^{jj}	–	[−3.0,3.0]	[−2.2,2.2]
f_{T5}/Λ^4	p_{T}^{jj}	1.1	[−9.9,9.9]	[−7.5,7.5]
f_{T6}/Λ^4	p_{T}^{jj}	1.3	[−7.4,7.6]	[−5.2,5.4]
f_{T7}/Λ^4	p_{T}^{jj}	–	[−3.8,3.9]	[−2.7,2.8]
f_{M0}/Λ^4	p_{T}^{l}	–	[−38,37]	[−38,37]
f_{M1}/Λ^4	p_{T}^{l}	–	[−57,58]	[−41,42]
f_{M2}/Λ^4	p_{T}^{l}	0.8	[−110,110]	[−88,82]
f_{M3}/Λ^4	p_{T}^{l}	1.1	[−100,110]	[−73,77]
f_{M4}/Λ^4	p_{T}^{l}	1.0	[−118,111]	[−89,83]
f_{M5}/Λ^4	p_{T}^{l}	1.3	[−57,80]	[−32,77]
f_{M7}/Λ^4	p_{T}^{l}	–	[−96,95]	[−69,68]

Acknowledgements We thank CERN for the very successful operation of the LHC and its injectors, as well as the support staff at CERN and at our institutions worldwide without whom ATLAS could not be operated efficiently. The crucial computing support from all WLCG partners is acknowledged gratefully, in particular from CERN, the ATLAS Tier-1 facilities at TRIUMF/SFU (Canada), NDGF (Denmark, Norway, Sweden), CC-IN2P3 (France), KIT/GridKA (Germany), INFN-CNAF (Italy), NL-T1 (Netherlands), PIC (Spain), RAL (UK) and BNL (USA), the Tier-2 facilities worldwide and large non-WLCG resource providers. Major contributors of computing resources are listed in Ref. [63]. We gratefully acknowledge the support of ANPCyT, Argentina; YerPhI, Armenia; ARC, Australia; BMWFW and FWF, Austria; ANAS, Azerbaijan; CNPq and FAPESP, Brazil; NSERC, NRC and CFI, Canada; CERN; ANID, Chile; CAS, MOST and NSFC, China; Minciencias, Colombia; MEYS CR, Czech Republic; DNRF and DNSRC, Denmark; IN2P3-CNRS and CEA-DRF/IRFU, France; SRNSFG, Georgia; BMBF, HGF and MPG, Germany; GSRI, Greece; RGC and Hong Kong SAR, China; ISF and Benoziyo Center, Israel; INFN, Italy; MEXT and JSPS, Japan; CNRST, Morocco; NWO, Netherlands; RCN, Norway; MNiSW, Poland; FCT, Portugal; MNE/IFA, Romania; MESTD, Serbia; MSSR, Slovakia; ARRS and MIZŠ, Slovenia; DSI/NRF, South Africa; MICINN, Spain; SRC and Wallenberg Foundation, Sweden; SERI, SNSF and Cantons of Bern and Geneva, Switzerland; NSTC, Taipei; TENMAK, Türkiye; STFC, United Kingdom; DOE and NSF, USA. Individual groups and members have received support from BCKDF, CANARIE, CRC and DRAC, Canada; CERN-CZ, PRIMUS 21/SCI/017 and UNCE SCI/013, Czech Republic; COST, ERC, ERDF, Horizon 2020, ICSC-NextGenerationEU and Marie Skłodowska-Curie Actions, European Union; Investissements d'Avenir Labex, Investissements d'Avenir Idex and ANR, France; DFG

and AvH Foundation, Germany; Herakleitos, Thales and Aristeia programmes co-financed by EU-ESF and the Greek NSRF, Greece; BSF-NSF and MINERVA, Israel; Norwegian Financial Mechanism 2014-2021, Norway; NCN and NAWA, Poland; La Caixa Banking Foundation, CERCA Programme Generalitat de Catalunya and PROMETEO and GenT Programmes Generalitat Valenciana, Spain; Göran Gustafssons Stiftelse, Sweden; The Royal Society and Leverhulme Trust, United Kingdom. In addition, individual members wish to acknowledge support from CERN: European Organization for Nuclear Research (CERN PJAS); Chile: Agencia Nacional de Investigación y Desarrollo (FONDECYT 1190886, FONDECYT 1210400, FONDECYT 1230812, FONDECYT 1230987); China: Chinese Ministry of Science and Technology (MOST-2023YFA1605700), National Natural Science Foundation of China (NSFC - 12175119, NSFC 12275265, NSFC-12075060); Czech Republic: PRIMUS Research Programme (PRIMUS/21/SCI/017); EU: H2020 European Research Council (ERC - 101002463); European Union: European Research Council (ERC - 948254, ERC 101089007), Horizon 2020 Framework Programme (MUCCA - CHIST-ERA-19-XAI-00), European Union, Future Artificial Intelligence Research (FAIR-NextGenerationEU PE00000013), Italian Center for High Performance Computing, Big Data and Quantum Computing (ICSC, NextGenerationEU); France: Agence Nationale de la Recherche (ANR-20-CE31-0013, ANR-21-CE31-0013, ANR-21-CE31-0022, ANR-22-EDIR-0002), Investissements d'Avenir Labex (ANR-11-LABX-0012); Germany: Baden-Württemberg Stiftung (BW Stiftung-Postdoc Eliteprogramme), Deutsche Forschungsgemeinschaft (DFG - 469666862, DFG - CR 312/5-2); Italy: Istituto Nazionale di Fisica Nucleare (ICSC, NextGenerationEU), Ministero dell'Università e della Ricerca (PRIN - 20223N7F8K - PNRR M4.C2.1.1); Japan: Japan Society for the Promotion of Science (JSPS KAKENHI JP21H05085, JSPS KAKENHI JP22H01227, JSPS KAKENHI JP22H04944, JSPS KAKENHI JP22KK0227); Netherlands: Netherlands Organisation for Scientific Research (NWO Veni 2020 - VI.Veni.202.179); Norway: Research Council of Norway (RCN-314472); Poland: Polish National Agency for Academic Exchange (PPN/PPO/2020/1/00002/U/00001), Polish National Science Centre (NCN 2021/42/E/ST2/00350, NCN OPUS nr 2022/47/B/ST2/03059, NCN UMO-2019/34/E/ST2/00393, UMO-2020/37/B/ST2/01043, UMO-2021/40/C/ST2/00187, UMO-2022/47/O/ST2/00148); Slovenia: Slovenian Research Agency (ARIS grant J1-3010); Spain: BBVA Foundation (LEO22-1-603), Generalitat Valenciana (Artemisa, FEDER, IDIFEDER/2018/048), Ministry of Science and Innovation (MCIN & NextGenEU PCI2022-135018-2, MICIN & FEDER PID2021-125273NB, RYC2019-028510-I, RYC2020-030254-I, RYC2021-031273-I, RYC2022-038164-I), PROMETEO and GenT Programmes Generalitat Valenciana (CIDEGENT/2019/023, CIDEGENT/2019/027); Sweden: Swedish Research Council (VR 2018-00482, VR 2022-03845, VR 2022-04683, VR grant 2021-03651), Knut and Alice Wallenberg Foundation (KAW 2017.0100, KAW 2018.0157, KAW 2018.0458, KAW 2019.0447, KAW 2022.0358); Switzerland: Swiss National Science Foundation (SNSF - PCEFP2_194658); United Kingdom: Leverhulme Trust (Leverhulme Trust RPG-2020-004), Royal Society (NIF-R1-231091); United States of America: U.S. Department of Energy (ECA DE-AC02-76SF00515), Neubauer Family Foundation.

Data Availability Statement This manuscript has no associated data. [Authors' comment: All ATLAS scientific output is published in journals, and preliminary results are made available in Conference Notes. All are openly available, without restriction on use by external parties beyond copyright law and the standard conditions agreed by CERN. Data associated with journal publications are also made available: tables and data from plots (e.g. cross section values, likelihood profiles, selection efficiencies, cross section limits, ...) are stored in appropriate repositories such as HEPDATA (http://hepdata.cedar.ac.uk/). ATLAS also strives to make additional material related to the paper available that allows a reinterpretation of the data in the context of new theoretical models. For example, an extended encapsulation of the analysis is often provided for measurements in the framework of RIVET (http://rivet.hepforge.org/). This information is taken from the ATLAS Data Access Policy, which is a public document that can be downloaded from http://opendata.cern.ch/record/413 [opendata.cern.ch].]

Code Availability Statement The manuscript has no associated code/software. [Author's comment: ATLAS collaboration software is open source, and all code necessary to recreate an analysis is publicly available. The Athena (http://gitlab.cern.ch/atlas/athena) software repository provides all code needed for calibration and uncertainty application, with configuration files that are also publicly available via Docker containers and cvmfs. The specific code and configurations written in support of this analysis are not public; however, these are internally preserved.]

Funded by SCOAP[3].

References

1. O.J.P. Éboli, M.C. Gonzalez-Garcia, S.M. Lietti, Bosonic quartic couplings at CERN LHC. Phys. Rev. D **69**, 095005 (2004). https://doi.org/10.1103/PhysRevD.69.095005. arXiv:hep-ph/0310141
2. O.J.P. Éboli, M.C. Gonzalez-Garcia, Classifying the bosonic quartic couplings. Phys. Rev. D **93**, 093013 (2016). https://doi.org/10.1103/PhysRevD.93.093013. arXiv:1604.03555 [hep-ph]
3. E. Accomando, A. Ballestrero, A. Belhouari, E. Maina, Isolating vector boson scattering at the CERN LHC: Gauge cancellations and the equivalent vector boson approximation versus complete calculations. Phys. Rev. D **74**, 073010 (2006). https://doi.org/10.1103/PhysRevD.74.073010. arXiv:hep-ph/0608019
4. C.M.S. Collaboration, Observation of electroweak production of $W\gamma$ with two jets in proton-proton collisions at $\sqrt{s} = 13\,TeV$. Phys. Lett. B **811**, 135988 (2020). https://doi.org/10.1016/j.physletb.2020.135988. arXiv:2008.10521 [hep-ex]
5. C.M.S. Collaboration, Measurement of the electroweak production of $W\gamma$ in association with two jets in proton-proton collisions at $\sqrt{s} = 13\,TeV$. Phys. Rev. D **108**, 032017 (2023). https://doi.org/10.1103/PhysRevD.108.032017. arXiv:2212.12592 [hep-ex]
6. T. Plehn, D. Rainwater, D. Zeppenfeld, Determining the structure of Higgs couplings at the LHC. Phys. Rev. Lett. **88** (2002). https://doi.org/10.1103/PhysRevLett.88.051801. arXiv:hep-ph/0105325
7. G. Klamke, D. Zeppenfeld, Higgs plus two jet production via gluon fusion as a signal at the CERN LHC. JHEP **0704**(2007). https://doi.org/10.1088/1126-6708/2007/04/052. arXiv:hep-ph/0703202
8. ATLAS Collaboration, The ATLAS Experiment at the CERN Large Hadron Collider. JINST **3**, S08003 (2008). https://doi.org/10.1088/1748-0221/3/08/S08003
9. ATLAS Collaboration, ATLAS Insertable B-Layer: Technical Design Report, ATLAS-TDR-19; CERN-LHCC-2010-013, 2010, https://cds.cern.ch/record/1291633, Addendum:

ATLAS-TDR-19-ADD-1; CERN-LHCC-2012-009, 2012, url: https://cds.cern.ch/record/1451888
10. B. Abbott et al., Production and integration of the ATLAS Insertable B-Layer. JINST **13**, T05008 (2018). https://doi.org/10.1088/1748-0221/13/05/T05008. arXiv:1803.00844 [physics.ins-det]
11. G. Avoni, The new LUCID-2 detector for luminosity measurement and monitoring in ATLAS. JINST **13**, P07017 (2018)
12. ATLAS Collaboration, Performance of the ATLAS trigger system in. Eur. Phys. J. C **77**(2017), 317 (2015). https://doi.org/10.1140/epjc/s10052-017-4852-3. arXiv:1611.09661 [hep-ex]
13. ATLAS Collaboration, The ATLAS Collaboration Software and Firmware, ATL-SOFT-PUB-2021-001, 2021. https://cds.cern.ch/record/2767187
14. E. Bothmann et al., Event generation with Sherpa 2.2. SciPost Phys. **7**, 034 (2019). https://doi.org/10.21468/SciPostPhys.7.3.034. arXiv:1905.09127 [hep-ph]
15. T. Gleisberg, S. Höche, Comix, a new matrix element generator. JHEP **12**, 039 (2008). https://doi.org/10.1088/1126-6708/2008/12/039. arXiv:0808.3674 [hep-ph]
16. S. Schumann, F. Krauss, A parton shower algorithm based on Catani-Seymour dipole factorisation. JHEP **03**, 038 (2008). https://doi.org/10.1088/1126-6708/2008/03/038. arXiv:0709.1027 [hep-ph]
17. S. Höche, F. Krauss, M. Schönherr, F. Siegert, A critical appraisal of NLO+ PS matching methods. JHEP **09**, 049 (2012). https://doi.org/10.1007/JHEP09(2012)049. arXiv:1111.1220 [hep-ph]
18. S. Höche, F. Krauss, M. Schönherr, F. Siegert, QCD matrix elements + parton showers. The NLO case. JHEP **04**, 027 (2013). https://doi.org/10.1007/JHEP04(2013)027. arXiv:1207.5030 [hep-ph]
19. S. Catani, F. Krauss, B.R. Webber, R. Kuhn, QCD matrix elements + Parton showers. JHEP **11**, 063 (2001). https://doi.org/10.1088/1126-6708/2001/11/063. arXiv:hep-ph/0109231
20. S. Höche, F. Krauss, S. Schumann, F. Siegert, QCD matrix elements and truncated showers. JHEP **05**, 053 (2009). https://doi.org/10.1088/1126-6708/2009/05/053. arXiv:0903.1219 [hep-ph]
21. NNPDF Collaboration, R.D. Ball et al., Parton distributions for the LHC run II. JHEP **04**, 040 (2015). https://doi.org/10.1007/JHEP04(2015)040. arXiv:1410.8849 [hep-ph]
22. J. Alwall et al., The automated computation of tree-level and next-to-leading order differential cross sections, and their matching to parton shower simulations. JHEP **07**, 079 (2014). https://doi.org/10.1007/JHEP07(2014)079. arXiv:1405.0301 [hep-ph]
23. ATLAS Collaboration, ATLAS Pythia 8 tunes to 7 TeV data, ATL-PHYS-PUB-2014-021, 2014. url: https://cds.cern.ch/record/1966419
24. D.J. Lange, The EvtGen particle decay simulation package. Nucl. Instrum. Methods A **462**, 152 (2001). https://doi.org/10.1016/S0168-9002(01)00089-4
25. S. Agostinelli et al., Geant4: a simulation toolkit. Nucl. Instrum. Methods A **506**, 250 (2003). https://doi.org/10.1016/S0168-9002(03)01368-8
26. T. Sjöstrand, S. Mrenna, P. Skands, A brief introduction to PYTHIA 8.1. Comput. Phys. Commun. **178**, 852 (2008). https://doi.org/10.1016/j.cpc.2008.01.036. arXiv:0710.3820 [hep-ph]
27. NNPDF Collaboration, R.D. Ball et al., Parton distributions with LHC data. Nucl. Phys. B **867**, 244 (2013). https://doi.org/10.1016/j.nuclphysb.2012.10.003. arXiv:1207.1303 [hep-ph]
28. ATLAS Collaboration, The Pythia 8 A3 tune description of ATLAS minimum bias and inelastic measurements incorporating the Donnachie–Landshoff diffractive model, ATL-PHYS-PUB-2016-017, 2016. https://cds.cern.ch/record/2206965
29. ATLAS Collaboration, Luminosity determination in *pp collisions at* $\sqrt{s} = 13\,TeV$ using the ATLAS detector at the LHC. Eur. Phys. J. C **83** (2023). https://doi.org/10.1140/epjc/s10052-023-11747-w. arXiv:2212.09379 [hep-ex]
30. ATLAS Collaboration, Performance of the ATLAS muon triggers in Run 2. JINST **15**, P09015 (2020). https://doi.org/10.1088/1748-0221/15/09/p09015. arXiv:2004.13447 [physics.ins-det]
31. ATLAS Collaboration, Performance of electron and photon triggers in ATLAS during LHC Run 2. Eur. Phys. J. C **80**, 47 (2020). https://doi.org/10.1140/epjc/s10052-019-7500-2. arXiv:1909.00761 [hep-ex]
32. ATLAS Collaboration, ATLAS data quality operations and performance for 2015–2018 data-taking. JINST **15**, P04003 (2020). https://doi.org/10.1088/1748-0221/15/04/P04003. arXiv:1911.04632 [physics.ins-det]
33. ATLAS Collaboration, Vertex Reconstruction Performance of the ATLAS Detector at $\sqrt{s} = 13\,TeV$, ATL-PHYS-PUB-2015-026, 2015. https://cds.cern.ch/record/2037717
34. ATLAS Collaboration, Muon reconstruction and identification efficiency in ATLAS using the full Run 2 *pp* collision data set at $\sqrt{s} = 13\,TeV$. Eur. Phys. J. C **81**, 578 (2021). https://doi.org/10.1140/epjc/s10052-021-09233-2. arXiv:2012.00578 [hep-ex]
35. ATLAS Collaboration, Electron and photon performance measurements with the ATLAS detector using the 2015–2017 LHC proton–proton collision data. JINST **14**, P12006 (2019). https://doi.org/10.1088/1748-0221/14/12/P12006. arXiv:1908.00005 [hep-ex]
36. ATLAS Collaboration, Jet reconstruction and performance using particle flow with the ATLAS Detector. Eur. Phys. J. C **77**, 466 (2017). https://doi.org/10.1140/epjc/s10052-017-5031-2. arXiv:1703.10485 [hep-ex]
37. M. Cacciari, G.P. Salam, G. Soyez, The anti-k_t jet clustering algorithm. JHEP **04**, 063 (2008). https://doi.org/10.1088/1126-6708/2008/04/063. arXiv:0802.1189 [hep-ph]
38. ATLAS Collaboration, Performance of pile-up mitigation techniques for jets in *pp* collisions at $\sqrt{s} = 8\,TeV$ using the ATLAS detector. Eur. Phys. J. C **76**, 581 (2016). https://doi.org/10.1140/epjc/s10052-016-4395-z. arXiv:1510.03823 [hep-ex]
39. ATLAS Collaboration, Selection of jets produced in 13 TeV proton–proton collisions with the ATLAS detector, ATLAS-CONF-2015-029, 2015. https://cds.cern.ch/record/2037702
40. ATLAS Collaboration, Optimisation and performance studies of the ATLAS *b*-tagging algorithms for the 2017-18 LHC run, ATL-PHYS-PUB-2017-013, 2017. https://cds.cern.ch/record/2273281
41. ATLAS Collaboration, Performance of missing transverse momentum reconstruction with the ATLAS detector using proton–proton collisions at $\sqrt{s} = 13\,TeV$. Eur. Phys. J. C **78**, 903 (2018). https://doi.org/10.1140/epjc/s10052-018-6288-9. arXiv:1802.08168 [hep-ex]
42. ATLAS Collaboration, Measurement of the inclusive isolated prompt photon cross section in *pp* collisions at $\sqrt{s} = 7$ TeV with the ATLAS detector. Phys. Rev. D **83**, 052005 (2011). https://doi.org/10.1103/PhysRevD.83.052005. arXiv:1012.4389 [hep-ex]
43. Gaiser, J., Charmonium spectroscopy from radiative decays of J/Ψ and Ψ', SLAC-R-255 (1982)
44. S. Bernstein, Proof of theorem of Weierstrass based on the calculus of probabilities. Commun. Kharkov Math. Soc. **13**(1) (1912)
45. ATLAS Collaboration, Measurement of the $Z(\to \ell^+\ell^-)_\gamma$ production cross-section in *pp* collisions at $\sqrt{s} = 13\,TeV$ with the ATLAS detector. JHEP **03**, 054 (2020). https://doi.org/10.1007/JHEP03(2020)054. arXiv:1911.04813 [hep-ex]
46. A.L. Maas, Rectifier nonlinearities improve neural network acoustic models, *Proceedings of the 30th International Conference on Machine Learning*, vol. 28, 3 (2013)
47. D.P. Kingma, J. Ba, Adam: a method for stochastic optimization (2014). arXiv:1412.6980 [hep-ex]
48. ATLAS Collaboration, Differential cross-section measurements for the electroweak production of dijets in association with a *Z*

boson in proton–proton collisions at ATLAS. Eur. Phys. J. C **81**, 163 (2021). https://doi.org/10.1140/epjc/s10052-020-08734-w. arXiv:2006.15458 [hep-ex]
49. R. Barlow, Extended maximum likelihood. Nucl. Instrum. Methods A **297**, 496 (1990). https://doi.org/10.1016/0168-9002(90)91334-8
50. M. Tanabashi, et al., (Particle Data Group), Review of Particle Physics. Phys. Rev. D **98**, 030001 (2018). https://doi.org/10.1103/PhysRevD.98.030001
51. ATLAS Collaboration, Evaluating statistical uncertainties and correlations using the bootstrap method, ATL-PHYS-PUB-2021-011, 2021. https://cds.cern.ch/record/2759945
52. G. D'Agostini, A multidimensional unfolding method based on Bayes' theorem. Nucl. Instrum. Methods A **362**, 487 (1995). ISSN:0168-9002. https://doi.org/10.1016/0168-9002(95)00274-X
53. T. Adye, Unfolding algorithms and tests using RooUnfold, *Proceedings, 2011 Workshop on Statistical Issues Related to Discovery Claims in Search Experiments and Unfolding (PHYSTAT 2011)* (CERN, Geneva, Switzerland, 17th–20th Jan. 2011) 313. arXiv:1105.1160 [physics.data-an]
54. G. Cowan, K. Cranmer, E. Gross, O. Vitells, Asymptotic formulae for likelihood-based tests of new physics. Eur. Phys. J. C **71**, 1554. https://doi.org/10.1140/epjc/s10052-011-1554-0. https://doi.org/10.1140/epjc/s10052-013-2501-z (Erratum: Eur. Phys. J. C 73(2013) 2501). arXiv:1007.1727 [physics.data-an]
55. ATLAS Collaboration, Jet energy scale and resolution measured in proton–proton collisions at $\sqrt{s} = 13\,TeV$ with the ATLAS detector. Eur. Phys. J. C **81**, 689 (2021). https://doi.org/10.1140/epjc/s10052-021-09402-3. arXiv:2007.02645 [hep-ex]
56. NNPDF Collaboration, Parton distributions from high-precision collider data. Eur. Phys. J. C **77** (2017). https://doi.org/10.48550/arXiv.1706.00428. arXiv:1706.00428 [hep-ex]
57. T.-J. Hou et al., Progress in the CTEQ-TEA NNLO global QCD analysis (2019). arXiv:1908.11394 [hep-ph]
58. S. Bailey, T. Cridge, L.A. Harland-Lang, A.D. Martin, R. Thorne, Parton distributions from LHC, HERA, Tevatron and fixed target data: MSHT20 PDFs. Eur. Phys. J. C **81** (2021). arXiv:2012.04684. https://doi.org/10.1140/epjc/s10052-021-09057-0
59. J. Butterworth et al., PDF4LHC recommendations for LHC Run II. J. Phys. G **43**, 023001 (2016). https://doi.org/10.1088/0954-3899/43/2/023001. arXiv:1510.03865 [hep-ph]
60. A. Ballestrero et al., Precise predictions for same-sign W-boson scattering at the LHC. Eur. Phys. J. C **78** (2018). https://doi.org/10.48550/arXiv.1803.07943. arXiv:1803.07943
61. S.S. Wilks, The large-sample distribution of the likelihood ratio for testing composite hypotheses. Ann. Math. Stat. **9**, 60 (1938). https://doi.org/10.1214/aoms/1177732360
62. E.D.S. Almeida, O.J.P. Éboli, M.C. Gonzalez-Garcia, Unitarity constraints on anomalous quartic couplings. Phys. Rev. D **101**, 113003 (2020). https://doi.org/10.1103/PhysRevD.101.113003. arXiv:2004.05174 [hep-ph]
63. ATLAS Collaboration, ATLAS Computing Acknowledgements, ATL-SOFT-PUB-2023-001, 2023. https://cds.cern.ch/record/2869272

ATLAS Collaboration[★]

G. Aad[103], E. Aakvaag[16], B. Abbott[121], K. Abeling[55], N. J. Abicht[49], S. H. Abidi[29], M. Aboelela[44], A. Aboulhorma[35e], H. Abramowicz[152], H. Abreu[151], Y. Abulaiti[118], B. S. Acharya[69a,69b,l], A. Ackermann[63a], C. Adam Bourdarios[4], L. Adamczyk[86a], S. V. Addepalli[26], M. J. Addison[102], J. Adelman[116], A. Adiguzel[21c], T. Adye[135], A. A. Affolder[137], Y. Afik[39], M. N. Agaras[13], J. Agarwala[73a,73b], A. Aggarwal[101], C. Agheorghiesei[27c], A. Ahmad[36], F. Ahmadov[38,y], W. S. Ahmed[105], S. Ahuja[96], X. Ai[62e], G. Aielli[76a,76b], A. Aikot[164], M. Ait Tamlihat[35e], B. Aitbenchikh[35a], I. Aizenberg[170], M. Akbiyik[101], T. P. A. Åkesson[99], A. V. Akimov[37], D. Akiyama[169], N. N. Akolkar[24], S. Aktas[21a], K. Al Khoury[41], G. L. Alberghi[23b], J. Albert[166], P. Albicocco[53], G. L. Albouy[60], S. Alderweireldt[52], Z. L. Alegria[122], M. Aleksa[36], I. N. Aleksandrov[38], C. Alexa[27b], T. Alexopoulos[10], F. Alfonsi[23b], M. Algren[56], M. Alhroob[142], B. Ali[133], H. M. J. Ali[92], S. Ali[149], S. W. Alibocus[93], M. Aliev[33c], G. Alimonti[71a], W. Alkakhi[55], C. Allaire[66], B. M. M. Allbrooke[147], J. F. Allen[52], C. A. Allendes Flores[138f], P. P. Allport[20], A. Aloisio[72a,72b], F. Alonso[91], C. Alpigiani[139], M. Alvarez Estevez[100], A. Alvarez Fernandez[101], M. Alves Cardoso[56], M. G. Alviggi[72a,72b], M. Aly[102], Y. Amaral Coutinho[83b], A. Ambler[105], C. Amelung[36], M. Amerl[102], C. G. Ames[110], D. Amidei[107], K. J. Amirie[156], S. P. Amor Dos Santos[131a], K. R. Amos[164], S. An[84], V. Ananiev[126], C. Anastopoulos[140], T. Andeen[11], J. K. Anders[36], S. Y. Andrean[47a,47b], A. Andreazza[71a,71b], S. Angelidakis[9], A. Angerami[41,aa], A. V. Anisenkov[37], A. Annovi[74a], C. Antel[56], M. T. Anthony[140], E. Antipov[146], M. Antonelli[53], F. Anulli[75a], M. Aoki[84], T. Aoki[154], J. A. Aparisi Pozo[164], M. A. Aparo[147], L. Aperio Bella[48], C. Appelt[18], A. Apyan[26], S. J. Arbiol Val[87], C. Arcangeletti[53], A. T. H. Arce[51], E. Arena[93], J.-F. Arguin[109], S. Argyropoulos[54], J.-H. Arling[48], O. Arnaez[4], H. Arnold[115], G. Artoni[75a,75b], H. Asada[112], K. Asai[119], S. Asai[154], N. A. Asbah[36], K. Assamagan[29], R. Astalos[28a], K. S. V. Astrand[99], S. Atashi[160], R. J. Atkin[33a], M. Atkinson[163], H. Atmani[35f], P. A. Atmasiddha[129], K. Augsten[133], S. Auricchio[72a,72b], A. D. Auriol[20], V. A. Austrup[102], G. Avolio[36], K. Axiotis[56], G. Azuelos[109,ae], D. Babal[28b], H. Bachacou[136], K. Bachas[153,p], A. Bachiu[34], F. Backman[47a,47b], A. Badea[39], T. M. Baer[107], P. Bagnaia[75a,75b], M. Bahmani[18], D. Bahner[54], K. Bai[124], J. T. Baines[135], L. Baines[95], O. K. Baker[173], E. Bakos[15], D. Bakshi Gupta[8], V. Balakrishnan[121], R. Balasubramanian[115], E. M. Baldin[37], P. Balek[86a], E. Ballabene[23a,23b], F. Balli[136], L. M. Baltes[63a], W. K. Balunas[32], J. Balz[101], E. Banas[87], M. Bandieramonte[130], A. Bandyopadhyay[24], S. Bansal[24], L. Barak[152], M. Barakat[48], E. L. Barberio[106], D. Barberis[57a,57b], M. Barbero[103], M. Z. Barel[115], K. N. Barends[33a], T. Barillari[111], M.-S. Barisits[36], T. Barklow[144], P. Baron[123], D. A. Baron Moreno[102], A. Baroncelli[62a], G. Barone[29], A. J. Barr[127], J. D. Barr[97], F. Barreiro[100], J. Barreiro Guimarães da Costa[14a], U. Barron[152], M. G. Barros Teixeira[131a], S. Barsov[37], F. Bartels[63a], R. Bartoldus[144], A. E. Barton[92], P. Bartos[28a], A. Basan[101], M. Baselga[49], A. Bassalat[66,b], M. J. Basso[157a], R. Bate[165], R. L. Bates[59], S. Batlamous[100], B. Batool[142], M. Battaglia[137], D. Battulga[18], M. Bauce[75a,75b], M. Bauer[36], P. Bauer[24], L. T. Bazzano Hurrell[30], J. B. Beacham[51], T. Beau[128], J. Y. Beaucamp[91], P. H. Beauchemin[159], P. Bechtle[24], H. P. Beck[19,o], K. Becker[168], A. J. Beddall[82], V. A. Bednyakov[38], C. P. Bee[146], L. J. Beemster[15], T. A. Beermann[36], M. Begalli[83d], M. Begel[29], A. Behera[146], J. K. Behr[48], J. F. Beirer[36], F. Beisiegel[24], M. Belfkir[117b], G. Bella[152], L. Bellagamba[23b], A. Bellerive[34], P. Bellos[20], K. Beloborodov[37], D. Benchekroun[35a], F. Bendebba[35a], Y. Benhammou[152], K. C. Benkendorfer[61], L. Beresford[48], M. Beretta[53], E. Bergeaas Kuutmann[162], N. Berger[4], B. Bergmann[133], J. Beringer[17a], G. Bernardi[5], C. Bernius[144], F. U. Bernlochner[24], F. Bernon[36,103], A. Berrocal Guardia[13], T. Berry[96], P. Berta[134], A. Berthold[50], S. Bethke[111], A. Betti[75a,75b], A. J. Bevan[95], N. K. Bhalla[54], M. Bhamjee[33c], S. Bhatta[146], D. S. Bhattacharya[167], P. Bhattarai[144], K. D. Bhide[54], V. S. Bhopatkar[122], R. M. Bianchi[130], G. Bianco[23a,23b], O. Biebel[110], R. Bielski[124], M. Biglietti[77a], C. S. Billingsley[44], M. Bindi[55], A. Bingul[21b], C. Bini[75a,75b], A. Biondini[93], C. J. Birch-sykes[102], G. A. Bird[32], M. Birman[170], M. Biros[134], S. Biryukov[147], T. Bisanz[49], E. Bisceglie[43a,43b], J. P. Biswal[135], D. Biswas[142], I. Bloch[48], A. Blue[59], U. Blumenschein[95], J. Blumenthal[101], V. S. Bobrovnikov[37], M. Boehler[54], B. Boehm[167], D. Bogavac[36], A. G. Bogdanchikov[37], C. Bohm[47a], V. Boisvert[96], P. Bokan[36], T. Bold[86a], M. Bomben[5], M. Bona[95], M. Boonekamp[136], C. D. Booth[96], A. G. Borbély[59], I. S. Bordulev[37], H. M. Borecka-Bielska[109], G. Borissov[92], D. Bortoletto[127], D. Boscherini[23b], M. Bosman[13], J. D. Bossio Sola[36], K. Bouaouda[35a], N. Bouchhar[164], J. Boudreau[130], E. V. Bouhova-Thacker[92], D. Boumediene[40], R. Bouquet[57a,57b], A. Boveia[120], J. Boyd[36], D. Boye[29], I. R. Boyko[38], J. Bracinik[20], N. Brahimi[4], G. Brandt[172], O. Brandt[32], F. Braren[48], B. Brau[104], J. E. Brau[124], R. Brener[170], L. Brenner[115], R. Brenner[162], S. Bressler[170], D. Britton[59], D. Britzger[111],

I. Brock[24], G. Brooijmans[41], E. Brost[29], L. M. Brown[166], L. E. Bruce[61], T. L. Bruckler[127], P. A. Bruckman de Renstrom[87], B. Brüers[48], A. Bruni[23b], G. Bruni[23b], M. Bruschi[23b], N. Bruscino[75a,75b], T. Buanes[16], Q. Buat[139], D. Buchin[111], A. G. Buckley[59], O. Bulekov[37], B. A. Bullard[144], S. Burdin[93], C. D. Burgard[49], A. M. Burger[36], B. Burghgrave[8], O. Burlayenko[54], J. T. P. Burr[32], C. D. Burton[11], J. C. Burzynski[143], E. L. Busch[41], V. Büscher[101], P. J. Bussey[59], J. M. Butler[25], C. M. Buttar[59], J. M. Butterworth[97], W. Buttinger[135], C. J. Buxo Vazquez[108], A. R. Buzykaev[37], S. Cabrera Urbán[164], L. Cadamuro[66], D. Caforio[58], H. Cai[130], Y. Cai[14a,14e], Y. Cai[14c], V. M. M. Cairo[36], O. Cakir[3a], N. Calace[36], P. Calafiura[17a], G. Calderini[128], P. Calfayan[68], G. Callea[59], L. P. Caloba[83b], D. Calvet[40], S. Calvet[40], M. Calvetti[74a,74b], R. Camacho Toro[128], S. Camarda[36], D. Camarero Munoz[26], P. Camarri[76a,76b], M. T. Camerlingo[72a,72b], D. Cameron[36], C. Camincher[166], M. Campanelli[97], A. Camplani[42], V. Canale[72a,72b], A. C. Canbay[3a], E. Canonero[96], J. Cantero[164], Y. Cao[163], F. Capocasa[26], M. Capua[43a,43b], A. Carbone[71a,71b], R. Cardarelli[76a], J. C. J. Cardenas[8], F. Cardillo[164], G. Carducci[43a,43b], T. Carli[36], G. Carlino[72a], J. I. Carlotto[13], B. T. Carlson[130,q], E. M. Carlson[157a,166], J. Carmignani[93], L. Carminati[71a,71b], A. Carnelli[136], M. Carnesale[75a,75b], S. Caron[114], E. Carquin[138f], S. Carrá[71a], G. Carratta[23a,23b], A. M. Carroll[124], T. M. Carter[52], M. P. Casado[13,i], M. Caspar[48], F. L. Castillo[4], L. Castillo Garcia[13], V. Castillo Gimenez[164], N. F. Castro[131a,131e], A. Catinaccio[36], J. R. Catmore[126], T. Cavaliere[4], V. Cavaliere[29], N. Cavalli[23a,23b], Y. C. Cekmecelioglu[48], E. Celebi[21a], S. Cella[36], F. Celli[127], M. S. Centonze[70a,70b], V. Cepaitis[56], K. Cerny[123], A. S. Cerqueira[83a], A. Cerri[147], L. Cerrito[76a,76b], F. Cerutti[17a], B. Cervato[142], A. Cervelli[23b], G. Cesarini[53], S. A. Cetin[82], D. Chakraborty[116], J. Chan[17a], W. Y. Chan[154], J. D. Chapman[32], E. Chapon[136], B. Chargeishvili[150b], D. G. Charlton[20], M. Chatterjee[19], C. Chauhan[134], Y. Che[14c], S. Chekanov[6], S. V. Chekulaev[157a], G. A. Chelkov[38,a], A. Chen[107], B. Chen[152], B. Chen[166], H. Chen[14c], H. Chen[29], J. Chen[62c], J. Chen[143], M. Chen[127], S. Chen[154], S. J. Chen[14c], X. Chen[62c,136], X. Chen[14b,ad], Y. Chen[62a], C. L. Cheng[171], H. C. Cheng[64a], S. Cheong[144], A. Cheplakov[38], E. Cheremushkina[48], E. Cherepanova[115], R. Cherkaoui El Moursli[35e], E. Cheu[7], K. Cheung[65], L. Chevalier[136], V. Chiarella[53], G. Chiarelli[74a], N. Chiedde[103], G. Chiodini[70a], A. S. Chisholm[20], A. Chitan[27b], M. Chitishvili[164], M. V. Chizhov[38], K. Choi[11], Y. Chou[139], E. Y. S. Chow[114], K. L. Chu[170], M. C. Chu[64a], X. Chu[14a,14e], J. Chudoba[132], J. J. Chwastowski[87], D. Cieri[111], K. M. Ciesla[86a], V. Cindro[94], A. Ciocio[17a], F. Cirotto[72a,72b], Z. H. Citron[170], M. Citterio[71a], D. A. Ciubotaru[27b], A. Clark[56], P. J. Clark[52], C. Clarry[156], J. M. Clavijo Columbie[48], S. E. Clawson[48], C. Clement[47a,47b], J. Clercx[48], Y. Coadou[103], M. Cobal[69a,69c], A. Coccaro[57b], R. F. Coelho Barrue[131a], R. Coelho Lopes De Sa[104], S. Coelli[71a], B. Cole[41], J. Collot[60], P. Conde Muiño[131a,131g], M. P. Connell[33c], S. H. Connell[33c], E. I. Conroy[127], F. Conventi[72a,af], H. G. Cooke[20], A. M. Cooper-Sarkar[127], F. A. Corchia[23a,23b], A. Cordeiro Oudot Choi[128], L. D. Corpe[40], M. Corradi[75a,75b], F. Corriveau[105,w], A. Cortes-Gonzalez[18], M. J. Costa[164], F. Costanza[4], D. Costanzo[140], B. M. Cote[120], G. Cowan[96], K. Cranmer[171], D. Cremonini[23a,23b], S. Crépé-Renaudin[60], F. Crescioli[128], M. Cristinziani[142], M. Cristoforetti[78a,78b], V. Croft[115], J. E. Crosby[122], G. Crosetti[43a,43b], A. Cueto[100], H. Cui[14a,14e], Z. Cui[7], W. R. Cunningham[59], F. Curcio[164], J. R. Curran[52], P. Czodrowski[36], M. M. Czurylo[36], M. J. Da Cunha Sargedas De Sousa[57a,57b], J. V. Da Fonseca Pinto[83b], C. Da Via[102], W. Dabrowski[86a], T. Dado[49], S. Dahbi[149], T. Dai[107], D. Dal Santo[19], C. Dallapiccola[104], M. Dam[42], G. D'amen[29], V. D'Amico[110], J. Damp[101], J. R. Dandoy[34], M. Danninger[143], V. Dao[36], G. Darbo[57b], S. J. Das[29,ag], F. Dattola[48], S. D'Auria[71a,71b], A. D'avanzo[72a,72b], C. David[33a], T. Davidek[134], B. Davis-Purcell[34], I. Dawson[95], H. A. Day-hall[133], K. De[8], R. De Asmundis[72a], N. De Biase[48], S. De Castro[23a,23b], N. De Groot[114], P. de Jong[115], H. De la Torre[116], A. De Maria[14c], A. De Salvo[75a], U. De Sanctis[76a,76b], F. De Santis[70a,70b], A. De Santo[147], J. B. De Vivie De Regie[60], D. V. Dedovich[38], J. Degens[93], A. M. Deiana[44], F. Del Corso[23a,23b], J. Del Peso[100], F. Del Rio[63a], L. Delagrange[128], F. Deliot[136], C. M. Delitzsch[49], M. Della Pietra[72a,72b], D. Della Volpe[56], A. Dell'Acqua[36], L. Dell'Asta[71a,71b], M. Delmastro[4], P. A. Delsart[60], S. Demers[173], M. Demichev[38], S. P. Denisov[37], L. D'Eramo[40], D. Derendarz[87], F. Derue[128], P. Dervan[93], K. Desch[24], C. Deutsch[24], F. A. Di Bello[57a,57b], A. Di Ciaccio[76a,76b], L. Di Ciaccio[4], A. Di Domenico[75a,75b], C. Di Donato[72a,72b], A. Di Girolamo[36], G. Di Gregorio[36], A. Di Luca[78a,78b], B. Di Micco[77a,77b], R. Di Nardo[77a,77b], M. Diamantopoulou[34], F. A. Dias[115], T. Dias Do Vale[143], M. A. Diaz[138a,138b], F. G. Diaz Capriles[24], M. Didenko[164], E. B. Diehl[107], S. Díez Cornell[48], C. Diez Pardos[142], C. Dimitriadi[24,162], A. Dimitrievska[20], J. Dingfelder[24], I.-M. Dinu[27b], S. J. Dittmeier[63b], F. Dittus[36], M. Divisek[134], F. Djama[103], T. Djobava[150b], C. Doglioni[99,102], A. Dohnalova[28a], J. Dolejsi[134], Z. Dolezal[134], K. M. Dona[39], M. Donadelli[83c], B. Dong[108], J. Donini[40], A. D'Onofrio[72a,72b],

M. D'Onofrio[93], J. Dopke[135], A. Doria[72a], N. Dos Santos Fernandes[131a], P. Dougan[102], M. T. Dova[91], A. T. Doyle[59], M. A. Draguet[127], E. Dreyer[170], I. Drivas-koulouris[10], M. Drnevich[118], M. Drozdova[56], D. Du[62a], T. A. du Pree[115], F. Dubinin[37], M. Dubovsky[28a], E. Duchovni[170], G. Duckeck[110], O. A. Ducu[27b], D. Duda[52], A. Dudarev[36], E. R. Duden[26], M. D'uffizi[102], L. Duflot[66], M. Dührssen[36], I. Duminica[27g], A. E. Dumitriu[27b], M. Dunford[63a], S. Dungs[49], K. Dunne[47a,47b], A. Duperrin[103], H. Duran Yildiz[3a], M. Düren[58], A. Durglishvili[150b], B. L. Dwyer[116], G. I. Dyckes[17a], M. Dyndal[86a], B. S. Dziedzic[87], Z. O. Earnshaw[147], G. H. Eberwein[127], B. Eckerova[28a], S. Eggebrecht[55], E. Egidio Purcino De Souza[128], L. F. Ehrke[56], G. Eigen[16], K. Einsweiler[17a], T. Ekelof[162], P. A. Ekman[99], S. El Farkh[35b], Y. El Ghazali[35b], H. El Jarrari[36], A. El Moussaouy[109], V. Ellajosyula[162], M. Ellert[162], F. Ellinghaus[172], N. Ellis[36], J. Elmsheuser[29], M. Elsawy[117a], M. Elsing[36], D. Emeliyanov[135], Y. Enari[154], I. Ene[17a], S. Epari[13], P. A. Erland[87], M. Errenst[172], M. Escalier[66], C. Escobar[164], E. Etzion[152], G. Evans[131a], H. Evans[68], L. S. Evans[96], A. Ezhilov[37], S. Ezzarqtouni[35a], F. Fabbri[23a,23b], L. Fabbri[23a,23b], G. Facini[97], V. Fadeyev[137], R. M. Fakhrutdinov[37], D. Fakoudis[101], S. Falciano[75a], L. F. Falda Ulhoa Coelho[36], P. J. Falke[24], F. Fallavollita[111], J. Faltova[134], C. Fan[163], Y. Fan[14a], Y. Fang[14a,14e], M. Fanti[71a,71b], M. Faraj[69a,69b], Z. Farazpay[98], A. Farbin[8], A. Farilla[77a], T. Farooque[108], S. M. Farrington[52], F. Fassi[35e], D. Fassouliotis[9], M. Faucci Giannelli[76a,76b], W. J. Fawcett[32], L. Fayard[66], P. Federic[134], P. Federicova[132], O. L. Fedin[37,a], M. Feickert[171], L. Feligioni[103], D. E. Fellers[124], C. Feng[62b], M. Feng[14b], Z. Feng[115], M. J. Fenton[160], L. Ferencz[48], R. A. M. Ferguson[92], S. I. Fernandez Luengo[138f], P. Fernandez Martinez[13], M. J. V. Fernoux[103], J. Ferrando[92], A. Ferrari[162], P. Ferrari[114,115], R. Ferrari[73a], D. Ferrere[56], C. Ferretti[107], F. Fiedler[101], P. Fiedler[133], A. Filipčič[94], E. K. Filmer[1], F. Filthaut[114], M. C. N. Fiolhais[131a,131c,c], L. Fiorini[164], W. C. Fisher[108], T. Fitschen[102], P. M. Fitzhugh[136], I. Fleck[142], P. Fleischmann[107], T. Flick[172], M. Flores[33d,ab], L. R. Flores Castillo[64a], L. Flores Sanz De Acedo[36], F. M. Follega[78a,78b], N. Fomin[16], J. H. Foo[156], A. Formica[136], A. C. Forti[102], E. Fortin[36], A. W. Fortman[17a], M. G. Foti[17a], L. Fountas[9,j], D. Fournier[66], H. Fox[92], P. Francavilla[74a,74b], S. Francescato[61], S. Franchellucci[56], M. Franchini[23a,23b], S. Franchino[63a], D. Francis[36], L. Franco[114], V. Franco Lima[36], L. Franconi[48], M. Franklin[61], G. Frattari[26], W. S. Freund[83b], Y. Y. Frid[152], J. Friend[59], N. Fritzsche[50], A. Froch[54], D. Froidevaux[36], J. A. Frost[127], Y. Fu[62a], S. Fuenzalida Garrido[138f], M. Fujimoto[103], K. Y. Fung[64a], E. Furtado De Simas Filho[83e], M. Furukawa[154], J. Fuster[164], A. Gabrielli[23a,23b], A. Gabrielli[156], P. Gadow[36], G. Gagliardi[57a,57b], L. G. Gagnon[17a], S. Gaid[161], S. Galantzan[152], E. J. Gallas[127], B. J. Gallop[135], K. K. Gan[120], S. Ganguly[154], Y. Gao[52], F. M. Garay Walls[138a,138b], B. Garcia[29], C. García[164], A. Garcia Alonso[115], A. G. Garcia Caffaro[173], J. E. García Navarro[164], M. Garcia-Sciveres[17a], G. L. Gardner[129], R. W. Gardner[39], N. Garelli[159], D. Garg[80], R. B. Garg[144,m], J. M. Gargan[52], C. A. Garner[156], C. M. Garvey[33a], P. Gaspar[83b], V. K. Gassmann[159], G. Gaudio[73a], V. Gautam[13], P. Gauzzi[75a,75b], I. L. Gavrilenko[37], A. Gavrilyuk[37], C. Gay[165], G. Gaycken[48], E. N. Gazis[10], A. A. Geanta[27b], C. M. Gee[137], A. Gekow[120], C. Gemme[57b], M. H. Genest[60], A. D. Gentry[113], S. George[96], W. F. George[20], T. Geralis[46], P. Gessinger-Befurt[36], M. E. Geyik[172], M. Ghani[168], K. Ghorbanian[95], A. Ghosal[142], A. Ghosh[160], A. Ghosh[7], B. Giacobbe[23b], S. Giagu[75a,75b], T. Giani[115], P. Giannetti[74a], A. Giannini[62a], S. M. Gibson[96], M. Gignac[137], D. T. Gil[86b], A. K. Gilbert[86a], B. J. Gilbert[41], D. Gillberg[34], G. Gilles[115], L. Ginabat[128], D. M. Gingrich[2,ae], M. P. Giordani[69a,69c], P. F. Giraud[136], G. Giugliarelli[69a,69c], D. Giugni[71a], F. Giuli[36], I. Gkialas[9,j], L. K. Gladilin[37], C. Glasman[100], G. R. Gledhill[124], G. Glemža[48], M. Glisic[124], I. Gnesi[43b,f], Y. Go[29], M. Goblirsch-Kolb[36], B. Gocke[49], D. Godin[109], B. Gokturk[21a], S. Goldfarb[106], T. Golling[56], M. G. D. Gololo[33g], D. Golubkov[37], J. P. Gombas[108], A. Gomes[131a,131b], G. Gomes Da Silva[142], A. J. Gomez Delegido[164], R. Gonçalo[131a,131c], L. Gonella[20], A. Gongadze[150c], F. Gonnella[20], J. L. Gonski[144], R. Y. González Andana[52], S. González de la Hoz[164], R. Gonzalez Lopez[93], C. Gonzalez Renteria[17a], M. V. Gonzalez Rodrigues[48], R. Gonzalez Suarez[162], S. Gonzalez-Sevilla[56], L. Goossens[36], B. Gorini[36], E. Gorini[70a,70b], A. Gorišek[94], T. C. Gosart[129], A. T. Goshaw[51], M. I. Gostkin[38], S. Goswami[122], C. A. Gottardo[36], S. A. Gotz[110], M. Gouighri[35b], V. Goumarre[48], A. G. Goussiou[139], N. Govender[33c], I. Grabowska-Bold[86a], K. Graham[34], E. Gramstad[126], S. Grancagnolo[70a,70b], C. M. Grant[1,136], P. M. Gravila[27f], F. G. Gravili[70a,70b], H. M. Gray[17a], M. Greco[70a,70b], C. Grefe[24], I. M. Gregor[48], K. T. Greif[160], P. Grenier[144], S. G. Grewe[111], A. A. Grillo[137], K. Grimm[31], S. Grinstein[13,s], J.-F. Grivaz[66], E. Gross[170], J. Grosse-Knetter[55], J. C. Grundy[127], L. Guan[107], C. Gubbels[165], J. G. R. Guerrero Rojas[164], G. Guerrieri[69a,69c], F. Guescini[111], R. Gugel[101], J. A. M. Guhit[107], A. Guida[18], E. Guilloton[168], S. Guindon[36], F. Guo[14a,14e], J. Guo[62c], L. Guo[48], Y. Guo[107], R. Gupta[48], R. Gupta[130], S. Gurbuz[24],

S. S. Gurdasani[54], G. Gustavino[36], M. Guth[56], P. Gutierrez[121], L. F. Gutierrez Zagazeta[129], M. Gutsche[50], C. Gutschow[97], C. Gwenlan[127], C. B. Gwilliam[93], E. S. Haaland[126], A. Haas[118], M. Habedank[48], C. Haber[17a], H. K. Hadavand[8], A. Hadef[50], S. Hadzic[111], A. I. Hagan[92], J. J. Hahn[142], E. H. Haines[97], M. Haleem[167], J. Haley[122], J. J. Hall[140], G. D. Hallewell[103], L. Halser[19], K. Hamano[166], M. Hamer[24], G. N. Hamity[52], E. J. Hampshire[96], J. Han[62b], K. Han[62a], L. Han[14c], L. Han[62a], S. Han[17a], Y. F. Han[156], K. Hanagaki[84], M. Hance[137], D. A. Hangal[41], H. Hanif[143], M. D. Hank[129], J. B. Hansen[42], P. H. Hansen[42], K. Hara[158], D. Harada[56], T. Harenberg[172], S. Harkusha[37], M. L. Harris[104], Y. T. Harris[127], J. Harrison[13], N. M. Harrison[120], P. F. Harrison[168], N. M. Hartman[111], N. M. Hartmann[110], R. Z. Hasan[96,135], Y. Hasegawa[141], S. Hassan[16], R. Hauser[108], C. M. Hawkes[20], R. J. Hawkings[36], Y. Hayashi[154], S. Hayashida[112], D. Hayden[108], C. Hayes[107], R. L. Hayes[115], C. P. Hays[127], J. M. Hays[95], H. S. Hayward[93], F. He[62a], M. He[14a,14e], Y. He[155], Y. He[48], Y. He[97], N. B. Heatley[95], V. Hedberg[99], A. L. Heggelund[126], N. D. Hehir[95,*], C. Heidegger[54], K. K. Heidegger[54], W. D. Heidorn[81], J. Heilman[34], S. Heim[48], T. Heim[17a], J. G. Heinlein[129], J. J. Heinrich[124], L. Heinrich[111,ac], J. Hejbal[132], A. Held[171], S. Hellesund[16], C. M. Helling[165], S. Hellman[47a,47b], R. C. W. Henderson[92], L. Henkelmann[32], A. M. Henriques Correia[36], H. Herde[99], Y. Hernández Jiménez[146], L. M. Herrmann[24], T. Herrmann[50], G. Herten[54], R. Hertenberger[110], L. Hervas[36], M. E. Hesping[101], N. P. Hessey[157a], M. Hidaoui[35b], E. Hill[156], S. J. Hillier[20], J. R. Hinds[108], F. Hinterkeuser[24], M. Hirose[125], S. Hirose[158], D. Hirschbuehl[172], T. G. Hitchings[102], B. Hiti[94], J. Hobbs[146], R. Hobincu[27e], N. Hod[170], M. C. Hodgkinson[140], B. H. Hodkinson[127], A. Hoecker[36], D. D. Hofer[107], J. Hofer[48], T. Holm[24], M. Holzbock[111], L. B. A. H. Hommels[32], B. P. Honan[102], J. Hong[62c], T. M. Hong[130], B. H. Hooberman[163], W. H. Hopkins[6], Y. Horii[112], S. Hou[149], A. S. Howard[94], J. Howarth[59], J. Hoya[6], M. Hrabovsky[123], A. Hrynevich[48], T. Hryn'ova[4], P. J. Hsu[65], S.-C. Hsu[139], T. Hsu[66], M. Hu[17a], Q. Hu[62a], S. Huang[64b], X. Huang[14a,14e], Y. Huang[140], Y. Huang[101], Y. Huang[14a], Z. Huang[102], Z. Hubacek[133], M. Huebner[24], F. Huegging[24], T. B. Huffman[127], C. A. Hugli[48], M. Huhtinen[36], S. K. Huiberts[16], R. Hulsken[105], N. Huseynov[12], J. Huston[108], J. Huth[61], R. Hyneman[144], G. Iacobucci[56], G. Iakovidis[29], I. Ibragimov[142], L. Iconomidou-Fayard[66], J. P. Iddon[36], P. Iengo[72a,72b], R. Iguchi[154], T. Iizawa[127], Y. Ikegami[84], N. Ilic[156], H. Imam[35a], M. Ince Lezki[56], T. Ingebretsen Carlson[47a,47b], G. Introzzi[73a,73b], M. Iodice[77a], V. Ippolito[75a,75b], R. K. Irwin[93], M. Ishino[154], W. Islam[171], C. Issever[18,48], S. Istin[21a,ai], H. Ito[169], R. Iuppa[78a,78b], A. Ivina[170], J. M. Izen[45], V. Izzo[72a], P. Jacka[132,133], P. Jackson[1], B. P. Jaeger[143], C. S. Jagfeld[110], G. Jain[157a], P. Jain[54], K. Jakobs[54], T. Jakoubek[170], J. Jamieson[59], K. W. Janas[86a], M. Javurkova[104], L. Jeanty[124], J. Jejelava[150a,z], P. Jenni[54,g], C. E. Jessiman[34], C. Jia[62b], J. Jia[146], X. Jia[61], X. Jia[14a,14e], Z. Jia[14c], C. Jiang[52], S. Jiggins[48], J. Jimenez Pena[13], S. Jin[14c], A. Jinaru[27b], O. Jinnouchi[155], P. Johansson[140], K. A. Johns[7], J. W. Johnson[137], D. M. Jones[147], E. Jones[48], P. Jones[32], R. W. L. Jones[92], T. J. Jones[93], H. L. Joos[36,55], R. Joshi[120], J. Jovicevic[15], X. Ju[17a], J. J. Junggeburth[104], T. Junkermann[63a], A. Juste Rozas[13,s], M. K. Juzek[87], S. Kabana[138e], A. Kaczmarska[87], M. Kado[111], H. Kagan[120], M. Kagan[144], A. Kahn[41], A. Kahn[129], C. Kahra[101], T. Kaji[154], E. Kajomovitz[151], N. Kakati[170], I. Kalaitzidou[54], C. W. Kalderon[29], N. J. Kang[137], D. Kar[33g], K. Karava[127], M. J. Kareem[157b], E. Karentzos[54], I. Karkanias[153], O. Karkout[115], S. N. Karpov[38], Z. M. Karpova[38], V. Kartvelishvili[92], A. N. Karyukhin[37], E. Kasimi[153], J. Katzy[48], S. Kaur[34], K. Kawade[141], M. P. Kawale[121], C. Kawamoto[88], T. Kawamoto[62a], E. F. Kay[36], F. I. Kaya[159], S. Kazakos[108], V. F. Kazanin[37], Y. Ke[146], J. M. Keaveney[33a], R. Keeler[166], G. V. Kehris[61], J. S. Keller[34], A. S. Kelly[97], J. J. Kempster[147], P. D. Kennedy[101], O. Kepka[132], B. P. Kerridge[135], S. Kersten[172], B. P. Kerševan[94], L. Keszeghova[28a], S. Ketabchi Haghighat[156], R. A. Khan[130], A. Khanov[122], A. G. Kharlamov[37], T. Kharlamova[37], E. E. Khoda[139], M. Kholodenko[37], T. J. Khoo[18], G. Khoriauli[167], J. Khubua[150b,*], Y. A. R. Khwaira[66], B. Kibirige[33g], A. Kilgallon[124], D. W. Kim[47a,47b], Y. K. Kim[39], N. Kimura[97], M. K. Kingston[55], A. Kirchhoff[55], C. Kirfel[24], F. Kirfel[24], J. Kirk[135], A. E. Kiryunin[111], C. Kitsaki[10], O. Kivernyk[24], M. Klassen[159], C. Klein[34], L. Klein[167], M. H. Klein[44], S. B. Klein[56], U. Klein[93], P. Klimek[36], A. Klimentov[29], T. Klioutchnikova[36], P. Kluit[115], S. Kluth[111], E. Kneringer[79], T. M. Knight[156], A. Knue[49], R. Kobayashi[88], D. Kobylianskii[170], S. F. Koch[127], M. Kocian[144], P. Kodyš[134], D. M. Koeck[124], P. T. Koenig[24], T. Koffas[34], O. Kolay[50], I. Koletsou[4], T. Komarek[123], K. Köneke[54], A. X. Y. Kong[1], T. Kono[119], N. Konstantinidis[97], P. Kontaxakis[56], B. Konya[99], R. Kopeliansky[41], S. Koperny[86a], K. Korcyl[87], K. Kordas[153,e], A. Korn[97], S. Korn[55], I. Korolkov[13], N. Korotkova[37], B. Kortman[115], O. Kortner[111], S. Kortner[111], W. H. Kostecka[116], V. V. Kostyukhin[142], A. Kotsokechagia[136], A. Kotwal[51], A. Koulouris[36], A. Kourkoumeli-Charalampidi[73a,73b], C. Kourkoumelis[9], E. Kourlitis[111,ac], O. Kovanda[124],

R. Kowalewski[166], W. Kozanecki[136], A. S. Kozhin[37], V. A. Kramarenko[37], G. Kramberger[94], P. Kramer[101], M. W. Krasny[128], A. Krasznahorkay[36], J. W. Kraus[172], J. A. Kremer[48], T. Kresse[50], J. Kretzschmar[93], K. Kreul[18], P. Krieger[156], S. Krishnamurthy[104], M. Krivos[134], K. Krizka[20], K. Kroeninger[49], H. Kroha[111], J. Kroll[132], J. Kroll[129], K. S. Krowpman[108], U. Kruchonak[38], H. Krüger[24], N. Krumnack[81], M. C. Kruse[51], O. Kuchinskaia[37], S. Kuday[3a], S. Kuehn[36], R. Kuesters[54], T. Kuhl[48], V. Kukhtin[38], Y. Kulchitsky[37,a], S. Kuleshov[138b,138d], M. Kumar[33g], N. Kumari[48], P. Kumari[157b], A. Kupco[132], T. Kupfer[49], A. Kupich[37], O. Kuprash[54], H. Kurashige[85], L. L. Kurchaninov[157a], O. Kurdysh[66], Y. A. Kurochkin[37], A. Kurova[37], M. Kuze[155], A. K. Kvam[104], J. Kvita[123], T. Kwan[105], N. G. Kyriacou[107], L. A. O. Laatu[103], C. Lacasta[164], F. Lacava[75a,75b], H. Lacker[18], D. Lacour[128], N. N. Lad[97], E. Ladygin[38], A. Lafarge[40], B. Laforge[128], T. Lagouri[173], F. Z. Lahbabi[35a], S. Lai[55], I. K. Lakomiec[86a], J. E. Lambert[166], S. Lammers[68], W. Lampl[7], C. Lampoudis[153,e], G. Lamprinoudis[101], A. N. Lancaster[116], E. Lançon[29], U. Landgraf[54], M. P. J. Landon[95], V. S. Lang[54], O. K. B. Langrekken[126], A. J. Lankford[160], F. Lanni[36], K. Lantzsch[24], A. Lanza[73a], A. Lapertosa[57a,57b], J. F. Laporte[136], T. Lari[71a], F. Lasagni Manghi[23b], M. Lassnig[36], V. Latonova[132], A. Laudrain[101], A. Laurier[151], S. D. Lawlor[140], Z. Lawrence[102], R. Lazaridou[168], M. Lazzaroni[71a,71b], B. Le[102], E. M. Le Boulicaut[51], L. T. Le Pottier[17a], B. Leban[23a,23b], A. Lebedev[81], M. LeBlanc[102], F. Ledroit-Guillon[60], S. C. Lee[149], S. Lee[47a,47b], T. F. Lee[93], L. L. Leeuw[33c], H. P. Lefebvre[96], M. Lefebvre[166], C. Leggett[17a], G. Lehmann Miotto[36], M. Leigh[56], W. A. Leight[104], W. Leinonen[114], A. Leisos[153,r], M. A. L. Leite[83c], C. E. Leitgeb[18], R. Leitner[134], K. J. C. Leney[44], T. Lenz[24], S. Leone[74a], C. Leonidopoulos[52], A. Leopold[145], C. Leroy[109], R. Les[108], C. G. Lester[32], M. Levchenko[37], J. Levêque[4], L. J. Levinson[170], G. Levrini[23a,23b], M. P. Lewicki[87], C. Lewis[139], D. J. Lewis[4], A. Li[5], B. Li[62b], C. Li[62a], C.-Q. Li[111], H. Li[62a], H. Li[62b], H. Li[14c], H. Li[14b], H. Li[62b], J. Li[62c], K. Li[139], L. Li[62c], M. Li[14a,14e], Q. Y. Li[62a], S. Li[14a,14e], S. Li[62c,62d,d], T. Li[5], X. Li[105], Z. Li[127], Z. Li[154], Z. Li[14a,14e], S. Liang[14a,14e], Z. Liang[14a], M. Liberatore[136], B. Liberti[76a], K. Lie[64c], J. Lieber Marin[83e], H. Lien[68], K. Lin[108], R. E. Lindley[7], J. H. Lindon[2], E. Lipeles[129], A. Lipniacka[16], A. Lister[165], J. D. Little[4], B. Liu[14a], B. X. Liu[143], D. Liu[62c,62d], E. H. L. Liu[20], J. B. Liu[62a], J. K. K. Liu[32], K. Liu[62d], K. Liu[62c,62d], M. Liu[62a], M. Y. Liu[62a], P. Liu[14a], Q. Liu[62c,62d,139], X. Liu[62a], X. Liu[62b], Y. Liu[14d,14e], Y. L. Liu[62b], Y. W. Liu[62a], J. Llorente Merino[143], S. L. Lloyd[95], E. M. Lobodzinska[48], P. Loch[7], T. Lohse[18], K. Lohwasser[140], E. Loiacono[48], M. Lokajicek[132,*], J. D. Lomas[20], J. D. Long[163], I. Longarini[160], L. Longo[70a,70b], R. Longo[163], I. Lopez Paz[67], A. Lopez Solis[48], N. Lorenzo Martinez[4], A. M. Lory[110], G. Löschcke Centeno[147], O. Loseva[37], X. Lou[47a,47b], X. Lou[14a,14e], A. Lounis[66], P. A. Love[92], G. Lu[14a,14e], M. Lu[66], S. Lu[129], Y. J. Lu[65], H. J. Lubatti[139], C. Luci[75a,75b], F. L. Lucio Alves[14c], F. Luehring[68], I. Luise[146], O. Lukianchuk[66], O. Lundberg[145], B. Lund-Jensen[145,*], N. A. Luongo[6], M. S. Lutz[36], A. B. Lux[25], D. Lynn[29], R. Lysak[132], E. Lytken[99], V. Lyubushkin[38], T. Lyubushkina[38], M. M. Lyukova[146], M.Firdaus M. Soberi[52], H. Ma[29], K. Ma[62a], L. L. Ma[62b], W. Ma[62a], Y. Ma[122], D. M. Mac Donell[166], G. Maccarrone[53], J. C. MacDonald[101], P. C. Machado De Abreu Farias[83e], R. Madar[40], T. Madula[97], J. Maeda[85], T. Maeno[29], H. Maguire[140], V. Maiboroda[136], A. Maio[131a,131b,131d], K. Maj[86a], O. Majersky[48], S. Majewski[124], N. Makovec[66], V. Maksimovic[15], B. Malaescu[128], Pa. Malecki[87], V. P. Maleev[37], F. Malek[60,n], M. Mali[94], D. Malito[96], U. Mallik[80], S. Maltezos[10], S. Malyukov[38], J. Mamuzic[13], G. Mancini[53], M. N. Mancini[26], G. Manco[73a,73b], J. P. Mandalia[95], I. Mandić[94], L. Manhaes de Andrade Filho[83a], I. M. Maniatis[170], J. Manjarres Ramos[90], D. C. Mankad[170], A. Mann[110], S. Manzoni[36], L. Mao[62c], X. Mapekula[33c], A. Marantis[153,r], G. Marchiori[5], M. Marcisovsky[132], C. Marcon[71a], M. Marinescu[20], S. Marium[48], M. Marjanovic[121], A. Markhoos[54], M. Markovitch[66], E. J. Marshall[92], Z. Marshall[17a], S. Marti-Garcia[164], T. A. Martin[168], V. J. Martin[52], B. Martin dit Latour[16], L. Martinelli[75a,75b], M. Martinez[13,s], P. Martinez Agullo[164], V. I. Martinez Outschoorn[104], P. Martinez Suarez[13], S. Martin-Haugh[135], G. Martinovicova[134], V. S. Martoiu[27b], A. C. Martyniuk[97], A. Marzin[36], D. Mascione[78a,78b], L. Masetti[101], T. Mashimo[154], J. Masik[102], A. L. Maslennikov[37], P. Massarotti[72a,72b], P. Mastrandrea[74a,74b], A. Mastroberardino[43a,43b], T. Masubuchi[154], T. Mathisen[162], J. Matousek[134], N. Matsuzawa[154], J. Maurer[27b], A. J. Maury[66], B. Maček[94], D. A. Maximov[37], A. E. May[102], R. Mazini[149], I. Maznas[116], M. Mazza[108], S. M. Mazza[137], E. Mazzeo[71a,71b], C. Mc Ginn[29], J. P. Mc Gowan[166], S. P. Mc Kee[107], C. C. McCracken[165], E. F. McDonald[106], A. E. McDougall[115], J. A. Mcfayden[147], R. P. McGovern[129], G. Mchedlidze[150b], R. P. Mckenzie[33g], T. C. Mclachlan[48], D. J. Mclaughlin[97], S. J. McMahon[135], C. M. Mcpartland[93], R. A. McPherson[166,w], S. Mehlhase[110], A. Mehta[93], D. Melini[164], B. R. Mellado Garcia[33g], A. H. Melo[55], F. Meloni[48], A. M. Mendes Jacques Da Costa[102], H. Y. Meng[156], L. Meng[92], S. Menke[111], M. Mentink[36],

E. Meoni[43a,43b], G. Mercado[116], C. Merlassino[69a,69c], L. Merola[72a,72b], C. Meroni[71a,71b], J. Metcalfe[6], A. S. Mete[6], C. Meyer[68], J.-P. Meyer[136], R. P. Middleton[135], L. Mijović[52], G. Mikenberg[170], M. Mikestikova[132], M. Mikuž[94], H. Mildner[101], A. Milic[36], D. W. Miller[39], E. H. Miller[144], L. S. Miller[34], A. Milov[170], D. A. Milstead[47a,47b], T. Min[14c], A. A. Minaenko[37], I. A. Minashvili[150b], L. Mince[59], A. I. Mincer[118], B. Mindur[86a], M. Mineev[38], Y. Mino[88], L. M. Mir[13], M. Miralles Lopez[59], M. Mironova[17a], A. Mishima[154], M. C. Missio[114], A. Mitra[168], V. A. Mitsou[164], Y. Mitsumori[112], O. Miu[156], P. S. Miyagawa[95], T. Mkrtchyan[63a], M. Mlinarevic[97], T. Mlinarevic[97], M. Mlynarikova[36], S. Mobius[19], P. Mogg[110], M. H. Mohamed Farook[113], A. F. Mohammed[14a,14e], S. Mohapatra[41], G. Mokgatitswane[33g], L. Moleri[170], B. Mondal[142], S. Mondal[133], K. Mönig[48], E. Monnier[103], L. Monsonis Romero[164], J. Montejo Berlingen[13], M. Montella[120], F. Montereali[77a,77b], F. Monticelli[91], S. Monzani[69a,69c], N. Morange[66], A. L. Moreira De Carvalho[48], M. Moreno Llácer[164], C. Moreno Martinez[56], P. Morettini[57b], S. Morgenstern[36], M. Morii[61], M. Morinaga[154], F. Morodei[75a,75b], L. Morvaj[36], P. Moschovakos[36], B. Moser[36], M. Mosidze[150b], T. Moskalets[54], P. Moskvitina[114], J. Moss[31,k], P. Moszkowicz[86a], A. Moussa[35d], E. J. W. Moyse[104], O. Mtintsilana[33g], S. Muanza[103], J. Mueller[130], D. Muenstermann[92], R. Müller[19], G. A. Mullier[162], A. J. Mullin[32], J. J. Mullin[129], D. P. Mungo[156], D. Munoz Perez[164], F. J. Munoz Sanchez[102], M. Murin[102], W. J. Murray[135,168], M. Muškinja[94], C. Mwewa[29], A. G. Myagkov[37,a], A. J. Myers[8], G. Myers[107], M. Myska[133], B. P. Nachman[17a], O. Nackenhorst[49], K. Nagai[127], K. Nagano[84], J. L. Nagle[29,ag], E. Nagy[103], A. M. Nairz[36], Y. Nakahama[84], K. Nakamura[84], K. Nakkalil[5], H. Nanjo[125], R. Narayan[44], E. A. Narayanan[113], I. Naryshkin[37], M. Naseri[34], S. Nasri[117b], C. Nass[24], G. Navarro[22a], J. Navarro-Gonzalez[164], R. Nayak[152], A. Nayaz[18], P. Y. Nechaeva[37], S. Nechaeva[23a,23b], F. Nechansky[48], L. Nedic[127], T. J. Neep[20], A. Negri[73a,73b], M. Negrini[23b], C. Nellist[115], C. Nelson[105], K. Nelson[107], S. Nemecek[132], M. Nessi[36,h], M. S. Neubauer[163], F. Neuhaus[101], J. Neundorf[48], R. Newhouse[165], P. R. Newman[20], C. W. Ng[130], Y. W. Y. Ng[48], B. Ngair[117a], H. D. N. Nguyen[109], R. B. Nickerson[127], R. Nicolaidou[136], J. Nielsen[137], M. Niemeyer[55], J. Niermann[55], N. Nikiforou[36], V. Nikolaenko[37,a], I. Nikolic-Audit[128], K. Nikolopoulos[20], P. Nilsson[29], I. Ninca[48], H. R. Nindhito[56], G. Ninio[152], A. Nisati[75a], N. Nishu[2], R. Nisius[111], J.-E. Nitschke[50], E. K. Nkadimeng[33g], T. Nobe[154], D. L. Noel[32], T. Nommensen[148], M. B. Norfolk[140], R. R. B. Norisam[97], B. J. Norman[34], M. Noury[35a], J. Novak[94], T. Novak[48], L. Novotny[133], R. Novotny[113], L. Nozka[123], K. Ntekas[160], N. M. J. Nunes De Moura Junior[83b], J. Ocariz[128], A. Ochi[85], I. Ochoa[131a], S. Oerdek[48,t], J. T. Offermann[39], A. Ogrodnik[134], A. Oh[102], C. C. Ohm[145], H. Oide[84], R. Oishi[154], M. L. Ojeda[48], Y. Okumura[154], L. F. Oleiro Seabra[131a], S. A. Olivares Pino[138d], G. Oliveira Correa[13], D. Oliveira Damazio[29], D. Oliveira Goncalves[83a], J. L. Oliver[160], Ö. O. Öncel[54], A. P. O'Neill[19], A. Onofre[131a,131e], P. U. E. Onyisi[11], M. J. Oreglia[39], G. E. Orellana[91], D. Orestano[77a,77b], N. Orlando[13], R. S. Orr[156], V. O'Shea[59], L. M. Osojnak[129], R. Ospanov[62a], G. Otero y Garzon[30], H. Otono[89], P. S. Ott[63a], G. J. Ottino[17a], M. Ouchrif[35d], F. Ould-Saada[126], T. Ovsiannikova[139], M. Owen[59], R. E. Owen[135], K. Y. Oyulmaz[21a], V. E. Ozcan[21a], F. Ozturk[87], N. Ozturk[8], S. Ozturk[82], H. A. Pacey[127], A. Pacheco Pages[13], C. Padilla Aranda[13], G. Padovano[75a,75b], S. Pagan Griso[17a], G. Palacino[68], A. Palazzo[70a,70b], J. Pampel[24], J. Pan[173], T. Pan[64a], D. K. Panchal[11], C. E. Pandini[115], J. G. Panduro Vazquez[96], H. D. Pandya[1], H. Pang[14b], P. Pani[48], G. Panizzo[69a,69c], L. Panwar[128], L. Paolozzi[56], S. Parajuli[163], A. Paramonov[6], C. Paraskevopoulos[53], D. Paredes Hernandez[64b], A. Pareti[73a,73b], K. R. Park[41], T. H. Park[156], M. A. Parker[32], F. Parodi[57a,57b], E. W. Parrish[116], V. A. Parrish[52], J. A. Parsons[41], U. Parzefall[54], B. Pascual Dias[109], L. Pascual Dominguez[152], E. Pasqualucci[75a], S. Passaggio[57b], F. Pastore[96], P. Patel[87], U. M. Patel[51], J. R. Pater[102], T. Pauly[36], C. I. Pazos[159], J. Pearkes[144], M. Pedersen[126], R. Pedro[131a], S. V. Peleganchuk[37], O. Penc[36], E. A. Pender[52], G. D. Penn[173], K. E. Penski[110], M. Penzin[37], B. S. Peralva[83d], A. P. Pereira Peixoto[139], L. Pereira Sanchez[144], D. V. Perepelitsa[29,ag], E. Perez Codina[157a], M. Perganti[10], H. Pernegger[36], O. Perrin[40], K. Peters[48], R. F. Y. Peters[102], B. A. Petersen[36], T. C. Petersen[42], E. Petit[103], V. Petousis[133], C. Petridou[153,e], T. Petru[134], A. Petrukhin[142], M. Pettee[17a], N. E. Pettersson[36], A. Petukhov[37], K. Petukhova[134], R. Pezoa[138f], L. Pezzotti[36], G. Pezzullo[173], T. M. Pham[171], T. Pham[106], P. W. Phillips[135], G. Piacquadio[146], E. Pianori[17a], F. Piazza[124], R. Piegaia[30], D. Pietreanu[27b], A. D. Pilkington[102], M. Pinamonti[69a,69c], J. L. Pinfold[2], B. C. Pinheiro Pereira[131a], A. E. Pinto Pinoargote[101,136], L. Pintucci[69a,69c], K. M. Piper[147], A. Pirttikoski[56], D. A. Pizzi[34], L. Pizzimento[64b], A. Pizzini[115], M.-A. Pleier[29], V. Plesanovs[54], V. Pleskot[134], E. Plotnikova[38], G. Poddar[95], R. Poettgen[99], L. Poggioli[128], I. Pokharel[55], S. Polacek[134], G. Polesello[73a], A. Poley[143,157a], A. Polini[23b], C. S. Pollard[168], Z. B. Pollock[120],

E. Pompa Pacchi[75a,75b], D. Ponomarenko[114], L. Pontecorvo[36], S. Popa[27a], G. A. Popeneciu[27d], A. Poreba[36], D. M. Portillo Quintero[157a], S. Pospisil[133], M. A. Postill[140], P. Postolache[27c], K. Potamianos[168], P. A. Potepa[86a], I. N. Potrap[38], C. J. Potter[32], H. Potti[1], J. Poveda[164], M. E. Pozo Astigarraga[36], A. Prades Ibanez[164], J. Pretel[54], D. Price[102], M. Primavera[70a], M. A. Principe Martin[100], R. Privara[123], T. Procter[59], M. L. Proffitt[139], N. Proklova[129], K. Prokofiev[64c], G. Proto[111], J. Proudfoot[6], M. Przybycien[86a], W. W. Przygoda[86b], A. Psallidas[46], J. E. Puddefoot[140], D. Pudzha[37], D. Pyatiizbyantseva[37], J. Qian[107], D. Qichen[102], Y. Qin[13], T. Qiu[52], A. Quadt[55], M. Queitsch-Maitland[102], G. Quetant[56], R. P. Quinn[165], G. Rabanal Bolanos[61], D. Rafanoharana[54], F. Ragusa[71a,71b], J. L. Rainbolt[39], J. A. Raine[56], S. Rajagopalan[29], E. Ramakoti[37], I. A. Ramirez-Berend[34], K. Ran[14e,48], N. P. Rapheeha[33g], H. Rasheed[27b], V. Raskina[128], D. F. Rassloff[63a], A. Rastogi[17a], S. Rave[101], B. Ravina[55], I. Ravinovich[170], M. Raymond[36], A. L. Read[126], N. P. Readioff[140], D. M. Rebuzzi[73a,73b], G. Redlinger[29], A. S. Reed[111], K. Reeves[26], J. A. Reidelsturz[172], D. Reikher[152], A. Rej[49], C. Rembser[36], M. Renda[27b], M. B. Rendel[111], F. Renner[48], A. G. Rennie[160], A. L. Rescia[48], S. Resconi[71a], M. Ressegotti[57a,57b], S. Rettie[36], J. G. Reyes Rivera[108], E. Reynolds[17a], O. L. Rezanova[37], P. Reznicek[134], H. Riani[35d], N. Ribaric[92], E. Ricci[78a,78b], R. Richter[111], S. Richter[47a,47b], E. Richter-Was[86b], M. Ridel[128], S. Ridouani[35d], P. Rieck[118], P. Riedler[36], E. M. Riefel[47a,47b], J. O. Rieger[115], M. Rijssenbeek[146], M. Rimoldi[36], L. Rinaldi[23a,23b], T. T. Rinn[29], M. P. Rinnagel[110], G. Ripellino[162], I. Riu[13], J. C. Rivera Vergara[166], F. Rizatdinova[122], E. Rizvi[95], B. R. Roberts[17a], S. H. Robertson[105,w], D. Robinson[32], C. M. Robles Gajardo[138f], M. Robles Manzano[101], A. Robson[59], A. Rocchi[76a,76b], C. Roda[74a,74b], S. Rodriguez Bosca[36], Y. Rodriguez Garcia[22a], A. Rodriguez Rodriguez[54], A. M. Rodríguez Vera[116], S. Roe[36], J. T. Roemer[160], A. R. Roepe-Gier[137], J. Roggel[172], O. Røhne[126], R. A. Rojas[104], C. P. A. Roland[128], J. Roloff[29], A. Romaniouk[37], E. Romano[73a,73b], M. Romano[23b], A. C. Romero Hernandez[163], N. Rompotis[93], L. Roos[128], S. Rosati[75a], B. J. Rosser[39], E. Rossi[127], E. Rossi[72a,72b], L. P. Rossi[61], L. Rossini[54], R. Rosten[120], M. Rotaru[27b], B. Rottler[54], C. Rougier[90], D. Rousseau[66], D. Rousso[48], A. Roy[163], S. Roy-Garand[156], A. Rozanov[103], Z. M. A. Rozario[59], Y. Rozen[151], A. Rubio Jimenez[164], A. J. Ruby[93], V. H. Ruelas Rivera[18], T. A. Ruggeri[1], A. Ruggiero[127], A. Ruiz-Martinez[164], A. Rummler[36], Z. Rurikova[54], N. A. Rusakovich[38], H. L. Russell[166], G. Russo[75a,75b], J. P. Rutherfoord[7], S. Rutherford Colmenares[32], K. Rybacki[92], M. Rybar[134], E. B. Rye[126], A. Ryzhov[44], J. A. Sabater Iglesias[56], P. Sabatini[164], H.F.-W. Sadrozinski[137], F. Safai Tehrani[75a], B. Safarzadeh Samani[135], S. Saha[1], M. Sahinsoy[111], A. Saibel[164], M. Saimpert[136], M. Saito[154], T. Saito[154], A. Sala[71a,71b], D. Salamani[36], A. Salnikov[144], J. Salt[164], A. Salvador Salas[152], D. Salvatore[43a,43b], F. Salvatore[147], A. Salzburger[36], D. Sammel[54], E. Sampson[92], D. Sampsonidis[153,e], D. Sampsonidou[124], J. Sánchez[164], V. Sanchez Sebastian[164], H. Sandaker[126], C. O. Sander[48], J. A. Sandesara[104], M. Sandhoff[172], C. Sandoval[22b], D. P. C. Sankey[135], T. Sano[88], A. Sansoni[53], L. Santi[75a,75b], C. Santoni[40], H. Santos[131a,131b], A. Santra[170], E. Sanzani[23a,23b], K. A. Saoucha[161], J. G. Saraiva[131a,131d], J. Sardain[7], O. Sasaki[84], K. Sato[158], C. Sauer[63b], F. Sauerburger[54], E. Sauvan[4], P. Savard[156,ae], R. Sawada[154], C. Sawyer[135], L. Sawyer[98], I. Sayago Galvan[164], C. Sbarra[23b], A. Sbrizzi[23a,23b], T. Scanlon[97], J. Schaarschmidt[139], U. Schäfer[101], A. C. Schaffer[44,66], D. Schaile[110], R. D. Schamberger[146], C. Scharf[18], M. M. Schefer[19], V. A. Schegelsky[37], D. Scheirich[134], F. Schenck[18], M. Schernau[160], C. Scheulen[55], C. Schiavi[57a,57b], M. Schioppa[43a,43b], B. Schlag[144,m], K. E. Schleicher[54], S. Schlenker[36], J. Schmeing[172], M. A. Schmidt[172], K. Schmieden[101], C. Schmitt[101], N. Schmitt[101], S. Schmitt[48], L. Schoeffel[136], A. Schoening[63b], P. G. Scholer[34], E. Schopf[127], M. Schott[101], J. Schovancova[36], S. Schramm[56], T. Schroer[56], H.-C. Schultz-Coulon[63a], M. Schumacher[54], B. A. Schumm[137], Ph. Schune[136], A. J. Schuy[139], H. R. Schwartz[137], A. Schwartzman[144], T. A. Schwarz[107], Ph. Schwemling[136], R. Schwienhorst[108], A. Sciandra[29], G. Sciolla[26], F. Scuri[74a], C. D. Sebastiani[93], K. Sedlaczek[116], P. Seema[18], S. C. Seidel[113], A. Seiden[137], B. D. Seidlitz[41], C. Seitz[48], J. M. Seixas[83b], G. Sekhniaidze[72a], L. Selem[60], N. Semprini-Cesari[23a,23b], D. Sengupta[56], V. Senthilkumar[164], L. Serin[66], L. Serkin[69a,69b], M. Sessa[76a,76b], H. Severini[121], F. Sforza[57a,57b], A. Sfyrla[56], Q. Sha[14a], E. Shabalina[55], A. H. Shah[32], R. Shaheen[145], J. D. Shahinian[129], D. Shaked Renous[170], L. Y. Shan[14a], M. Shapiro[17a], A. Sharma[36], A. S. Sharma[165], P. Sharma[80], P. B. Shatalov[37], K. Shaw[147], S. M. Shaw[102], A. Shcherbakova[37], Q. Shen[5,62c], D. J. Sheppard[143], P. Sherwood[97], L. Shi[97], X. Shi[14a], C. O. Shimmin[173], J. D. Shinner[96], I. P. J. Shipsey[127], S. Shirabe[89], M. Shiyakova[38,u], J. Shlomi[170], M. J. Shochet[39], J. Shojaii[106], D. R. Shope[126], B. Shrestha[121], S. Shrestha[120,ah], E. M. Shrif[33g], M. J. Shroff[166], P. Sicho[132], A. M. Sickles[163], E. Sideras Haddad[33g], A. C. Sidley[115], A. Sidoti[23b], F. Siegert[50], Dj. Sijacki[15], F. Sili[91], J. M. Silva[52], M. V. Silva Oliveira[29], S. B. Silverstein[47a], S. Simion[66], R. Simoniello[36],

E. L. Simpson[102], H. Simpson[147], L. R. Simpson[107], N. D. Simpson[99], S. Simsek[82], S. Sindhu[55], P. Sinervo[156], S. Singh[156], S. Sinha[48], S. Sinha[102], M. Sioli[23a,23b], I. Siral[36], E. Sitnikova[48], J. Sjölin[47a,47b], A. Skaf[55], E. Skorda[20], P. Skubic[121], M. Slawinska[87], V. Smakhtin[170], B. H. Smart[135], S.Yu. Smirnov[37], Y. Smirnov[37], L. N. Smirnova[37,a], O. Smirnova[99], A. C. Smith[41], D. R. Smith[160], E. A. Smith[39], H. A. Smith[127], J. L. Smith[102], R. Smith[144], M. Smizanska[92], K. Smolek[133], A. A. Snesarev[37], S. R. Snider[156], H. L. Snoek[115], S. Snyder[29], R. Sobie[166,w], A. Soffer[152], C. A. Solans Sanchez[36], E.Yu. Soldatov[37], U. Soldevila[164], A. A. Solodkov[37], S. Solomon[26], A. Soloshenko[38], K. Solovieva[54], O. V. Solovyanov[40], P. Sommer[36], A. Sonay[13], W. Y. Song[157b], A. Sopczak[133], A. L. Sopio[97], F. Sopkova[28b], J. D. Sorenson[113], I. R. Sotarriva Alvarez[155], V. Sothilingam[63a], O. J. Soto Sandoval[138b,138c], S. Sottocornola[68], R. Soualah[161], Z. Soumaimi[35e], D. South[48], N. Soybelman[170], S. Spagnolo[70a,70b], M. Spalla[111], D. Sperlich[54], G. Spigo[36], S. Spinali[92], D. P. Spiteri[59], M. Spousta[134], E. J. Staats[34], R. Stamen[63a], A. Stampekis[20], M. Standke[24], E. Stanecka[87], W. Stanek-Maslouska[48], M. V. Stange[50], B. Stanislaus[17a], M. M. Stanitzki[48], B. Stapf[48], E. A. Starchenko[37], G. H. Stark[137], J. Stark[90], P. Staroba[132], P. Starovoitov[63a], S. Stärz[105], R. Staszewski[87], G. Stavropoulos[46], J. Steentoft[162], P. Steinberg[29], B. Stelzer[143,157a], H. J. Stelzer[130], O. Stelzer-Chilton[157a], H. Stenzel[58], T. J. Stevenson[147], G. A. Stewart[36], J. R. Stewart[122], M. C. Stockton[36], G. Stoicea[27b], M. Stolarski[131a], S. Stonjek[111], A. Straessner[50], J. Strandberg[145], S. Strandberg[47a,47b], M. Stratmann[172], M. Strauss[121], T. Strebler[103], P. Strizenec[28b], R. Ströhmer[167], D. M. Strom[124], R. Stroynowski[44], A. Strubig[47a,47b], S. A. Stucci[29], B. Stugu[16], J. Stupak[121], N. A. Styles[48], D. Su[144], S. Su[62a], W. Su[62d], X. Su[62a], D. Suchy[28a], K. Sugizaki[154], V. V. Sulin[37], M. J. Sullivan[93], D. M. S. Sultan[127], L. Sultanaliyeva[37], S. Sultansoy[3b], T. Sumida[88], S. Sun[107], S. Sun[171], O. Sunneborn Gudnadottir[162], N. Sur[103], M. R. Sutton[147], H. Suzuki[158], M. Svatos[132], M. Swiatlowski[157a], T. Swirski[167], I. Sykora[28a], M. Sykora[134], T. Sykora[134], D. Ta[101], K. Tackmann[48,t], A. Taffard[160], R. Tafirout[157a], J. S. Tafoya Vargas[66], Y. Takubo[84], M. Talby[103], A. A. Talyshev[37], K. C. Tam[64b], N. M. Tamir[152], A. Tanaka[154], J. Tanaka[154], R. Tanaka[66], M. Tanasini[146], Z. Tao[165], S. Tapia Araya[138f], S. Tapprogge[101], A. Tarek Abouelfadl Mohamed[108], S. Tarem[151], K. Tariq[14a], G. Tarna[27b], G. F. Tartarelli[71a], M. J. Tartarin[90], P. Tas[134], M. Tasevsky[132], E. Tassi[43a,43b], A. C. Tate[163], G. Tateno[154], Y. Tayalati[35e,v], G. N. Taylor[106], W. Taylor[157b], A. S. Tee[171], R. Teixeira De Lima[144], P. Teixeira-Dias[96], J. J. Teoh[156], K. Terashi[154], J. Terron[100], S. Terzo[13], M. Testa[53], R. J. Teuscher[156,w], A. Thaler[79], O. Theiner[56], N. Themistokleous[52], T. Theveneaux-Pelzer[103], O. Thielmann[172], D. W. Thomas[96], J. P. Thomas[20], E. A. Thompson[17a], P. D. Thompson[20], E. Thomson[129], R. E. Thornberry[44], Y. Tian[55], V. Tikhomirov[37,a], Yu.A. Tikhonov[37], S. Timoshenko[37], D. Timoshyn[134], E. X. L. Ting[1], P. Tipton[173], S. H. Tlou[33g], K. Todome[155], S. Todorova-Nova[134], S. Todt[50], L. Toffolin[69a,69c], M. Togawa[84], J. Tojo[89], S. Tokár[28a], K. Tokushuku[84], O. Toldaiev[68], R. Tombs[32], M. Tomoto[84,112], L. Tompkins[144,m], K. W. Topolnicki[86b], E. Torrence[124], H. Torres[90], E. Torró Pastor[164], M. Toscani[30], C. Tosciri[39], M. Tost[11], D. R. Tovey[140], A. Traeet[16], I. S. Trandafir[27b], T. Trefzger[167], A. Tricoli[29], I. M. Trigger[157a], S. Trincaz-Duvoid[128], D. A. Trischuk[26], B. Trocmé[60], L. Truong[33c], M. Trzebinski[87], A. Trzupek[87], F. Tsai[146], M. Tsai[107], A. Tsiamis[153,e], P. V. Tsiareshka[37], S. Tsigaridas[157a], A. Tsirigotis[153,r], V. Tsiskaridze[156], E. G. Tskhadadze[150a], M. Tsopoulou[153], Y. Tsujikawa[88], I. I. Tsukerman[37], V. Tsulaia[17a], S. Tsuno[84], K. Tsuri[119], D. Tsybychev[146], Y. Tu[64b], A. Tudorache[27b], V. Tudorache[27b], A. N. Tuna[61], S. Turchikhin[57a,57b], I. Turk Cakir[3a], R. Turra[71a], T. Turtuvshin[38,x], P. M. Tuts[41], S. Tzamarias[153,e], E. Tzovara[101], F. Ukegawa[158], P. A. Ulloa Poblete[138b,138c], E. N. Umaka[29], G. Unal[36], A. Undrus[29], G. Unel[160], J. Urban[28b], P. Urquijo[106], P. Urrejola[138a], G. Usai[8], R. Ushioda[155], M. Usman[109], Z. Uysal[82], V. Vacek[133], B. Vachon[105], T. Vafeiadis[36], A. Vaitkus[97], C. Valderanis[110], E. Valdes Santurio[47a,47b], M. Valente[157a], S. Valentinetti[23a,23b], A. Valero[164], E. Valiente Moreno[164], A. Vallier[90], J. A. Valls Ferrer[164], D. R. Van Arneman[115], T. R. Van Daalen[139], A. Van Der Graaf[49], P. Van Gemmeren[6], M. Van Rijnbach[126], S. Van Stroud[97], I. Van Vulpen[115], P. Vana[134], M. Vanadia[76a,76b], W. Vandelli[36], E. R. Vandewall[122], D. Vannicola[152], L. Vannoli[53], R. Vari[75a], E. W. Varnes[7], C. Varni[17b], T. Varol[149], D. Varouchas[66], L. Varriale[164], K. E. Varvell[148], M. E. Vasile[27b], L. Vaslin[84], G. A. Vasquez[166], A. Vasyukov[38], R. Vavricka[101], F. Vazeille[40], T. Vazquez Schroeder[36], J. Veatch[31], V. Vecchio[102], M. J. Veen[104], I. Veliscek[29], L. M. Veloce[156], F. Veloso[131a,131c], S. Veneziano[75a], A. Ventura[70a,70b], S. Ventura Gonzalez[136], A. Verbytskyi[111], M. Verducci[74a,74b], C. Vergis[95], M. Verissimo De Araujo[83b], W. Verkerke[115], J. C. Vermeulen[115], C. Vernieri[144], M. Vessella[104], M. C. Vetterli[143,ae], A. Vgenopoulos[153,e], N. Viaux Maira[138f], T. Vickey[140], O. E. Vickey Boeriu[140], G. H. A. Viehhauser[127], L. Vigani[63b], M. Villa[23a,23b], M. Villaplana Perez[164], E. M. Villhauer[52], E. Vilucchi[53], M. G. Vincter[34], A. Visibile[115],

C. Vittori[36], I. Vivarelli[23a,23b], E. Voevodina[111], F. Vogel[110], J. C. Voigt[50], P. Vokac[133], Yu. Volkotrub[86b], J. Von Ahnen[48], E. Von Toerne[24], B. Vormwald[36], V. Vorobel[134], K. Vorobev[37], M. Vos[164], K. Voss[142], M. Vozak[115], L. Vozdecky[121], N. Vranjes[15], M. Vranjes Milosavljevic[15], M. Vreeswijk[115], N. K. Vu[62c,62d], R. Vuillermet[36], O. Vujinovic[101], I. Vukotic[39], S. Wada[158], C. Wagner[104], J. M. Wagner[17a], W. Wagner[172], S. Wahdan[172], H. Wahlberg[91], M. Wakida[112], J. Walder[135], R. Walker[110], W. Walkowiak[142], A. Wall[129], E. J. Wallin[99], T. Wamorkar[6], A. Z. Wang[137], C. Wang[101], C. Wang[11], H. Wang[17a], J. Wang[64c], R.-J. Wang[101], R. Wang[61], R. Wang[6], S. M. Wang[149], S. Wang[62b], S. Wang[14a], T. Wang[62a], W. T. Wang[80], W. Wang[14a], X. Wang[14c], X. Wang[163], X. Wang[62c], Y. Wang[62d], Y. Wang[14c], Z. Wang[107], Z. Wang[51,62c,62d], Z. Wang[107], A. Warburton[105], R. J. Ward[20], N. Warrack[59], S. Waterhouse[96], A. T. Watson[20], H. Watson[59], M. F. Watson[20], E. Watton[59,135], G. Watts[139], B. M. Waugh[97], J. M. Webb[54], C. Weber[29], H. A. Weber[18], M. S. Weber[19], S. M. Weber[63a], C. Wei[62a], Y. Wei[54], A. R. Weidberg[127], E. J. Weik[118], J. Weingarten[49], M. Weirich[101], C. Weiser[54], C. J. Wells[48], T. Wenaus[29], B. Wendland[49], T. Wengler[36], N. S. Wenke[111], N. Wermes[24], M. Wessels[63a], A. M. Wharton[92], A. S. White[61], A. White[8], M. J. White[1], D. Whiteson[160], L. Wickremasinghe[125], W. Wiedenmann[171], M. Wielers[135], C. Wiglesworth[42], D. J. Wilbern[121], H. G. Wilkens[36], J. J. H. Wilkinson[32], D. M. Williams[41], H. H. Williams[129], S. Williams[32], S. Willocq[104], B. J. Wilson[102], P. J. Windischhofer[39], F. I. Winkel[30], F. Winklmeier[124], B. T. Winter[54], J. K. Winter[102], M. Wittgen[144], M. Wobisch[98], T. Wojtkowski[60], Z. Wolffs[115], J. Wollrath[160], M. W. Wolter[87], H. Wolters[131a,131c], M. C. Wong[137], E. L. Woodward[41], S. D. Worm[48], B. K. Wosiek[87], K. W. Woźniak[87], S. Wozniewski[55], K. Wraight[59], C. Wu[20], M. Wu[14d], M. Wu[114], S. L. Wu[171], X. Wu[56], Y. Wu[62a], Z. Wu[4], J. Wuerzinger[111,ac], T. R. Wyatt[102], B. M. Wynne[52], S. Xella[42], L. Xia[14c], M. Xia[14b], J. Xiang[64c], M. Xie[62a], X. Xie[62a], S. Xin[14a,14e], A. Xiong[124], J. Xiong[17a], D. Xu[14a], H. Xu[62a], L. Xu[62a], R. Xu[129], T. Xu[107], Y. Xu[14b], Z. Xu[52], Z. Xu[14c], B. Yabsley[148], S. Yacoob[33a], Y. Yamaguchi[155], E. Yamashita[154], H. Yamauchi[158], T. Yamazaki[17a], Y. Yamazaki[85], J. Yan[62c], S. Yan[59], Z. Yan[104], H. J. Yang[62c,62d], H. T. Yang[62a], S. Yang[62a], T. Yang[64c], X. Yang[36], X. Yang[14a], Y. Yang[44], Y. Yang[62a], Y. Yang[105], Z. Yang[62a], W.-M. Yao[17a], H. Ye[14c], H. Ye[55], J. Ye[14a], S. Ye[29], X. Ye[62a], Y. Yeh[97], I. Yeletskikh[38], B. K. Yeo[17b], M. R. Yexley[97], T. P. Yildirim[127], P. Yin[41], K. Yorita[169], S. Younas[27b], C. J. S. Young[36], C. Young[144], C. Yu[14a,14e], Y. Yu[62a], M. Yuan[107], R. Yuan[62c,62d], L. Yue[97], M. Zaazoua[62a], B. Zabinski[87], E. Zaid[52], Z. K. Zak[87], T. Zakareishvili[164], N. Zakharchuk[34], S. Zambito[56], J. A. Zamora Saa[138b,138d], J. Zang[154], D. Zanzi[54], O. Zaplatilek[133], C. Zeitnitz[172], H. Zeng[14a], J. C. Zeng[163], D. T. Zenger Jr[26], O. Zenin[37], T. Ženiš[28a], S. Zenz[95], S. Zerradi[35a], D. Zerwas[66], M. Zhai[14a,14e], D. F. Zhang[140], J. Zhang[62b], J. Zhang[6], K. Zhang[14a,14e], L. Zhang[62a], L. Zhang[14c], P. Zhang[14a,14e], R. Zhang[171], S. Zhang[107], S. Zhang[44], T. Zhang[154], X. Zhang[62c], X. Zhang[62b], Y. Zhang[5,62c], Y. Zhang[97], Y. Zhang[14c], Z. Zhang[17a], Z. Zhang[66], H. Zhao[139], T. Zhao[62b], Y. Zhao[137], Z. Zhao[62a], Z. Zhao[62a], A. Zhemchugov[38], J. Zheng[14c], K. Zheng[163], X. Zheng[62a], Z. Zheng[144], D. Zhong[163], B. Zhou[107], H. Zhou[7], N. Zhou[62c], Y. Zhou[14c], Y. Zhou[7], C. G. Zhu[62b], J. Zhu[107], X. Zhu[62d], Y. Zhu[62c], Y. Zhu[62a], X. Zhuang[14a], K. Zhukov[37], N. I. Zimine[38], J. Zinsser[63b], M. Ziolkowski[142], L. Živković[15], A. Zoccoli[23a,23b], K. Zoch[61], T. G. Zorbas[140], O. Zormpa[46], W. Zou[41], L. Zwalinski[36]

[1] Department of Physics, University of Adelaide, Adelaide, Australia
[2] Department of Physics, University of Alberta, Edmonton, AB, Canada
[3] [(a)]Department of Physics, Ankara University, Ankara, Turkey; [(b)]Division of Physics, TOBB University of Economics and Technology, Ankara, Turkey
[4] LAPP, Université Savoie Mont Blanc, CNRS/IN2P3, Annecy, France
[5] APC, Université Paris Cité, CNRS/IN2P3, Paris, France
[6] High Energy Physics Division, Argonne National Laboratory, Argonne, IL, USA
[7] Department of Physics, University of Arizona, Tucson, AZ, USA
[8] Department of Physics, University of Texas at Arlington, Arlington, TX, USA
[9] Physics Department, National and Kapodistrian University of Athens, Athens, Greece
[10] Physics Department, National Technical University of Athens, Zografou, Greece
[11] Department of Physics, University of Texas at Austin, Austin, TX, USA
[12] Institute of Physics, Azerbaijan Academy of Sciences, Baku, Azerbaijan
[13] Institut de Física d'Altes Energies (IFAE), Barcelona Institute of Science and Technology, Barcelona, Spain

[14] [(a)]Institute of High Energy Physics, Chinese Academy of Sciences, Beijing, China; [(b)]Physics Department, Tsinghua University, Beijing, China; [(c)]Department of Physics, Nanjing University, Nanjing, China; [(d)]School of Science, Shenzhen Campus of Sun Yat-sen University, China; [(e)]University of Chinese Academy of Science (UCAS), Beijing, China
[15] Institute of Physics, University of Belgrade, Belgrade, Serbia
[16] Department for Physics and Technology, University of Bergen, Bergen, Norway
[17] [(a)]Physics Division, Lawrence Berkeley National Laboratory, Berkeley, CA, USA; [(b)]University of California, Berkeley, CA, USA
[18] Institut für Physik, Humboldt Universität zu Berlin, Berlin, Germany
[19] Albert Einstein Center for Fundamental Physics and Laboratory for High Energy Physics, University of Bern, Bern, Switzerland
[20] School of Physics and Astronomy, University of Birmingham, Birmingham, UK
[21] [(a)]Department of Physics, Bogazici University, Istanbul, Turkey; [(b)]Department of Physics Engineering, Gaziantep University, Gaziantep, Turkey; [(c)]Department of Physics, Istanbul University, Istanbul, Turkey
[22] [(a)]Facultad de Ciencias y Centro de Investigaciónes, Universidad Antonio Nariño, Bogotá, Colombia; [(b)]Departamento de Física, Universidad Nacional de Colombia, Bogotá, Colombia
[23] [(a)]Dipartimento di Fisica e Astronomia A. Righi, Università di Bologna, Bologna, Italy; [(b)]INFN Sezione di Bologna, Bologna, Italy
[24] Physikalisches Institut, Universität Bonn, Bonn, Germany
[25] Department of Physics, Boston University, Boston, MA, USA
[26] Department of Physics, Brandeis University, Waltham, MA, USA
[27] [(a)]Transilvania University of Brasov, Brasov, Romania; [(b)]Horia Hulubei National Institute of Physics and Nuclear Engineering, Bucharest, Romania; [(c)]Department of Physics, Alexandru Ioan Cuza University of Iasi, Iasi, Romania; [(d)]National Institute for Research and Development of Isotopic and Molecular Technologies, Physics Department, Cluj-Napoca, Romania; [(e)]National University of Science and Technology Politechnica, Bucharest, Romania; [(f)]West University in Timisoara, Timisoara, Romania; [(g)]Faculty of Physics, University of Bucharest, Bucharest, Romania
[28] [(a)]Faculty of Mathematics, Physics and Informatics, Comenius University, Bratislava, Slovak Republic; [(b)]Department of Subnuclear Physics, Institute of Experimental Physics of the Slovak Academy of Sciences, Kosice, Slovak Republic
[29] Physics Department, Brookhaven National Laboratory, Upton, NY, USA
[30] Departamento de Física, y CONICET, Instituto de Física de Buenos Aires (IFIBA), Facultad de Ciencias Exactas y Naturales, Universidad de Buenos Aires, Buenos Aires, Argentina
[31] California State University, Long Beach, CA, USA
[32] Cavendish Laboratory, University of Cambridge, Cambridge, UK
[33] [(a)]Department of Physics, University of Cape Town, Cape Town, South Africa; [(b)]iThemba Labs, Western Cape, South Africa; [(c)]Department of Mechanical Engineering Science, University of Johannesburg, Johannesburg, South Africa; [(d)]National Institute of Physics, University of the Philippines Diliman (Philippines), Quezon City, Philippines; [(e)]University of South Africa, Department of Physics, Pretoria, South Africa; [(f)]University of Zululand, KwaDlangezwa, South Africa; [(g)]School of Physics, University of the Witwatersrand, Johannesburg, South Africa
[34] Department of Physics, Carleton University, Ottawa, ON, Canada
[35] [(a)]Faculté des Sciences Ain Chock, Université Hassan II de Casablanca, Morocco; [(b)]Faculté des Sciences, Université Ibn-Tofail, Kenitra, Morocco; [(c)]Faculté des Sciences Semlalia, Université Cadi Ayyad, LPHEA-Marrakech, Marrakesh, Morocco; [(d)]LPMR, Faculté des Sciences, Université Mohamed Premier, Oujda, Morocco; [(e)]Faculté des sciences, Université Mohammed V, Rabat, Morocco; [(f)]Institute of Applied Physics, Mohammed VI Polytechnic University, Ben Guerir, Morocco
[36] CERN, Geneva, Switzerland
[37] Affiliated with an institute covered by a cooperation agreement with CERN, Geneva, Switzerland
[38] Affiliated with an international laboratory covered by a cooperation agreement with CERN, Geneva, Switzerland
[39] Enrico Fermi Institute, University of Chicago, Chicago, IL, USA
[40] LPC, Université Clermont Auvergne, CNRS/IN2P3, Clermont-Ferrand, France
[41] Nevis Laboratory, Columbia University, Irvington, NY, USA
[42] Niels Bohr Institute, University of Copenhagen, Copenhagen, Denmark

[43] [(a)]Dipartimento di Fisica, Università della Calabria, Rende, Italy; [(b)]INFN Gruppo Collegato di Cosenza, Laboratori Nazionali di Frascati, Frascati, Italy
[44] Physics Department, Southern Methodist University, Dallas, TX, USA
[45] Physics Department, University of Texas at Dallas, Richardson, TX, USA
[46] National Centre for Scientific Research "Demokritos", Agia Paraskevi, Greece
[47] [(a)]Department of Physics, Stockholm University, Stockholm, Sweden; [(b)]Oskar Klein Centre, Stockholm, Sweden
[48] Deutsches Elektronen-Synchrotron DESY, Hamburg and Zeuthen, Germany
[49] Fakultät Physik , Technische Universität Dortmund, Dortmund, Germany
[50] Institut für Kern- und Teilchenphysik, Technische Universität Dresden, Dresden, Germany
[51] Department of Physics, Duke University, Durham, NC, USA
[52] SUPA-School of Physics and Astronomy, University of Edinburgh, Edinburgh, UK
[53] INFN e Laboratori Nazionali di Frascati, Frascati, Italy
[54] Physikalisches Institut, Albert-Ludwigs-Universität Freiburg, Freiburg, Germany
[55] II. Physikalisches Institut, Georg-August-Universität Göttingen, Göttingen, Germany
[56] Département de Physique Nucléaire et Corpusculaire, Université de Genève, Geneve, Switzerland
[57] [(a)]Dipartimento di Fisica, Università di Genova, Genoa, Italy; [(b)]INFN Sezione di Genova, Genoa, Italy
[58] II. Physikalisches Institut, Justus-Liebig-Universität Giessen, Giessen, Germany
[59] SUPA-School of Physics and Astronomy, University of Glasgow, Glasgow, UK
[60] LPSC, Université Grenoble Alpes, CNRS/IN2P3, Grenoble INP, Grenoble, France
[61] Laboratory for Particle Physics and Cosmology, Harvard University, Cambridge, MA, USA
[62] [(a)]Department of Modern Physics and State Key Laboratory of Particle Detection and Electronics, University of Science and Technology of China, Hefei, China; [(b)]Institute of Frontier and Interdisciplinary Science and Key Laboratory of Particle Physics and Particle Irradiation (MOE), Shandong University, Qingdao, China; [(c)]School of Physics and Astronomy, Shanghai Jiao Tong University, Key Laboratory for Particle Astrophysics and Cosmology (MOE), SKLPPC, Shanghai, China; [(d)]Tsung-Dao Lee Institute, Shanghai, China; [(e)]School of Physics and Microelectronics, Zhengzhou University, China
[63] [(a)]Kirchhoff-Institut für Physik, Ruprecht-Karls-Universität Heidelberg, Heidelberg, Germany; [(b)]Physikalisches Institut, Ruprecht-Karls-Universität Heidelberg, Heidelberg, Germany
[64] [(a)]Department of Physics, Chinese University of Hong Kong, Shatin N.T., Hong Kong, China; [(b)]Department of Physics, University of Hong Kong, Hong Kong, China; [(c)]Department of Physics and Institute for Advanced Study, Hong Kong University of Science and Technology, Clear Water Bay, Kowloon, Hong Kong, China
[65] Department of Physics, National Tsing Hua University, Hsinchu, Taiwan
[66] IJCLab, Université Paris-Saclay, CNRS/IN2P3, 91405 Orsay, France
[67] Centro Nacional de Microelectrónica (IMB-CNM-CSIC), Barcelona, Spain
[68] Department of Physics, Indiana University, Bloomington, IN, USA
[69] [(a)]INFN Gruppo Collegato di Udine, Sezione di Trieste, Udine, Italy; [(b)]ICTP, Trieste, Italy; [(c)]Dipartimento Politecnico di Ingegneria e Architettura, Università di Udine, Udine, Italy
[70] [(a)]INFN Sezione di Lecce, Lecce, Italy; [(b)]Dipartimento di Matematica e Fisica, Università del Salento, Lecce, Italy
[71] [(a)]INFN Sezione di Milano, Milan, Italy; [(b)]Dipartimento di Fisica, Università di Milano, Milan, Italy
[72] [(a)]INFN Sezione di Napoli, Naples, Italy; [(b)]Dipartimento di Fisica, Università di Napoli, Naples, Italy
[73] [(a)]INFN Sezione di Pavia, Pavia, Italy; [(b)]Dipartimento di Fisica, Università di Pavia, Pavia, Italy
[74] [(a)]INFN Sezione di Pisa, Pisa, Italy; [(b)]Dipartimento di Fisica E. Fermi, Università di Pisa, Pisa, Italy
[75] [(a)]INFN Sezione di Roma, Rome, Italy; [(b)]Dipartimento di Fisica, Sapienza Università di Roma, Rome, Italy
[76] [(a)]INFN Sezione di Roma Tor Vergata, Rome, Italy; [(b)]Dipartimento di Fisica, Università di Roma Tor Vergata, Rome, Italy
[77] [(a)]INFN Sezione di Roma Tre, Rome, Italy; [(b)]Dipartimento di Matematica e Fisica, Università Roma Tre, Rome, Italy
[78] [(a)]INFN-TIFPA, Rome, Italy; [(b)]Università degli Studi di Trento, Trento, Italy
[79] Universität Innsbruck, Department of Astro and Particle Physics, Innsbruck, Austria
[80] University of Iowa, Iowa City, IA, USA
[81] Department of Physics and Astronomy, Iowa State University, Ames, IA, USA
[82] Istinye University, Sariyer, Istanbul, Turkey
[83] [(a)]Departamento de Engenharia Elétrica, Universidade Federal de Juiz de Fora (UFJF), Juiz de Fora,

Brazil; [b]Universidade Federal do Rio De Janeiro COPPE/EE/IF, Rio de Janeiro, Brazil; [c]Instituto de Física, Universidade de São Paulo, São Paulo, Brazil; [d]Rio de Janeiro State University, Rio de Janeiro, Brazil; [e]Federal University of Bahia, Bahia, Brazil
[84] KEK, High Energy Accelerator Research Organization, Tsukuba, Japan
[85] Graduate School of Science, Kobe University, Kobe, Japan
[86] [a]AGH University of Krakow, Faculty of Physics and Applied Computer Science, Krakow, Poland; [b]Marian Smoluchowski Institute of Physics, Jagiellonian University, Kraków, Poland
[87] Institute of Nuclear Physics Polish Academy of Sciences, Kraków, Poland
[88] Faculty of Science, Kyoto University, Kyoto, Japan
[89] Research Center for Advanced Particle Physics and Department of Physics, Kyushu University, Fukuoka , Japan
[90] L2IT, Université de Toulouse, CNRS/IN2P3, UPS, Toulouse, France
[91] Instituto de Física La Plata, Universidad Nacional de La Plata and CONICET, La Plata, Argentina
[92] Physics Department, Lancaster University, Lancaster, UK
[93] Oliver Lodge Laboratory, University of Liverpool, Liverpool, UK
[94] Department of Experimental Particle Physics, Jožef Stefan Institute and Department of Physics, University of Ljubljana, Ljubljana, Slovenia
[95] School of Physics and Astronomy, Queen Mary University of London, London, UK
[96] Department of Physics, Royal Holloway University of London, Egham, UK
[97] Department of Physics and Astronomy, University College London, London, UK
[98] Louisiana Tech University, Ruston, LA, USA
[99] Fysiska institutionen, Lunds universitet, Lund, Sweden
[100] Departamento de Física Teorica C-15 and CIAFF, Universidad Autónoma de Madrid, Madrid, Spain
[101] Institut für Physik, Universität Mainz, Mainz, Germany
[102] School of Physics and Astronomy, University of Manchester, Manchester, UK
[103] CPPM, Aix-Marseille Université, CNRS/IN2P3, Marseille, France
[104] Department of Physics, University of Massachusetts, Amherst, MA, USA
[105] Department of Physics, McGill University, Montreal, QC, Canada
[106] School of Physics, University of Melbourne, Melbourne, VIC, Australia
[107] Department of Physics, University of Michigan, Ann Arbor, MI, USA
[108] Department of Physics and Astronomy, Michigan State University, East Lansing, MI, USA
[109] Group of Particle Physics, University of Montreal, Montreal, QC, Canada
[110] Fakultät für Physik, Ludwig-Maximilians-Universität München, Munich, Germany
[111] Max-Planck-Institut für Physik (Werner-Heisenberg-Institut), Munich, Germany
[112] Graduate School of Science and Kobayashi-Maskawa Institute, Nagoya University, Nagoya, Japan
[113] Department of Physics and Astronomy, University of New Mexico, Albuquerque, NM, USA
[114] Institute for Mathematics, Astrophysics and Particle Physics, Radboud University/Nikhef, Nijmegen, Netherlands
[115] Nikhef National Institute for Subatomic Physics and University of Amsterdam, Amsterdam, Netherlands
[116] Department of Physics, Northern Illinois University, DeKalb, IL, USA
[117] [a]New York University Abu Dhabi, Abu Dhabi, United Arab Emirates; [b]United Arab Emirates University, Al Ain, United Arab Emirates
[118] Department of Physics, New York University, New York, NY, USA
[119] Ochanomizu University, Otsuka, Bunkyo-ku, Tokyo, Japan
[120] Ohio State University, Columbus, OH, USA
[121] Homer L. Dodge Department of Physics and Astronomy, University of Oklahoma, Norman, OK, USA
[122] Department of Physics, Oklahoma State University, Stillwater, OK, USA
[123] Palacký University, Joint Laboratory of Optics, Olomouc, Czech Republic
[124] Institute for Fundamental Science, University of Oregon, Eugene, OR, USA
[125] Graduate School of Science, Osaka University, Osaka, Japan
[126] Department of Physics, University of Oslo, Oslo, Norway
[127] Department of Physics, Oxford University, Oxford, UK
[128] LPNHE, Sorbonne Université, Université Paris Cité, CNRS/IN2P3, Paris, France
[129] Department of Physics, University of Pennsylvania, Philadelphia, PA, USA
[130] Department of Physics and Astronomy, University of Pittsburgh, Pittsburgh, PA, USA

[131] [(a)]Laboratório de Instrumentação e Física Experimental de Partículas-LIP, Lisbon, Portugal; [(b)]Departamento de Física, Faculdade de Ciências, Universidade de Lisboa, Lisbon, Portugal; [(c)]Departamento de Física, Universidade de Coimbra, Coimbra, Portugal; [(d)]Centro de Física Nuclear da Universidade de Lisboa, Lisbon, Portugal; [(e)]Departamento de Física, Universidade do Minho, Braga, Portugal; [(f)]Departamento de Física Teórica y del Cosmos, Universidad de Granada, Granada, Spain; [(g)]Departamento de Física, Instituto Superior Técnico, Universidade de Lisboa, Lisbon, Portugal
[132] Institute of Physics of the Czech Academy of Sciences, Prague, Czech Republic
[133] Czech Technical University in Prague, Prague, Czech Republic
[134] Charles University, Faculty of Mathematics and Physics, Prague, Czech Republic
[135] Particle Physics Department, Rutherford Appleton Laboratory, Didcot, UK
[136] IRFU, CEA, Université Paris-Saclay, Gif-sur-Yvette, France
[137] Santa Cruz Institute for Particle Physics, University of California Santa Cruz, Santa Cruz, CA, USA
[138] [(a)]Departamento de Física, Pontificia Universidad Católica de Chile, Santiago, Chile; [(b)]Millennium Institute for Subatomic physics at high energy frontier (SAPHIR), Santiago, Chile; [(c)]Instituto de Investigación Multidisciplinario en Ciencia y Tecnología y Departamento de Física, Universidad de La Serena, La Serena, Chile; [(d)]Universidad Andres Bello, Department of Physics, Santiago, Chile; [(e)]Instituto de Alta Investigación, Universidad de Tarapacá, Arica, Chile; [(f)]Departamento de Física, Universidad Técnica Federico Santa María, Valparaiso, Chile
[139] Department of Physics, University of Washington, Seattle, WA, USA
[140] Department of Physics and Astronomy, University of Sheffield, Sheffield, UK
[141] Department of Physics, Shinshu University, Nagano, Japan
[142] Department Physik, Universität Siegen, Siegen, Germany
[143] Department of Physics, Simon Fraser University, Burnaby, BC, Canada
[144] SLAC National Accelerator Laboratory, Stanford, CA, USA
[145] Department of Physics, Royal Institute of Technology, Stockholm, Sweden
[146] Departments of Physics and Astronomy, Stony Brook University, Stony Brook, NY, USA
[147] Department of Physics and Astronomy, University of Sussex, Brighton, UK
[148] School of Physics, University of Sydney, Sydney, Australia
[149] Institute of Physics, Academia Sinica, Taipei, Taiwan
[150] [(a)]E. Andronikashvili Institute of Physics, Iv. Javakhishvili Tbilisi State University, Tbilisi, Georgia; [(b)]High Energy Physics Institute, Tbilisi State University, Tbilisi, Georgia; [(c)]University of Georgia, Tbilisi, Georgia
[151] Department of Physics, Technion, Israel Institute of Technology, Haifa, Israel
[152] Raymond and Beverly Sackler School of Physics and Astronomy, Tel Aviv University, Tel Aviv, Israel
[153] Department of Physics, Aristotle University of Thessaloniki, Thessaloniki, Greece
[154] International Center for Elementary Particle Physics and Department of Physics, University of Tokyo, Tokyo, Japan
[155] Department of Physics, Tokyo Institute of Technology, Tokyo, Japan
[156] Department of Physics, University of Toronto, Toronto, ON, Canada
[157] [(a)]TRIUMF, Vancouver, BC, Canada; [(b)]Department of Physics and Astronomy, York University, Toronto, ON, Canada
[158] Division of Physics and Tomonaga Center for the History of the Universe, Faculty of Pure and Applied Sciences, University of Tsukuba, Tsukuba, Japan
[159] Department of Physics and Astronomy, Tufts University, Medford, MA, USA
[160] Department of Physics and Astronomy, University of California Irvine, Irvine, CA, USA
[161] University of Sharjah, Sharjah, United Arab Emirates
[162] Department of Physics and Astronomy, University of Uppsala, Uppsala, Sweden
[163] Department of Physics, University of Illinois, Urbana, IL, USA
[164] Instituto de Física Corpuscular (IFIC), Centro Mixto Universidad de Valencia - CSIC, Valencia, Spain
[165] Department of Physics, University of British Columbia, Vancouver, BC, Canada
[166] Department of Physics and Astronomy, University of Victoria, Victoria, BC, Canada
[167] Fakultät für Physik und Astronomie, Julius-Maximilians-Universität Würzburg, Würzburg, Germany
[168] Department of Physics, University of Warwick, Coventry, UK
[169] Waseda University, Tokyo, Japan
[170] Department of Particle Physics and Astrophysics, Weizmann Institute of Science, Rehovot, Israel
[171] Department of Physics, University of Wisconsin, Madison, WI, USA
[172] Fakultät für Mathematik und Naturwissenschaften, Fachgruppe Physik, Bergische Universität Wuppertal, Wuppertal, Germany

[173] Department of Physics, Yale University, New Haven, CT, USA

[a] Also Affiliated with an institute covered by a cooperation agreement with CERN, Geneva, Switzerland
[b] Also at An-Najah National University, Nablus, Palestine
[c] Also at Borough of Manhattan Community College, City University of New York, New York, NY, USA
[d] Also at Center for High Energy Physics, Peking University, China
[e] Also at Center for Interdisciplinary Research and Innovation (CIRI-AUTH), Thessaloniki, Greece
[f] Also at Centro Studi e Ricerche Enrico Fermi, Rome, Italy
[g] Also at CERN, Geneva, Switzerland
[h] Also at Département de Physique Nucléaire et Corpusculaire, Université de Genève, Geneve, Switzerland
[i] Also at Departament de Fisica de la Universitat Autonoma de Barcelona, Barcelona, Spain
[j] Also at Department of Financial and Management Engineering, University of the Aegean, Chios, Greece
[k] Also at Department of Physics, California State University, Sacramento, USA
[l] Also at Department of Physics, King's College London, London, UK
[m] Also at Department of Physics, Stanford University, Stanford, CA, USA
[n] Also at Department of Physics, Stellenbosch University, South Africa
[o] Also at Department of Physics, University of Fribourg, Fribourg, Switzerland
[p] Also at Department of Physics, University of Thessaly, Greece
[q] Also at Department of Physics, Westmont College, Santa Barbara, USA
[r] Also at Hellenic Open University, Patras, Greece
[s] Also at Institucio Catalana de Recerca i Estudis Avancats, ICREA, Barcelona, Spain
[t] Also at Institut für Experimentalphysik, Universität Hamburg, Hamburg, Germany
[u] Also at Institute for Nuclear Research and Nuclear Energy (INRNE) of the Bulgarian Academy of Sciences, Sofia, Bulgaria
[v] Also at Institute of Applied Physics, Mohammed VI Polytechnic University, Ben Guerir, Morocco
[w] Also at Institute of Particle Physics (IPP), Vancouver, Canada
[x] Also at Institute of Physics and Technology, Mongolian Academy of Sciences, Ulaanbaatar, Mongolia
[y] Also at Institute of Physics, Azerbaijan Academy of Sciences, Baku, Azerbaijan
[z] Also at Institute of Theoretical Physics, Ilia State University, Tbilisi, Georgia
[aa] Also at Lawrence Livermore National Laboratory, Livermore, USA
[ab] Also at National Institute of Physics, University of the Philippines Diliman (Philippines), Quezon City, Philippines
[ac] Also at Technical University of Munich, Munich, Germany
[ad] Also at The Collaborative Innovation Center of Quantum Matter (CICQM), Beijing, China
[ae] Also at TRIUMF, Vancouver, BC, Canada
[af] Also at Università di Napoli Parthenope, Naples, Italy
[ag] Also at University of Colorado Boulder, Department of Physics, Colorado, USA
[ah] Also at Washington College, Chestertown, MD, USA
[ai] Also at Yeditepe University, Physics Department, Istanbul, Turkey
* Deceased